Université de Montréal

Ultrasonography-Based Evaluation and Simulation of the Hemodynamic Consequences of Arterial Stenoses

par
Brigitte C. Lamontagne

Institut de génie biomédical
Faculté de Médecine

Mémoire présenté à la Faculté des études supérieures
en vue de l'obtention du grade de Maître ès sciences appliquées (M.Sc.A.)
en génie biomédical
option: Instrumentation et imagerie biomédicale

Janvier, 2002

Université de Montréal

Faculté des études supérieures

Ce mémoire intitulé:
Ultrasonography-Based Evaluation and Simulation of the Hemodynamic Consequences of Arterial Stenoses

présenté par:
Brigitte C. Lamontagne

a été évalué par un jury composé des personnes suivantes:

Jean Meunier, Ph.D.
président-rapporteur

Guy Cloutier, Ph.D., M.Sc.A., Ing.
directeur de recherche

Louis-Gilles Durand, Ph.D., M.Sc.A., Ing.
codirecteur

Gilles Soulez, M.D., M.Sc.
membre du jury

RESUME

Pour diagnostiquer l'acrosyndrome vasculaire, la justesse d'un index clinique, le ratio de vélocité ($VR = PSV_2/PSV_1$), et les gradients des pression ($\Delta P = P_1-P_2$) à une sténose d'intérêt (SOI), ont été étudiés dans les cas d'une sténose simple et pour plusieurs configurations de sténoses doubles. PSV_1 et PSV_2 sont les vitesses systoliques maximales proximales ou distales à la SOI, et à la SOI, respectivement, et P_1 et P_2 sont les pressions proximales et distales à la SOI. Plusieurs points de mesure de PSV_1 (2D proximal, et 2D et 10D distal à la SOI) et de P_2 (à la SOI, et 2D, 5D, et 10D distal à la SOI) ont été étudiés par simulation en éléments finis et par des expériences *in vitro*, en débit continu. Les VRs pour la sténose simple étaient inférieurs à la prédiction de la théorie, par contre, les mesures proximales du PSV_1 fournissaient les meilleurs VRs. Les sténoses étagées pouvaient davantage réduire les VRs dépendant du point de mesure du PSV_1. En présence d'une sténose proximale (SP), les mesures du PSV_1 à 10D distal à la SOI ont donné les meilleurs approximations de la sévérité du SOI. D'autre part, pour une grande distance intersténotique (10D), une mesure de PSV_1 à 2D proximal donnait des résultats similaires. En présence d'une sténose distale, PSV_1 mesuré à 2D proximal était le plus près de la théorie. Pour toutes les configurations, les positions de mesure du PSV_1 choisit aveuglement résultaient en des courbes VR au moins aussi bien que celles des positions fixes. Les gradients de pression à la SOI étaient consistants selon la position de mesure de P_2, mais les valeurs *in vitro* étaient inférieures aux simulations. Ces gradients n'étaient pas affectés par la présence d'une sténose adjacente dans les simulations. *In vitro*, une sténose à 3D ou 6D proximal affectait légèrement les gradients, et ils augmentaient de façon significative à 10D. Une sténose distale réduisait les gradients à la SOI peu importe la distance intersténotique.

Mots clés: Ultrasonographie duplex Doppler, acrosyndrome vasculaire, ratio de vélocité, vitesse systolique maximale, gradient de pression, sténose, sténoses étagées, simulations, *in vitro*.

ABSTRACT

The diagnosis of Peripheral Vascular Disease was studied using a clinical index based on a ratio of Peak Systolic Velocities (PSV), the Velocity Ratio ($VR = PSV_2/PSV_1$), and using the pressure gradients ($\Delta P = P_1-P_2$) at a stenosis of interest (SOI). PSV_1 is proximal or distal to SOI, PSV_2 is at SOI, and P_1 and P_2 are proximal and distal to SOI, respectively. Various measurement positions for PSV_1 (2D proximal, and 2D and 10D distal to the SOI) and P_2 (at the SOI, and 2D, 5D, and 10D distal to the SOI) were studied for several stenosis configurations in Finite Element simulations and *in vitro* experiments in steady flow. The VRs at a single stenosis were lower than in theory, and the proximal PSV_1 measurements resulted in the best VRs. Multilevel disease could further reduce the VRs depending on the PSV_1 measurement position. Globally, with a proximal stenosis, PSV_1 measured 10D distal to SOI allowed the most accurate severity estimations, however, when SP was at 10D, a 2D proximal position was acceptable. For a distal stenosis, PSV_1 measured 2D proximal to SOI was best. In all cases, blinded velocity measurements resulted in VR curves comparable to or more accurate than the best fixed positions. The pressure gradients at SOI appeared consistent with the P_2 measurement position, though they were generally lower *in vitro* than in the simulations and were not affected by an adjacent stenosis in the simulations. For a stenosis at 3D or 6D proximal, the *in vitro* gradients varied slightly, and increased visibly at 10D. For a distal stenosis, the gradients decreased at all interstenotic distances.

Keywords: Duplex Doppler ultrasound, Peripheral Vascular Disease, Velocity Ratio, Peak Systolic Velocity, pressure gradient, stenosis, multilevel disease, simulations, *in vitro*.

TABLE OF CONTENTS

Page

Page

Page

Page

LIST OF TABLES

Page

LIST OF FIGURES

Page

Page

Page

LIST OF ABBREVIATIONS

CVD	Cardiovascular disease
CW	Continuous-Wave
EC	Endothelial cells
FE	Finite Element
KE	Kinetic energy
LD	Interstenotic distance between SOI and SD
LP	Interstenotic distance between SP and SOI
MRI	Magnetic Resonance Imaging
PRF	Pulse Repetition Frequency
PSV	Peak Systolic Velocity
PVD	Peripheral Vascular Disease
PW	Pulsed-Wave
SOI	Stenosis of Interest
SD	Stenosis distal to the SOI
SP	Stenosis proximal to the SOI
US	Ultrasound
VR	Velocity Ratio

A mon mari Mathieu et notre petit Félix

ACKNOWLEDGEMENTS

Je tiens à remercier Guy Cloutier et Louis-Gilles Durand pour leurs conseils judicieux et leur soutien, ainsi que Richard Cimon et Zhao Qin pour leur aide dans la mise en œuvre des expériences *in vitro*.

Je garderai aussi un très bon souvenir de tous les membres de l'équipe du laboratoire qui, par leur à propos et leur sympathie, ont contribué à faire de ma maîtrise une expérience réussie.

CHAPTER 1.

Cardiovascular Disease and Clinical Assessment

1.1 Atherosclerosis : Epidemiology and Risk Factors

Cardiovascular diseases (CVD) are a growing problem throughout the world. Such diseases include myocardial infarction, ischemic heart disease, valvular cardiopathy, arrhythmia, hypertension, stroke, and peripheral vascular disease (PVD). Risk factors for CVD include cigarette smoking, hypertension, hypercholesterolemia, diabetes mellitus, obesity and a sedentary lifestyle, alcohol consumption, stress, aging, and socio-economic status. The increasing incidence of CVD in developing countries may be attributed to longer life expectancies, higher risk factor levels, and special susceptibilities of certain populations (e.g., due to specific genes), compared to Western populations [a].

1.1.1 Target Population

In Canada, CVD are the principal causes for hospitalization in both men and women. In 1997, they caused 79 457 deaths and were the third cause of premature death for those younger than 75 years of age. Myocardial infarction and ischemic heart disease become serious problems toward the age of 45 years in men and towards 55 years in women. In 1993, CVD for Canadians cost $19,7 billion, the highest total costs of all pathologies (Health Canada website). In 1996 in the United States, 5% of men and 2.5% of women 60 years of age or older had symptoms of intermittent claudication[66,103]. However, the prevalence of arterial insufficiency reported in asymptomatic and symptomatic individuals depends on the diagnostic test used which may be more or less sensitive[29].

---

[a]http\\cardiology.medscape.com/Medscape/cardiology/2000/v04.n02/mc0428.ounp/mc0428.ounp.html, The Global Burden of Cardiovascular Disease, Stephanie Ounpuu, Sonia Anand, Salim Yusuf, Medscape Cardiology, 2000.

1.1.2 Peripheral Vascular Disease

Peripheral vascular disease (PVD), a specific cardiovascular disease, is the pathological narrowing of the arteries supplying oxygenated blood to the limbs. The most common form of PVD is atherosclerosis[138], the forming of yellowish plaques (atheromas or stenoses) containing lipid material, cholesterol, and lipophages, for which smoking is the most important related risk factor[54]. It is a generalized disease, and most patients with PVD have widespread occlusive arterial disease elsewhere in the body possibly leading to other clinical events[7,66,103,135]. Population studies show an increased incidence of cerebrovascular disease in patients with PVD, with a stroke incidence three times that of controls[49]. More specifically, at least 10% of PVD patients have cerebrovascular disease and 28% have coronary heart disease[135]. Of patients with lower extremity arterial disease, 75% will die of a coronary or cerebrovascular event[68]. In fact, the relative risk of death in patients with PVD is increased by a factor of 2 after 5 years and 2.5 after 10 years. About half the mortality is due to coronary artery disease[76], which emphasizes its close relationship to PVD.

Atherosclerosis is mainly a disease of large- and medium-sized arteries (e.g. the femoral artery) and most frequently involves the forming of stenoses (see Figure 1, page 2) at branch points and bifurcations[138].

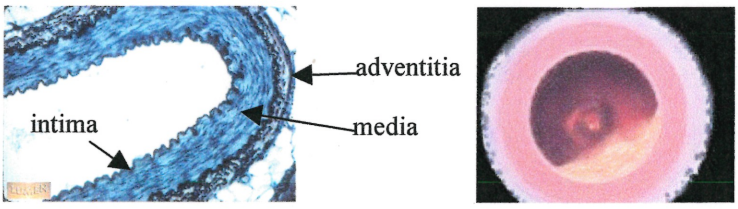

Figure 1. a) Cross-section of a muscular artery (e.g. femoral artery) showing the three layers of the wall: the intima, the media, and the adventitia (http://www.meddean.luc.edu/lumen/meded/Histo/HistoImages/ hl4-12.jpg). b) A schematic of an artery with an eccentric stenosis (from http://www.nobel.se/announcement-98/medanim/images.html).

An atheroma can increase in size and harden over time, reducing blood flow to the distal vascular bed, and can potentially result in a thrombosis or bleeding and subsequently clotting off of the artery, possibly leading to myocardial infarction or

cerebrovascular ischemia. Therefore, the importance of identifying patients with PVD extends beyond its impact on the lower extremity vascular system[138].

PVD may occur as part of the process in several recognized diseases. Its various forms may manifest themselves as (1) asymptomatic arterial insufficiency, (2) symptomatic disease presenting as intermittent claudication with positive noninvasive tests, and (3) critical leg ischemia, that is, symptomatic lower extremity arterial disease in which the ischemic process endangers part or all of the lower extremity[108]. Symptoms may only arise once the disease process is well advanced and they progress rather slowly over time[31,64].

The superficial femoral and popliteal arteries are the vessels most commonly affected by the atherosclerotic process in peripheral vessels, therefore, the pain of intermittent claudication is most often localized to the calf. The distal aorta, the aorto-iliac bifurcation and the iliac arteries are the next most frequent sites of involvement, producing pain in the buttocks or thighs as well as the legs[138].

Clinical symptoms of PVD are aching pains in the arms, legs, and feet due to ischemia of the tissues. In general, such symptoms are intensified with the onset of physical activity and are alleviated when ended, which is also known as intermittent claudication. Critical ischemia leads to more severe symptoms including continuous pain in the foot at rest, foot sores that heal slowly (ischemic ulceration), especially in patients with diabetes, and possibly gangrene, threatening limb loss. In fact, people living with diabetes are vulnerable to foot problems associated with peripheral vascular disease and neuropathy, producing a decreased sensation to pain and touch [b], and have 15 times greater risk of requiring lower extremity amputation than those without diabetes [c]. This is the end result of PVD and usually requires multiple sites of obstruction that severely reduce blood flow to the tissues[57,80]. However, the particular symptoms experienced depend on the overall physiological condition of the person, such as the degree of collateral flow and the severity of occlusion of the arteries[138], both of which affect distal blood supply.

---

[b] http://www.hc-sc.gc.ca/hpb/lcdc/publicat/ccdr/97vol23/vol23s8/fcb_e.html
[c] http://www.hc-sc.gc.ca/hpb/lcdc/publicat/diabet99/d12_e.html#10

The disease process in the femoral artery is a progression, though symptoms often occur stepwise[12]. Thrombotic occlusion occurs at sites with a critical stenosis (75% cross sectional area reduction of the arterial lumen), with acute worsening in symptoms, followed by gradual improvement due to collateral compensation[79]. The collateral circulation develops from the widening of existing arteries and provides a parallel pathway for blood flow[12]. The site and the severity of the arterial constriction in relation to the collateral flow determines the degree of limb ischemia[54], and hence, the severity of the symptoms[138]. In the thigh, there is extensive collateral potential via the numerous branches from the deep femoral artery when the superficial femoral artery is occluded. This is the main reason why patients who develop chronic occlusion of the superficial femoral artery without affecting the deep femoral artery have either no symptoms or mild symptoms of intermittent claudication. However, as soon as the origin of the deep femoral artery is also stenosed, the symptoms worsen. Thus, critical limb ischemia is rarely a consequence of isolated occlusion of the superficial femoral artery but occurs in the presence of multilevel disease, when the deep femoral artery is also affected or when there are stenoses and occlusions in the iliac and infrapopliteal arteries[12].

1.1.3 Clinical Implications

In light of the significance of such diseases, the awareness in the population of the association between PVD and its risk factors should be emphasized and the diagnosis of PVD should be available at a primary care level in order to limit the physical and economic burden of CVD on the population[17,55].

1.2 Human Physiology

1.2.1 Blood Properties and Macrocirculation

Blood behaves as a non-Newtonian liquid, which implies that its viscosity varies based on the flow conditions. However, it may be considered Newtonian in non-constricted arteries with a diameter superior to 1 mm (where the shear is high)[140]. It has a viscosity of $3x10^{-3}$ to $4.5x10^{-3}$ $N{\cdot}s/m^2$ [140], varying with the rate of flow, the size of the vessel,

and the blood hematocrit[84], and it is incompressible with a density of approximately 1050 kg/m^3 [140].

The movement of blood throughout the arterial system occurs due to variations in driving pressures in the order of 100 mmHg. However, the greatest pressure drop occurs at the arterioles, also known as the resistance vessels that have diameters ranging from 500 to 50 μm. The macrocirculation is the group of vessels with a diameter superior to 300 μm[28]. Due to high pressures, arteries are generally circular in cross-section, a fairly good assumption for modeling purposes, whereas veins are more or less flattened[28]. In the lower limbs, the following peripheral macrovessels are found. The *common femoral artery* (see Figure 2, page 6), the continuation of the *external iliac artery*, is situated at the hip level in the arterial tree and divides into the superficial and profunda femoral arteries. The *superficial femoral artery* is mainly a transport vessel to the below-knee muscles, has very few branches, is positioned towards the surface of the skin, and is a relatively straight artery, characteristics that favor its use in the diagnosis of PVD. The *profunda femoris artery* is the largest branch of the femoral artery and is the chief artery to the thigh[90].

1.2.2 Blood Flow Properties in the Macrocirculation

Blood flows through the arterial system in a periodic fashion with an average frequency of 70-75 beats/min. Accordingly, the pressure and the velocity of blood are periodic, but become almost constant in the capillaries. The flow may be assumed laminar and is highly pulsatile for arteries of diameter superior to 1 mm[140]. Normally, among the hemodynamic parameters that vary are the average flow rate, the vascular resistance, and the frequency of heartbeats. Though the heart flow rate may increase by a factor of five during physical activity, the average arterial pressure remains relatively constant[28]. The maximum velocity attained during a cardiac cycle is termed the Peak Systolic Velocity (PSV) (see Figure 3, page 7). The normal range is 119 ± 22 cm/s in the common external iliac artery, 114 ± 25 cm/s in the common femoral artery, and 91 to 94 $\pm$ 14 cm/s in the superficial femoral artery[116].

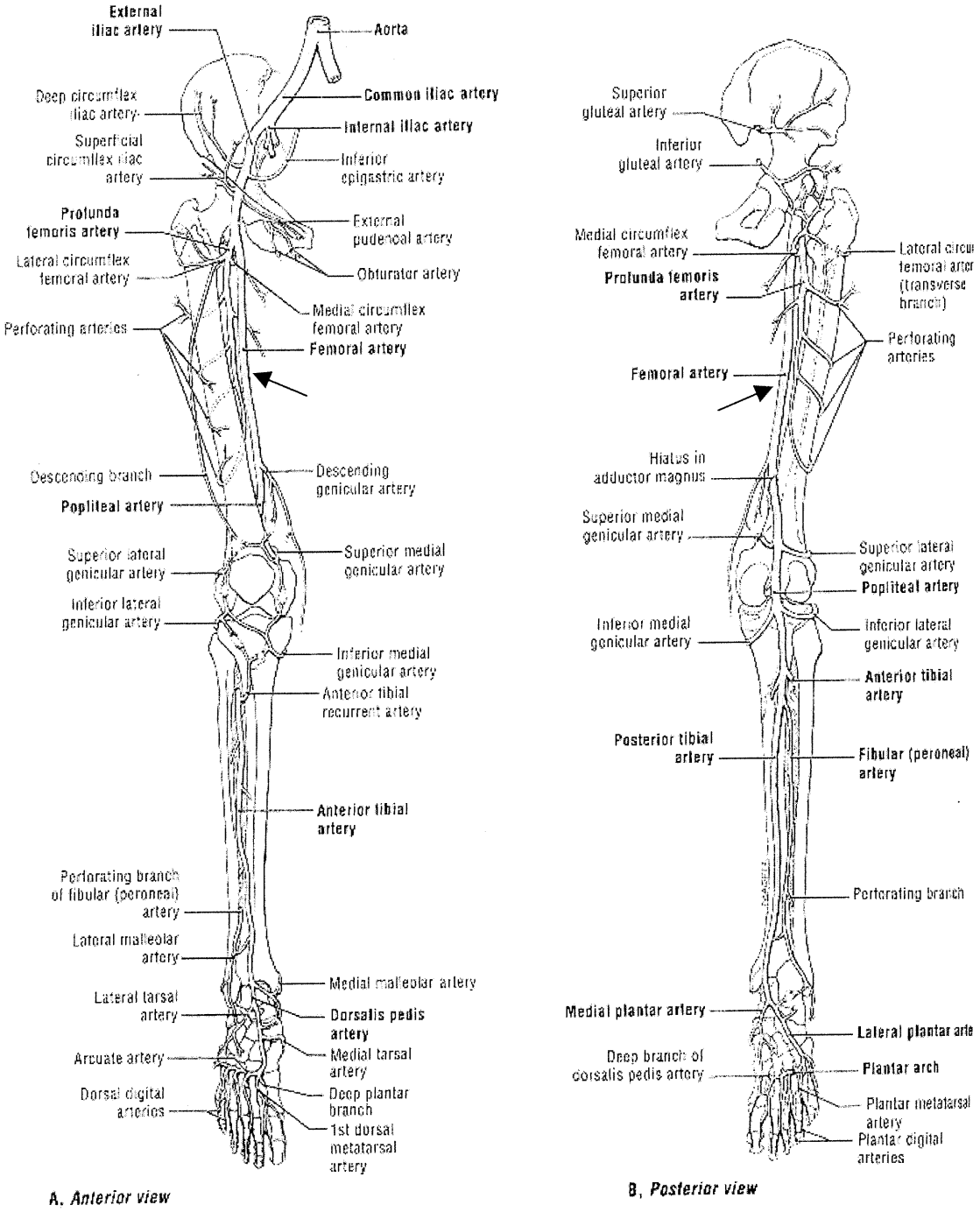

Figure 2. Arteries of the lower limb. Note the superficial femoral artery just distal to the hip joint[90].

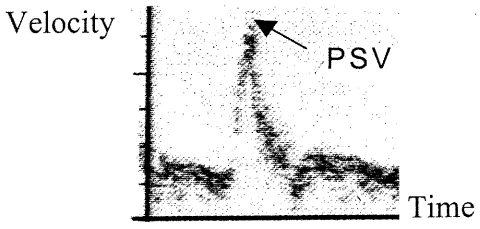

Figure 3. The pulsatility of a cardiac cycle indicating the Peak Systolic Velocity (PSV).

1.3 Hemodynamic and Homeostatic Consequences of Atherosclerotic Disease Progression

The static pressure measured at a point in the arterial system is indicative of the driving pressure created by the heart. However, the presence of a vessel constriction or projection into the lumen may change the pressure value measured depending on the measurement position relative to the stenosis. This may occur when an acceleration and deceleration of the blood is caused by the stenosis, as well as disturbed or turbulent flow conditions[42], resulting in friction and viscous losses, and thus, a pressure drop. Should the acceleration be significant, large pressure drops may arise, though the exact value measured depends on the flow conditions: flow rate, peripheral resistance, and driving pressure[140]. At each branching or bifurcation in the arterial tree, the velocity profiles are disturbed and secondary flows may arise. Following each disturbance, a certain distance is required for the profile to return to its fully developed parabolic shape. Moreover, the presence of a lesion (increased impedance) causes a reduction in the amplitude of flow waves proximally and distally, and of the pressure wave distally but little change is observed proximally[45]. The pressure and flow pulsations are most sensitive to changes in caliber of the artery. That is, changes in the pressure waves are noted with lesser degrees of stenosis than those required to cause change in mean flow or pressure gradient across the stenosis[94].

1.3.1 Endothelium

As mentioned earlier, healthy arteries are composed of three layers of tissue, the intima (endothelium), the media (muscle fibers), and the adventitia (collagen) (see Figure 1,

page 2). The intima is a monolayer of endothelial cells (ECs) forming the inner lining at the blood/vessel interface for hemodynamic control (flow rate, pressure, fluidity, coagulability of blood) through various metabolic activities[114]. This intima is normally anti-thrombotic and anti-adhesive to ensure blood fluidity. The regulation of these factors, however, can be affected by flow either through direct activation or by mechano-transduction (local blood flow conditions)[34,37,51,114].

Specific arterial sites such as branches, bifurcations, and curvatures, cause characteristic alterations in blood flow, including decreased shear stress and increased turbulence[56,87]. On the occurrence of a stimulus that characterizes vascular dysfunction (non-physiological conditions such as abnormal local shear stresses), mechano-sensitive structures are activated, which modify endothelial membrane receptor activity[39]. In turn, EC morphology and metabolism are affected[24,35,41,107,114,136], and the endothelium can reverse its "blood fluidifying" functions[114]. Therefore, the nature of the flow appears to be important in determining whether lesions occur at a given vascular site[106]. Endothelial vasomotor dysfunction has been demonstrated in coronary and peripheral arteries[134].

More recent work by Ross et al.[106] shows that atherosclerosis can best be described as an inflammatory disease. The endothelial dysfunction that results from an injury to the vessel leads to compensatory responses (inflammation) that alter the normal homeostatic properties of the intima. If this response does not effectively remove the offending agents, it can continue, stimulating migration and proliferation of smooth muscle cells that become intermixed with the area of inflammation to form an intermediate lesion. Eventually, the artery wall can thicken, and gradual dilation or "remodeling" of the artery occurs so that up to a point, the lumen remains unaltered[53]. The lesion may worsen and eventually lead to focal necrosis[44]. This behavior corresponds to the need to eliminate destroyed tissue or to protect it from hemorrhage[114,133]. At some point, the artery can no longer compensate by dilation and the lesion may then intrude into the lumen and alter blood flow[106].

1.4 Diagnosis of Peripheral Vascular Obstructions

In general, biological flow phenomena may be measured using at least one of three variables: displacement, pressure, and velocity/flow rate. Such variables may be measured either directly, indirectly (noninvasively, ex. measuring Korotkoff sounds and relating them to a given disease), or relatively (using a model to recreate an *in vivo* situation)[15]. Ideally, screening examinations for the detection of PVD should be noninvasive, yet provide quantitative information from a direct measurement. A common method is to calculate clinical indices based on velocity measurements obtained within an artery using Doppler ultrasound (US). Modern US machines are portable and relatively inexpensive, and the examination is rapid (real-time imaging), noninvasive, and non-ionizing. However, the accuracy of such diagnoses varies according to the characteristics of the ultrasound system, to the clinical index of severity employed (i.e. the interpretation of the measurements), and to the level of experience of the medical operator and consultant[42]. However, Doppler (mainly duplex) US already has an established success in diagnosing problems relating to cardiac valves, to venous and arterial stenoses, and other hemodynamic problems. Since disease progression depends on the hemodynamic conditions, it is becoming the principal tool used in its detection. Yet even though disease prevention depends on the early detection of stenoses, the diagnostic process will only be initiated in the presence of clinical symptoms[52].

Diagnosis of PVD has been performed using many different indices, however, noninvasive assessment by Doppler ultrasound is recommended to determine the extent of the disease when symptoms are related to blood flow[42,54]. In patients with indications for intervention (disabling claudication or critical limb ischemia), most centers use the combination of color-coded duplex US scanning and angiography[12]. Magnetic resonance imaging (MRI) may replace angiography in the future but US, because of its low cost, should continue to be the most utilized screening tool for PVD.

Presently, PVD is grossly categorized by the morphological importance of a stenosis, reflecting the imprecision of the diagnostic techniques and the difficulty in interpreting the hemodynamic measurements. Though it is the hemodynamic

consequences of a stenosis which are of interest, which hemodynamic criteria best reflect the importance of a stenosis is difficult to determine, especially in the context of serial stenoses located on either a single arterial segment or on multiple segments.

1.4.1 Imaging

Angiography (see Figure 4, page 10) was first used in 1937[89] for antemortem diagnosis of carotid artery disease. The method became the gold standard to which other approaches to stenosis lumen estimation were compared. However, it is an invasive procedure associated with complications, and bed rest is required after the procedure[98]. Furthermore, if pictured in one plane, it can underestimate the extent of disease and does not provide any information about the functional hemodynamic significance of a lesion[137]. Angiography cannot reliably determine the relative importance of a stenosis unless it is combined with invasive intra-arterial pressure measurements[69]. Therefore, it is no longer a gold standard, and common practice in some vascular units is now to plan intervention based on duplex US imaging alone[98].

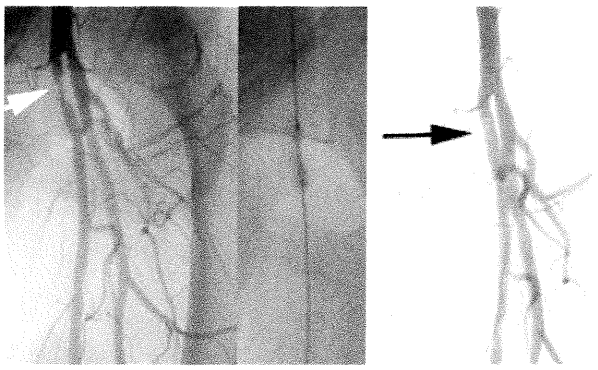

a) b)

Figure 4. An angiogram of a tight stenosis in the superficial femoral artery, a) before and b) after balloon angioplasty (from http//www.westsubcardiology.com/pages/cases/vascular/sfa.htm).

B-mode ultrasound is an imaging modality which provides important information on the presence, severity, and architecture of echogenic stenoses[10], though its most recent use has been to image arterial wall thickness (intimal-medial thickening)[32,100]. However, it does not provide sufficient resolution to accurately

determine the degree of narrowing[138], even though 3D imaging is now possible. Furthermore, any given arterial morphology does not imply the same clinical symptoms, this being more directly related to the global hemodynamic state of the patient.

1.4.2 Doppler Ultrasound Techniques

The current trend for diagnosing PVD is for the method to be noninvasive, so as to create the least discomfort for the patients, and to be non-toxic to allow frequent follow-up examinations. Several Doppler techniques have been investigated including continuous-wave (CW), pulsed-wave (PW), color (velocity and power), the combination of PW with spectral analysis, and duplex (PW and B-mode imaging)[32].

Doppler techniques for diagnosing atherosclerosis are focused on spectral analysis. The Doppler spectrum can provide crucial quantitative hemodynamic information[38,95,97] related to the instantaneous velocity distribution of the blood flowing through the ultrasound beam, reflecting the hemodynamic state in the artery. The nature of this signal is analyzed based on certain criteria, and the severity of the disease inferred based on these criteria. Therefore, the accuracy of the diagnosis is closely related to the correctness of the clinical index, and is limited by the quality of the ultrasound equipment, the ultrasound technique employed, the experience of the technician, and the complexity of the flow phenomenon. However, before being able to interpret the readings and choose an appropriate index, the general flow characteristics in the presence of a stenosis must be understood and is briefly discussed.

The flow field in the region of a moderately severe axi-symmetric stenosis can be qualitatively described by dividing the distal region into four zones[96,97]. Just beyond the stenosis, a stable jet and a well-defined flow separation zone are present. Further downstream, the vortices generated within the shear layer of the jet begin to break down, and the flow exhibits a transition to turbulence. Distal to this region, fully turbulent flow develops, followed by relaminarization where the velocity profile begins to return to the pre-stenotic state. The properties of these zones depend on the Reynolds number ($Re = \rho DU/\mu$, where ρ is the fluid density, D is the arterial diameter, U is the average spatial velocity, and μ is the fluid viscosity) and on the precise stenosis

geometry[10]. That is, a Reynolds number as low as 200 may create turbulence downstream to a severe stenosis (90% area reduction)[140]. Therefore, depending on the measurement position chosen, the accuracy of Doppler US may be impaired due to different flow phenomena.

The first study using duplex in the peripheral arterial circulation was published in 1985[65]. Initially, the validity of Doppler ultrasound was determined by comparing stenosis severity obtained by Doppler with angiography in the carotid arteries of the same patients[21]. As diagnostic challenges are similar in the carotid and femoral arteries, the outcome of such studies is discussed. The sensitivity and specificity were good for differentiation of angiographically demonstrable carotid stenoses greater than, or less than 50% diameter reduction. However, analysis of Doppler "spectral broadening" [105] permitted more precise quantification of stenoses with division into six rather than 2 categories (0%, 1-15%, 16-49%, 50-79%, 80-99% diameter reduction, and 100% occlusion) that corresponded well with percent stenosis measured by angiography. Spectral broadening is defined by Taylor et al.[127] as a filling in of the systolic "window" under the time-velocity envelope. It may also be defined as a widening of the range of velocities within the Doppler sample volume positioned in the vessel in the presence of disturbed flow. In 1992, Suton-Tyrrell[121] performed studies which provided confidence that the Doppler method accurately identified carotid artery lesions and supported its usefulness for studies relating obstructive disease to clinical outcome[32]. In 1996, Bascom et al.[10] performed an *in vitro* study where pulsed Doppler recordings were made within the artery distal to a 70% area reduction (almost critical) asymmetric stenosis. In the post-stenotic flow field, the variability of the spectrum showed a strong spatial and temporal dependence, due in part to a deviated jet, particularly when small Doppler sample volumes were used to quantify the flow disturbance. Displacement of the sample volume by as little as 1 mm into the separation region could produce remarkably different values for the various Doppler indices. They concluded that the most useful diagnostic parameters were the peak frequency and the grading of the severity of the stenosis from spectral broadening. However, with symmetric stenoses such as in the present study, the deviation in the jet will likely be absent, thereby reducing the variability within the post-stenotic flow field.

Many different measurement techniques have been studied to quantify stenosis severity, yet it is recognized that no single Doppler measurement can accurately quantify the severity of a stenosis because of the complex three-dimensional nature of the post-stenotic flow field[10]. For example, spectral broadening which allowed more precise quantification of stenosis severity is considered to be a subjective diagnostic tool[70] as it can arise not only from the flow field but also from factors that are intrinsic to the measurement system. Furthermore, this intrinsic spectral broadening[9] can have a significant effect on the received pulsed Doppler spectrum when a small sample volume is placed at the center of the vessel[8]. Nonetheless, quantification of pulsed Doppler spectra may still be feasible if the sample volume is appropriately placed[10,71]. That is, reproducible peak velocity measurements were obtained only if the Doppler sample volume was positioned at or very near the throat of the stenosis, where peak velocity is maximum, and at an appropriate radial site that is not necessarily at the center of the vessel[10]. And since a direct relationship exists between the peak Doppler frequency, or peak velocity, and the severity of a stenosis[38,95,97], and that it is the only Doppler measurement related to the severity, many readings should be taken when trying to characterize a flow field[10] to minimize variability.

1.4.3 Duplex in the Peripheral Arteries of the Lower Limbs

The normal pressure relations in the limb as well as the patterns of flow velocity are altered distal to sites of disease. Normally, the arterial velocity patterns in the lower limb at rest have a triphasic shape, i.e., forward flow, reverse flow, and late forward flow during diastole[115] (see Figure 5 (A), page 14). Pressure- and flow-reducing lesions create: (1) an increase in PSV at the site of narrowing, (2) turbulence distal to the lesion, (3) loss of the reverse flow component, and (4) a reduction in PSV distally[116]. For iliac (and femoral) artery stenoses, reverse flow is preserved until the velocity in the stenosis is great enough to cause an appreciable pressure decrease, causing the pressure gradient to favor forward flow throughout the entire cardiac cycle. This loss of reverse flow, though qualitative, may be the most important indicator of hemodynamically important stenoses[69], whereas blood flow velocity determined by duplex is a quantitative indicator which was proven to be accurate in identifying peripheral arterial disease[119].

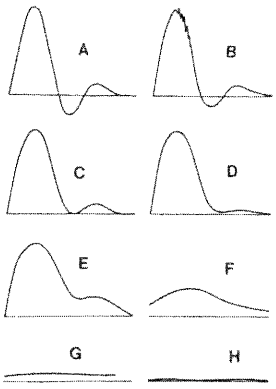

Figure 5. Typical flow velocity waveforms in a peripheral artery with disease progression to total occlusion (H)[94].

At present, a lesion that reduces pressure and flow supply to the lower limbs under resting circumstances is considered "critical" [82]. Although a reduction in arterial size greater or equal to 50% diameter reduction (75% area reduction) is usually required to produce such an effect, less severe lesions may produce symptoms during exercise (increased flow rates) if the flow distal to the stenotic segment is disturbed[22]. In this situation, there is a loss of potential energy, or pressure, that can lead to a flow reduction to the active muscle groups. This is most commonly observed with lesions in the iliac arteries.

Estimation of the degree of stenosis by duplex scanning[65,74] depends on changes in peak systolic velocity that occur from one arterial segment to another[138], that is, the PSV at the site of the arterial stenosis to that at a normal proximal site. This is the most reliable method for determining the degree of arterial narrowing[77]. However, the overall clinical criteria used for classing stenoses are the following: a normal artery shows a triphasic velocity wave form; a minimal wall lesion (1% to 19% diameter reduction) is defined as spectral broadening alone; and a 20% to 49% (diameter) stenosis is indicated by an increase in peak systolic velocity between 30% and 100% from the preceding segment accompanied by reverse flow, even though spectral broadening may be present. A critical stenosis (50% to 99% diameter reduction) is indicated by a 100% increase in

PSV from one segment to the next, although some investigators have found a 150% increase to be more reliable. Finally, no flow indicates total occlusion[116,138].

This ratio of peak systolic velocities is also called the Velocity Ratio (VR) index, and is discussed in greater detail further on in the text. However, certain practical difficulties in obtaining such a ratio are described here. Briefly, the theory of the VR index assumes that the velocity profiles at both measurement positions are the same[73,77,101]. However, it is known that the velocity profile within the throat of a stenosis flattens under steady or pulsatile flow conditions. During the acceleration phase of a pulsatile flow cycle, the velocity profile before the stenosis is flat, little or no change occurs in the shape of the velocity profile at the stenosis, and the mean and maximum velocities increase at the stenosis. The ratio of the mean to maximum velocity also increases at the stenosis, indicating that the velocity profile is flatter. At six diameters distal to the stenosis, the velocity envelope may effectively return to its pre-stenotic value[10]. Because of changes in the velocity profile along stenosed vessels, the VR may be limited in some circumstances[2], though carefully chosen measurement positions may compensate for this difficulty, as is to be verified in this study.

In practice, best diagnostic results are obtained when the arteries of interest are first identified by color Doppler and then spectral analysis is used to quantify the velocity changes across the detected lesion[59,60]. This combination of color Doppler to localize and duplex to quantify the severity of the disease is also referred to as color-coded duplex[77].

1.4.4 Catheter Pressure Measurement

For the hemodynamic assessment of aortoiliac occlusive disease, the "pull through" intra-arterial catheter pressure measurement method is accepted as the best standard, and is considered more objective than other pressure measurement methods. Nevertheless, any pressure drop across a stenotic region is dependent on the velocities in the blood flow, and a significant aortoiliac obstruction may be overlooked if there is outflow impairment caused by the presence of distal disease. The pressure readings using this technique seem to depend on the lateral or axial intraluminal position of the catheter tip. Variable pressure readings may be found at the immediate post-stenotic

region, due to flow induced pressure changes caused by the stenosis and local recirculation, but are absent further downstream.

Pressure recordings taken at the immediate throat only account for the pressure drop at that position and thereby correspond to the energy loss across the tunnel. Though the total effects of a stenosis must include both the post-stenotic phenomena of energy loss occurring across the turbulent region, and the lateral pressure recovery, if it is to assess stenosis significance accurately. Furthermore, if measurements are taken further downstream at the point of relaminarization, the intraluminal position of the catheter, whether axial or lateral, would make little difference in the final reading[137]. Nonetheless, unless the tip of the catheter has its opening at right angles to the stream, the pressure recorded is not accurately the static pressure existing at that point in the blood since some of the flow may enter directly into the catheter opening[18]. The added value to the static pressure may range between $+\frac{1}{2}\ \rho v^2$ (the kinetic energy transformed to pressure if the catheter opening was facing against the flow), where ρ and v are the blood density and the blood velocity, respectively, and $-0.8\ \rho v^2$ (for an opening facing downstream)[86]. Similarly, for static pressure taps used in an *in vitro* model such as in this study, ideally, the tap is placed exactly perpendicular to the streamlines of the fluid (see Figures 6a, or 6b, third case, page 16). No burrs must be created at the opening, since this could induce a local deceleration of the fluid (Figure 6b, first case) and hence a greater pressure than in reality, or a local acceleration of the fluid (Figure 6b, second case) past the opening creating a lower pressure than in reality.

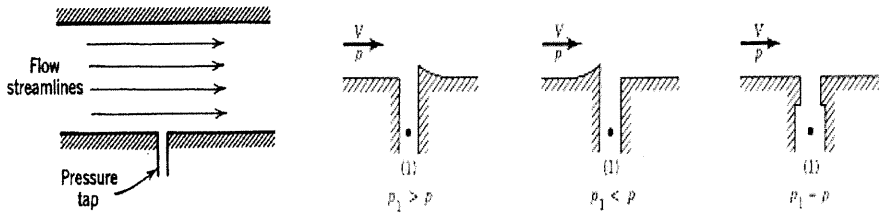

Figure 6. a) Schematic of an ideal wall tap, with flow streamlines perpendicular to the axis of the tap, to measure static pressure within a tube. b) The presence of burrs causes perturbations in the flow streamlines and, hence, the pressure measured is not the static pressure. P_1 is the measured value and P is the actual value of static pressure in the fluid[91].

Clinically, either a peak systolic pressure gradient of 5 mm Hg, or a decrease in femoral artery pressure of more than 15% with reactive hyperaemia[14], or a gradient of 10 mm Hg at rest and of 20 mm Hg after vasodilation[131] is considered significant. A resting systolic gradient of 29 mm Hg is indicative of an iliac stenosis of 50% area reduction or more[5].

The introduction of a catheter in the artery may cause variations in the recorded pressure gradient[86]. Namely, previous work on a femoral artery model suggests that, when a catheter is placed across a stenosis, the true pressure gradient is overestimated in a predictable manner which is dependent on the ratio of the catheter diameter to the stenosis diameter[75], as it reduces the vessel lumen area. In clinical practice, this effect may be sufficient to alter the interventional management of the patient. The optimum method of measuring a pressure gradient involves simultaneous pressure recording from bilateral femoral artery catheters without crossing the stenosis. With the pullback technique, the main disadvantage is that the measurements are sequential rather than simultaneous and cannot compensate for error due to beat to beat variations in blood pressure and transitory pressure changes after vasodilatation. Yet the measurement errors do tend to cancel out when gradients are calculated[86]. Though, with all the measurement uncertainties, it can be useful to find an alternative method of measuring intra-arterial pressures.

1.4.5 Doppler Pressure Measurement

Duplex ultrasound estimation of pressure drop is generally based on the Simplified Bernoulli equation ($\Delta P_{max} = 4*PSV^2$). This technique is commonly used in cardiology to measure pressure drop across heart valves. However, in the case of the peripheral arteries, the flow phenomenon is different and this equation needs appropriate validation.

An initial look at this clinical pressure measurement technique reveals that the pressure gradient measured conventionally is the maximum gradient (Pproximal-Pjet). However, by catheter, it is approximately the minimum gradient measurable (Pproximal-Pdistal). Given that downstream from a stenosis, a certain amount of pressure recovery is expected[140], discrepancies between both measurements will exist,

especially for severely stenosed arteries where the post-stenotic pressure recovery may be more significant[137]. Furthermore, although pressure gradient measurements alone are commonly used in clinical practice, it is important to recognize that, if *in vivo* measurements are made during conditions of low flow, then no significant gradient may be recorded across a potentially important iliac stenosis[86]. As well, angiographers must be aware of the limitations of the technique[86]. A more detailed discussion on these subjects will be considered in the following chapter.

1.5 Clinical Objectives

The goals of clinical therapy are to eliminate ischemic symptoms, and to prevent progression to occlusion and cardiovascular complications[138]. These goals may be reached by planning management strategies and by using the correct imaging techniques. Global efforts are currently being made to reduce the adverse effects of CVD through early diagnosis, more effective treatments and follow-up examinations, and by an improved understanding of the pathological processes. Patients with chronic critical limb ischemia require lifelong follow-up after intervention for rehabilitation, and to assess graft patency. Authorities recommend periodic surveillance with duplex ultrasonography[138,139] to maximize the chance that re-stenosis in such circumstances is identified early, when it is more amenable to repair[12]. The current study will attempt to give further insight into the applications and limitations of duplex ultrasound in the diagnosis of peripheral arterial disease and its associated complex flow phenomena.

CHAPTER 2.
Fluid Dynamics

2.1 Mathematical Models

In general, the characteristics of fluid flow that must be considered are steadiness, rotation, compressibility, and viscosity. In *steady flow*, the fluid velocity at a point is constant in time, which can be achieved at low flow speeds. In unsteady flow, velocities at a point are a function of time, and in turbulent flow, they vary erratically with time and from point to point. In *rotational flow*, angular momentum plays a role, and the flow includes vortex motion, such as whirlpools or eddies, and motion in which the velocity vector varies in the transverse direction, whereas no net angular velocity exists for irrotational flow. A fluid in motion is considered *incompressible* when its density is a constant independent of x, y, z, and t. *Viscosity* in fluid flow is the analog of friction in the motion of solids. It introduces tangential forces between laminae of fluid in relative motion (shear stress) and results in dissipation of mechanical energy. It is dependent on the temperature of the fluid and its constituents[102]. Whole blood has properties which most closely resemble those of a shear thinning fluid (non-Newtonian), where the apparent viscosity decreases with increasing shear rate[91]. However, blood is considered to behave as a Newtonian fluid in large arteries, and otherwise in the distal or peripheral parts of the cardiovascular system[28]. Assuming blood is Newtonian throughout the network may be an oversimplification, especially in areas of flow stasis and recirculation, though is common for modeling purposes. Furthermore, many conclusions may be drawn based on the physiological data obtained at different levels of the arterial system[28] when using such an assumption.

2.1.1 The Continuity Equation

For steady flow in a tube of constant diameter, the velocity streamlines are parallel to the wall. Therefore, the mass flux (dm/dt) at a given point in the tube is ρAV, where ρ is the fluid density, A is the cross sectional area perpendicular to the streamlines, and V is the speed of the fluid. In the absence of "sources" or "sinks" of flow, the mass crossing each section of the tube per unit of time must be the same: ρAV = constant. If the fluid is incompressible, the equation simplifies to: AV = constant, the product of which is the volume flux or flow rate of the fluid. This predicts that, in steady incompressible flow, the speed of flow varies inversely with the cross-sectional area, being larger in narrower parts of the tube. Thereby, widely spaced streamlines indicate regions of low speed, and closely spaced streamlines indicate regions of high speed[102].

The pressure within the fluid represents the internal forces, and the pressure along the artery represents external forces. In a mechanical system, such as an artery, the internal forces and torques cancel one another, leaving only the external forces and torques to contribute to the momentum[102]. A deceleration of a fluid in a horizontal tube can come about from a *difference in pressure* along the artery. Hence, in steady horizontal flow, the pressure is greater where the speed is least[102].

2.1.2 The Bernoulli Equation

Most fluid mechanics models were developed observing fluid flow in a straight tube. The most fundamental model is the Bernoulli equation derived from the basic laws of Newtonian mechanics. It is essentially a statement of the work-energy theorem ($W = \Delta KE$) for fluid flow, stating that *the work* (W) *done by the resultant force acting on a system is equal to the change in kinetic energy* (ΔKE) *of the system (a fluid volume)*. For a non-viscous, steady, incompressible flow, the resultant work is the sum of the pressure force and the force of gravity. By inserting these variables and the change of kinetic energy into the theorem and rearranging the terms, we obtain the general Bernoulli equation:

$$P + \tfrac{1}{2}\rho V^2 + \rho g h = \text{constant.} \qquad (1)$$

The individual components of the equation correspond to the following hemodynamic terms:

$P + \rho gh$ = static pressure, i.e., the pressure measured when $V = 0$ (pressure and gravity terms), and

$\frac{1}{2} \rho V^2$ = dynamic pressure (mass times acceleration),

where V = average velocity, g = acceleration due to gravity, and h = the height of the tube center relative to a reference value.

The assumptions made in deriving this equation are that viscous effects are negligible, the flow is steady and incompressible, and that the equation is applicable along a streamline. Since the fluid is non-viscous (no friction within an ideal fluid), it implies a flat velocity profile and an irrotational flow. As well, the problem is isothermal since the temperature of the fluid cannot be changed by mechanical means if there are no viscous energy losses. In practice, these assumptions are not exactly true. A violation of one or more of these assumptions is a common cause of discrepancies between the "real world" and solutions obtained by use of the Bernoulli equation[91]. Furthermore, errors arise in modeling the physiological system due to the fact that the flow is unlike that in a straight tube and also because living tissues are perpetually evolving causing *in vitro* and *in vivo* experimental results to diverge[28]. Nonetheless, some simple models, such as Bernoulli, may give important insight into the flow phenomena.

The Bernoulli equation may be reorganized and simplified under certain conditions to obtain a pressure drop value. If the tube is horizontal, the change in h is negligible from one point in the tube to the next and so the potential energy (ρgh) of the fluid is ignored. It follows that the pressure drop induced by a reduction in lumen diameter of a horizontal tube may be calculated as:

$$\Delta P = P_1 - P_2 = (\rho /2) (V_2^2 - V_1^2), \qquad (2)$$

where the subscripts 1 and 2 indicate the proximal and distal positions of the measurements, respectively, on either side of the vessel narrowing. For a fluid density of $\rho = 1.06 \times 10^3$ kg/m^3, and for velocity and pressure measurements expressed in m/s

and mmHg (1 mmHg = 133.3 kg/ms^2), respectively, the equation becomes approximately:

$$\Delta P_{MAX} = 4 * (V_{MAX}^2 - V_{PROX}^2), \quad (3)$$

where ΔP_{MAX} is the maximum pressure gradient created by the stenosis, V_{MAX} is the maximum jet velocity, and V_{PROX} is the proximal peak velocity. Assuming that the kinetic energy in the stenotic jet is completely dissipated beyond the stenosis by viscous losses during turbulence, this equation accurately reflects the maximal pressure gradient[69]. In fact, it assumes that all of the kinetic energy of flow in the stenosis is converted to heat rather than to static pressure in the post stenotic region, accounting for the pressure decrease across the stenosis[93]. This implies that the static pressure is unrecoverable post-stenotically. In reality, however, some of the static pressure is recovered post-stenotically, though some is converted to heat (see Figure 7, page 22).

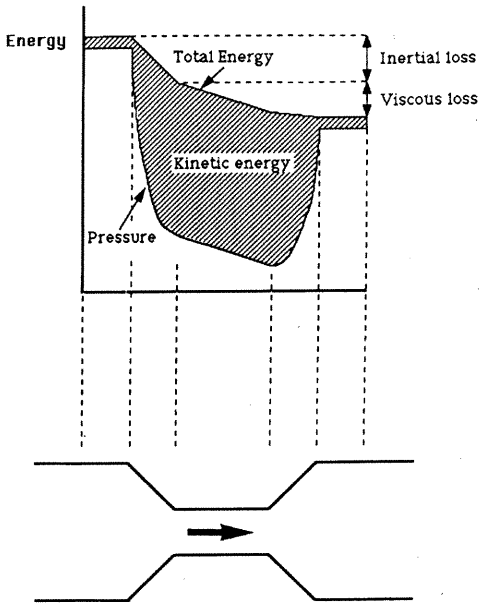

Figure 7. Viscous and inertial energy losses in a stenosis with laminar flow. The amount of inertial loss depends on the geometry of the narrowing[91].

Applied to cardiac valve stenoses, the calculation of the pressure drop is again simplified to the following form known as the Simplified Bernoulli equation:

$$\Delta P = 4V_{MAX}^2. \quad (4)$$

The additional assumption ignores kinetic energy proximal to the stenosis relative to that within the stenosis. This approach works well for stenotic cardiac valves, whose sudden area expansion encourages viscous energy losses, and may be useful for some short, severe peripheral stenoses that are associated with relatively high Reynolds numbers (Re > 500, when viscous forces are negligible). However, for mild stenoses in the peripheral arteries, the Bernoulli equations may overestimate pressure gradients because the kinetic energy may not be converted to heat by viscous losses during turbulence, but rather the kinetic energy in the stenotic jet is converted back into pressure beyond the stenosis (pressure recovery). The expression may underestimate gradients for lengthy, irregular, and very tight peripheral artery stenoses where viscous energy losses dominate[69].

In a clinical study by Kohler et al.[69], the pressure gradients calculated using the Simplified Bernoulli equation did not correlate well with measured catheter values in human iliac arteries. They found that a significant pressure drop between positions proximal and distal to a stenosis did not develop, during peak systole, until a stenosis of 60% diameter reduction (84% area reduction) was reached. As the lumen narrowed further, the pressure gradient increased rapidly. The gradients were consistently overestimated for mild stenoses having pressure drops inferior to 20 mmHg, and the variability was great. The absence of reverse flow in diastole at the site of the stenosis or a resting pressure gradient of greater than 15 mm Hg were more reliable indicators of a hemodynamically significant stenosis[69].

In vitro, Ahmed and Giddens[1] studied axi-symmetric stenoses under pulsatile flow at a physiological Reynolds number (600) and found turbulence only with stenoses greater than 75% area reduction (50% diameter reduction). Similarly, Thiele et al.[129] found increased velocities *in vivo* in mild stenoses, but no pressure gradient. In fact, pressure gradients are generally not observed until stenoses exceed 75% of the lumen area, the point at which turbulence causes energy dissipation. Below this level, the increased velocity causes the Bernoulli equation to predict a pressure gradient when none exists[69].

2.1.3 Poiseuille Flow

In steady state flow of a viscous fluid within a rigid uniform diameter tube, the velocity profile depends on its distance from the entrance region. As the fluid travels along the tube, the velocity profile will change as shear occurs between the fluid and the wall, and between the various laminae of fluid. This phenomenon is described by the *Boundary Layer Theory*, and the thickness of fluid affected by the shearing forces is known as the boundary layer. The theory states that, for steady flow, the boundary layer thickness is equal to the radius of the tube at a distance from the entrance of $X = 0.06\, d * Re$ for laminar flow, and $X = 4.4\, d * (Re)^{1/6}$ for turbulent flow[91], where d is the tube diameter and Re is the Reynolds number (see Figure 8, page 24). At this point, the velocity profile is considered "fully developed" since it will remain unchanged unless an additional factor comes into play. This is also known as Poiseuille flow, which assumes a parabolic velocity profile.

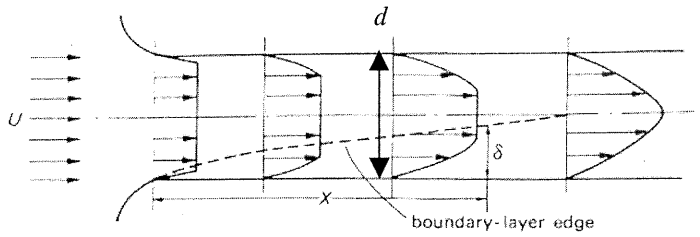

Figure 8. Progression of a boundary layer in the entrance region of a tube into fully-developed flow.

Poiseuille's model is empirical and states that the pressure drop (ΔP) through a pipe is directly proportional to the rate of flow (Q), to the viscosity (μ), and to the length of the pipe (L) and is inversely proportional to the fourth power of the radius (R):

$$\Delta P = Q\left[\frac{8\mu L}{\pi R^4}\right], \qquad V_{MAX} = \frac{\Delta P R^2}{4\mu L}, \qquad V_{AVG} = V_{MAX}/2, \tag{5}$$

where V_{MAX} is the maximum centerline velocity and V_{AVG} is the spatially averaged velocity. The underlying assumptions are steady, laminar, fully developed flow in a straight, rigid, cylindrical vessel. The fluid is Newtonian and incompressible and at a constant temperature[94]. For a liquid flowing in a cylindrical tube, as in Figure 8, the fully developed flow has a parabolic velocity profile of the form $V(r) = V_{MAX}(1 - r^2/R^2)$,

where r is the radial position from the central axis. However, if the flow through the tube is continuously increased there comes a point when the resistance to flow increases quite sharply and the Poiseuille relation no longer applies. This is when the flow becomes turbulent[102].

Poiseuille's equation, however, is generally not used to study blood flow since it considers energy losses only due to viscous effects, and not due to inertia, and so, is less accurate as the stenosis severity increases. As well, the rheological properties of the fluid must be known and the flow is assumed steady, which is not the case physiologically. However, understanding the Poiseuille equation is fundamental to hemodynamics[94] and some of its underlying concepts are of interest in the current project.

2.1.4 Pressure Loss and Recovery

Biological fluids have a viscosity that is dependent on the shear rate and on the temperature. For a viscous fluid, when there is friction with the vessel wall, vortices will appear, whereas no vorticity exists for a non-viscous fluid. Vortices are transported along the artery and create turbulence downstream. Moreover, an obstacle projecting into a stream, such as a stenosis, will cause eddies to form. Small eddies die away rapidly, however, if the disturbance is large, the eddies will grow in size and ultimately cause a complete breakdown of laminar flow. The size of obstacle which causes laminar flow break-down, represents a fraction of the width of the channel, and depends on the *Re* and to a certain extent on the shape of the obstacle[94]. Therefore, fluid viscosity and obstacle geometry are important factors when studying flow phenomena surrounding a stenosis.

In the human body, a certain amount of energy loss is expected in the presence of flow obstructions. Several investigators have described and characterized these losses and their relationships to pressure gradient and percentage stenosis[13,141]. Energy loss arises from three causes: (a) the viscous turbulent losses, which are strongly dependent on the geometry of the stenosis including the shape, length, and percent stenosis, (b) the nonlinear losses as a result of the convergence and divergence of the blood as it enters and leaves the stenosis, and (c) the losses arising from the inertia of the blood itself[13].

As fluid passes through a slightly stenotic segment the need for kinetic energy increases. Static lateral energy is converted, in part, into kinetic energy, and the rate of flow is maintained. With progressively smaller stenotic lumens, the demand for kinetic energy at some point is surpassed and the rate of flow will decrease. The cross-sectional area beyond which this phenomenon occurs has been termed the "critical" area of stenosis[137]. The stenosis has to be substantial with an area reduction of at least 70% to create a pressure drop[12]. Downstream, pressure recovery is expected since the pressure loss is due both to convective inertial and viscous effects. The major pressure loss and recovery may take place over 10 lumen diameters[140]. A more complex look at the flow behaviour, however, may be obtained using the Navier-Stokes equations, as discussed in the following section.

2.1.5 Navier-Stokes Equations

In general, the governing equations of blood flow are the three-dimensional (*x*, *y* and *z)* Navier-Stokes equations (conservation of momentum) of motion (Eq. 6) combined with the conservation of mass equation (Eq. 7), written here in their general forms, provide a complete mathematical description of the flow of an incompressible Newtonian fluid (viscous flow)[28,91,94]:

Navier-Stokes:
$$\rho\left(\frac{\partial \vec{u}}{\partial t} + \vec{u}\cdot\nabla\vec{u}\right) = -\nabla p + \rho\vec{g} + \mu(\nabla^2\vec{u}) \qquad (6)$$

Conservation of mass:
$$div(\vec{u})=0 \qquad (7)$$

where ρ = constant density, $\vec{u}$ = fluid velocity (3D), p = driving pressure = static pressure + pressure due to gravity (ρgh, negligible if horizontal), g is the gravitational acceleration, and μ is the fluid viscosity.

The Navier-Stokes equations represent the conservation of momentum related to the accelerations and the forces (in 3D) of the fluid. Conservation of mass describes the incompressibility of the fluid. Therefore, there are four equations and four unknowns (three velocities and pressure).

The complexity of the Navier-Stokes equations (non-linear, second order, partial differential equations), however, does not allow exact mathematical solutions. Certain simplifying assumptions yield numerical solutions to the problem, and if the solution converges, it will be more or less accurate based on the assumptions.

In theory or numerically, complex models such as Navier-Stokes are typically used in describing and in trying to understand the complex nature of the flow *in vivo*. However, their practical application is difficult, and they are indeterminate and must be resolved numerically. The simpler mathematical models applied to blood dynamics such as Bernoulli or Poiseuille are not realistic, however, useful information may be obtained from their use, leading to a situation which is currently difficult to resolve. The current models are limited from the beginning since cardiovascular disease and the complexity of the fluid phenomena is not fully understood[42]. Furthermore, in order to study a given rigid arterial segment, these equations must be coupled to boundary conditions, a phenomena which is not yet fully defined. However, two types of boundary conditions are identified: parietal (wall) conditions describing the level of friction at the wall (slip or no slip) or the extent of wall deformation due to the transmural pressure, and extremity or end conditions, describing the difference in driving pressures from one end of the arterial segment to the other[28]. Errors made in estimating such conditions may further reduce the accuracy of the solution.

Considerable efforts have been made to understand the fluid mechanics of the flow through a stenotic tube[36,47,48,72,109,140]. In the majority of these analytical studies, the blood was treated as a Newtonian fluid whereas several researchers have begun to depart from modeling blood as Newtonian[92,99,111,122,123,124,125]. More specifically, some have begun to model blood as a non-Newtonian fluid using Navier-Stokes and a modified Casson's fluid model. The Casson's model represents the effect of red blood cell aggregation on flow[33]. The approach is, therefore, taken from a numerical analysis perspective, where the governing equations are solved by using the finite element method. Although of high interest, treating the flow of a non-Newtonian fluid was not considered in the present study, though the results of a few such studies are discussed in the following section.

2.1.6 Arterial non-Newtonian Flow in the Presence of Multiple Stenoses

This section deals with the modeling of fluid flow through multiple axi-symmetric and equivalent stenoses with the assumption that the fluid is non-Newtonian, as may be found in a physiological situation.

Young et al.[140] and Fox[50], in the study of velocities created at various Reynold's numbers (20, 50, 100), found that the maximum velocity in the case of a single stenosis occurred at the throat, while for double stenoses it occurred downstream just behind the throats of the stenoses.

Drumel[40] and Tandon[126], both studying double axi-symmetric and identical stenoses in series using a tube model of a coronary artery and a non-Newtonian fluid (Re = 20, 50, 100) found that, from the central line velocity distribution, the peak of the velocity in the diverging section of the distal stenosis was higher as compared to that in the proximal equivalent stenosis. As the Reynold's number increased, the fluid acceleration increased due to the formation of vortices between the two stenoses. In Newtonian fluids, this prevents the retardation of the fluid at the central line. In the same studies, the pressure was found to decrease sharply in the converging section of the proximal stenosis and partially recover in its diverging section. In the converging part of the distal stenosis, the pressure again started decreasing before it could fully recover. Thus, the pressure recovery following the proximal stenosis was hindered by the presence of the distal equivalent stenosis. The flow through the distal stenosis was less accelerated due to a formation of vortices between the two stenoses, leading to lesser energy dissipation by the wall (lower wall shear stress). Consequently, equivalent double stenoses of the same severity produced lower total pressure drop as compared to that produced by a same severity single stenosis. However, the pressure drop across both stenoses combined increased as the interstenotic distance decreased. It also reduced the lengths of the flow reversal zones. Finally, the magnitude of the pressure drop at a point decreased with increasing values of the Reynolds number, which is always higher in the non-Newtonian fluids than in the Newtonian fluids. Accordingly, Caro[19] and Forestrom[46] found that the non-Newtonian character of blood possesses an in-built property which helps lower the wall shear-stresses, thus reducing the flow reversal zones and other ill effects. Moreover, the separation and reattachment points

were observed only in the diverging section of the distal stenosis. Thus, the non-Newtonian effect of blood has the tendency to reduce pressure drop and the lengths of the flow reversal zones[126].

2.1.7 Young's model

An empirical equation describing the hemodynamics of blood flow in arteries has been developed, by Young[140], which may be more accurate since the equation was proposed and validated *in vitro* for steady and pulsatile flow in peripheral arteries. Young's pressure drop measurement across an iliac stenosis takes into account the degree of collateralization, becoming a parameter of hemodynamic significance. Thus, different degrees of collateralization for the same stenosis will modify in different manners the transtenotic jet velocity and the pressure gradients[43]. The equation for the pressure drop across a stenosis of length L_s is the following:

$$\Delta p = \frac{K_v \mu}{D} U + \frac{K_t}{2}\left(\frac{A_0}{A_1} - 1\right)^2 \rho |U| U + K_u \rho L_s \frac{dU}{dt}, \qquad (8)$$

due to viscous effects

due to non-linear effects from convergence/ divergence of flow and turbulence

due to the acceleration of the fluid

where μ is the fluid viscosity, U is the velocity, D is the non-stenosed vessel diameter, A_0 is the non-stenosed cross-sectional area of the artery, A_1 is the minimal cross-sectional area of the stenosis, ρ is the fluid density, and dU/dt is the acceleration of the fluid (see Figure 9, page 30). K_v, the viscous coefficient, and K_t, the turbulence coefficient, depend on the non-dimentional geometric ratios L/D, L_s/D, and d/D (L is the artery length investigated, and d is the diameter within the stenosis), and are obtained by steady-flow tests where pressure drops are measured as a function of Re for a given geometry. K_u is the inertial coefficient which absorbs the added mass effect plus any corrections to the viscous-turbulence terms that are proportional to dU/dt.

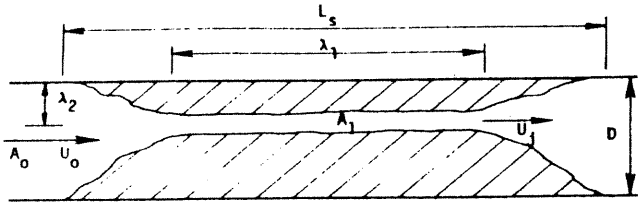

Figure 9. A schematic representation of the defined geometrical variables used to describe a stenosis for Young's model[140], where A_0 is the unobstructed lumen area, A_1 is the minimum cross-sectional area, D is the unobstructed lumen diameter, L_s and λ_1 are stenosis lengths, λ_2 is some measure of eccentricity, and U_0 and U_1 are characteristic velocities at the entrance and exit of the stenosis.

In its dimensionless form (divided by ρU^2), for steady flow conditions (no acceleration term, 3rd term), the equation becomes:

$$\frac{\Delta p}{\rho U^2} = \frac{K_v \mu U}{D\rho U^2} + \frac{K_t}{2\rho U^2}\left(\frac{A_0}{A_1} - 1\right)^2 \rho |U| U = \frac{K_v}{\mathrm{Re}} + \frac{K_t}{2}\left(\frac{A_0}{A_1} - 1\right)^2 . \qquad (9)$$

This equation is obtained by dimensional analysis if it is recognized that at very low *Re*, pressure drop must be linearly related to the velocity (viscous effects dominate), and at high *Re*, pressure drop depends on the square of the velocity (turbulence losses dominate). The equation is thus a linear combination of low and high Reynolds number regimes. In the present study, because of its complexity, Young's model was not considered.

2.1.8 Effect of Stenosis Geometry

May et al.[81] found that the jet velocity used in the Simplified Bernoulli equation is insufficient to estimate pressure gradient since it ignores the effects of stenosis length, roughness, and irregularity, as well as arterial tapering, tortuosity, and branching. Effectively, Kohler et al.[69] found that increasing stenosis length from 1 to 4 cm in a canine iliac artery decreased the flow by 25%, indicating the importance of viscous forces since kinetic energy losses are not influenced by stenosis length[69]. Furthermore, reflection of the pressure wave at the stenosis[69], and vessel compliance, are ignored.

However, Young found that the vessels may be assumed rigid and the arterial taper negligible when considering local flow characteristics[140].

It seems likely that the accurate estimation of pressure gradient in most peripheral arterial stenoses of appreciable length, with significant area reductions and low Reynolds numbers, requires frictional loss equations. Such equations are not likely to be clinically useful, however, because the 3D geometry of the stenosis must be precisely known to apply these adequately[69]. Conversely, another group reported excellent agreement between calculated and measured pressure gradients over a wide range of degrees and lengths of stenosis in an *in vivo* model[43,112]. Their results raised the possibility that the Simplified Bernoulli equation may still be useful in the peripheral circulation[69].

Others also found that for stenoses less than 2 cm long and larger than 0.3 cm in diameter, the frictional loss and flow acceleration are negligibly low relative to the amount of convective acceleration represented by the term $4*V_{MAX}^2$ [58,61,128]. This is also supported by the results of Strauss et al.[118], in which the length of iliac stenoses encountered ranged from 0.3 to 1.7 cm.

2.2 Finite Element Simulations

The governing transport equations for a fluid with a constant viscosity are mathematical representations of the principles of conservation of mass and momentum. The Navier-Stokes equations combined with the continuity equation provide a complete mathematical description of viscous flow for an incompressible fluid (four equations, four unknowns: three velocities, u, and pressure, p). The equations may be represented as follows:

1) The Navier-Stokes (conservation of momentum) equations:

$$\rho\left(\frac{\partial \vec{u}}{\partial t} + \vec{u} \cdot \nabla \vec{u}\right) = -\nabla p + \rho \vec{g} + \mu(\nabla^2 \vec{u}) \qquad (10)$$

where ρ is the fluid density, g is the acceleration due to gravity, μ is the fluid viscosity, *(u. Vu)* is the convective term in the momentum equations;

2) The Continuity Equation (ρ = constant):

$$div(\vec{u}) = 0 \tag{11}$$

The complexity of the Navier-Stokes equations (non-linear, second order, partial differential equations) rarely allows an exact mathematical solution. However, a numerical solution may be found by making certain simplifying assumptions. The solution, if it converges, will be more or less accurate based on the assumptions made for the particular flow in question.

The problem was defined in Fidap 8.0 (Fluent Inc.) as: INCOMPRESSIBLE, STEADY, NON-LINEAR (convective term), NEWTONIAN, AXI-SYMMETRIC, MOMENTUM (momentum and continuity equations solved for velocity and pressure fields), ISOTHERMAL (no temperature dependence), FIXED (geometry of the problem is unchanging), and LAMINAR (laminar flow problem, that is, no divergence term representing turbulence, and the streamlines never cross).

For an axi-symmetric problem defined in the r, z, θ coordinate system (see Figure 10, page 32), there is no dependence of the terms on θ, and the equations solved become:

$$\rho\left(\frac{\partial u_r}{\partial t} + u_r\frac{\partial u_r}{\partial r} + u_z\frac{\partial u_r}{\partial z}\right) = \rho g_r - \frac{\partial p}{\partial r} + \mu\left\{\frac{\partial}{\partial r}\left(\frac{1}{r}\frac{\partial}{\partial r}(ru_r)\right) + \frac{\partial^2 u_r}{\partial z^2}\right\}$$

$$\rho\left(\frac{\partial u_z}{\partial t} + u_r\frac{\partial u_z}{\partial r} + u_z\frac{\partial u_z}{\partial z}\right) = \rho g_z - \frac{\partial p}{\partial z} + \mu\left\{\frac{1}{r}\frac{\partial}{\partial r}\left(r\frac{\partial u_z}{\partial r}\right) + \frac{\partial^2 u_z}{\partial z^2}\right\} \tag{12}$$

$$\frac{1}{r}\frac{\partial}{\partial r}(ru_r) + \frac{\partial}{\partial z}(u_z) = 0$$

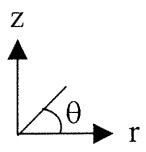

Figure 10. The r, z, θ coordinate system, where r is the radial coordinate of the artery, z is the longitudinal coordinate of the artery, and θ is the counterclockwise angle coordinate of the cross-section of the artery.

2.2.1 Discretization of the Problem

The first step in the finite element (FE) method consists of dividing the continuum problem, with its infinite number of degrees of freedom, into a discrete problem described by a system of algebraic equations having a finite number of degrees of freedom. The FE procedure begins with the division of the continuum region into a number of elements. An Eulerian description is used for setting up the partial differential equations, and so, the elements are assumed to be fixed in space. For each element, the dependent variables (velocity, pressure, etc.) are interpolated by functions of compatible order, in terms of values to be determined at a set of nodal points.

Within each element, the velocity and pressure fields are approximated by:

$$\left.\begin{aligned} u_i(\bar{x},t) &= \varphi^T \mathbf{U}_i(t) \\ p_x(\bar{x},t) &= \psi^T \mathbf{P}_x(t) \end{aligned}\right\} \tag{13}$$

where $\boldsymbol{U}_i$, and $\boldsymbol{P}_x$ are column vectors of element nodal point unknowns, $\bar{x}$ is the spatial coordinate, t is the time, and φ and ψ are column vectors of the interpolation functions. Herein the same interpolation functions are employed for all components of the velocity. Substitution of these approximations into the field equations and boundary conditions yields a set of equations:

Momentum: $$\mathbf{f}_1(\varphi,\psi,\mathbf{U}_i,\mathbf{P}_x) = \mathbf{R}_1 \tag{14}$$

Mass conservation: $$\mathbf{f}_2(\varphi,\mathbf{U}_i) = \mathbf{R}_2 \tag{15}$$

where $\boldsymbol{R}_1$ and $\boldsymbol{R}_2$ are the residuals, or errors, resulting from the use of the approximations of the previous equations. The Galerkin form of the Method of Weighted Residuals seeks to reduce the solution errors to zero, in a weighted sense, by making the residuals orthogonal to the interpolation functions of each element (that is, φ for the velocity, and ψ for the pressure degrees of freedom).

The result is the equation for a single element, and the discrete representation of the entire continuum region of interest is obtained through an assemblage of elements such that inter-element continuity of velocity is enforced. This continuity requirement is

met through the appropriate summation of equations for nodes common to adjacent elements – the direct stiffness approach.

2.2.2 Element and Mesh Definitions

The flow within the vessel was assumed to be symmetric about the z axis (axi-symmetric), therefore, the problem was reduced to two dimensions, independent of θ. Furthermore, only the upper half of the longitudinal cross-section through the axis of the vessel was considered. This section was divided into 4-node quadrilateral finite elements (see Figure 11, page 34). The mesh was refined towards the axis wall (successive ratio = 0.9), and the number of elements were chosen so as to assure convergence of the solution.

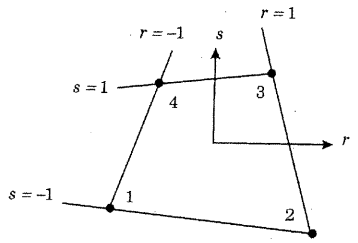

Figure 11. Element definition for the FE simulations in Fidap 8.0. The order of the interpolation functions corresponds to the ordering of the nodes, and the interpolation functions are expressed in terms of the normalized or natural coordinates for the element, r and s, which vary from –1 to +1.

2.2.3 Boundary Conditions and Parameter Calculations

Boundary conditions are required on all boundaries of the computational domain as either specified nodal values or specified fluxes across element sides for each of the active degrees of freedom in the simulation. At a given boundary, only one of these types of conditions may be specified. If none is applied at a boundary node for a degree of freedom, the default boundary condition is zero flux for that degree of freedom. The time derivatives in all the equations (momentum, energy, turbulent kinetic energy, turbulent dissipation, and species) are discarded. The velocity degree of freedom is associated with the nodal points and is approximated using bilinear interpolation functions. The pressure degree of freedom, when using a segregated solver such as successive substitution, uses a piecewise constant discontinuous, linear pressure approximation by default. The pressures are associated with the element centroid,

however, the pressure solution at all the nodes in the mesh is interpolated (in FIPOST or post-processing) for plotting purposes. No initial conditions are required in steady flow.

2.2.4 Solution Method

The Galerkin solution approach was applied to the stationary Navier-Stokes equations, resulting in a group of non-linear algebraic equations represented in matrix form as follows:

$$\mathbf{K(u)u = F} \tag{16}$$

where $\boldsymbol{K}$ is the global matrix of equations, $\boldsymbol{u}$ is the global matrix of unknowns (velocity, pressure, etc.), and $\boldsymbol{F}$ is a vector including the effects of the boundary conditions. The coefficient matrix $\boldsymbol{K(u)}$ has a scattered bandwidth which, for steady flow simulations, is decomposed into: $\mathbf{K(u)} = \mathbf{K}_c\mathbf{(u)} + \mathbf{K}_d$, where $\boldsymbol{K_c(u)}$ is the non-symmetrical convection matrix, and $\boldsymbol{K_d}$ is the symmetric matrix containing the diffusion, pressure, and continuity terms.

The convective term is very important for $Re \gg 1$, as in this study, where the non-linear character of the equations is dominant, and the choice of the solution algorithm becomes key to obtain convergence. The problem was solved in a fully coupled fashion, that is, where the conservation equations are solved simultaneously for relatively simple 2D problems. The non-linearity of the equations requires an iterative solution method, therefore, Successive Substitution was used owing to its robustness (large radius of convergence) and the relatively simple geometry of the flow region. A relaxation factor of 0.5 was used to improve the rate of convergence of the iterative procedure for the solution. When used, a value of 0.5 is usually chosen by default since no general rules apply in such a choice.

In FE computations of incompressible flows, there are two main sources of potential numerical instabilities associated with the Galerkin formulation of the problem. One is due to the presence of the advection terms, which can result in spurious node-to-node oscillations primarily in the velocity field. The other arises if an inappropriate combination of interpolation functions is used for the velocity and pressure. This instability usually appears as oscillations primarily in the pressure field.

Both of these instabilities can be stabilized by the addition of two extra terms to the standard Galerkin formulation of the problem. Pressure stabilization was not performed as it tends to only produce more stable solutions in cases where the computational grid is predominantly made up of linear triangles (2D). However, it is preferable and strongly recommended to adhere to a well established practice of using pressure interpolation functions one order lower than those used for velocities, because the results obtained in this manner are superior in quality to those obtained using pressure stabilization. The pressure degree of freedom is reduced in most situations upon specification of the element type.

2.3 Ultrasound in Medicine

Ultrasound in medicine originated in Scotland towards the 1950s, Ian Donald being the main figure involved[85]. Applications were mainly in obstetrics and gynecology where differences in the signals obtained from solid and simple cystic tissues were found. He discovered that the higher the signal frequency of ultrasound, the less the penetration in the tissues, and also the effect of tissue density on reverberation. Human safety in the presence of diagnostic ultrasound was verified and no damage to tissues was found[85].

During the 1950s, developments in ultrasound were also in progress in Japan (Wagai), Australia (Kossoff), and the United States (Holmes). In the 1960s, there was an explosion of technological advancement in obstetric ultrasound which was then applied to the study of blood flow measurement. Marked contributions to the development of Doppler ultrasound technology applied to blood flow were made by Satomura, in Japan, in 1957 for blood flow measurement, and by Pourcelot, in France, in 1988 (since 1960) for a Doppler cardiovascular surveillance system for astronauts in space[85].

2.3.1 Physical Principles of Ultrasound

Diagnostic ultrasonics uses frequencies, for transcutaneous applications, in the range of 2 MHz (deep abdominal and obstetric studies) to 10 MHz (peripheral vascular studies)[127]. For endovascular applications, common frequencies for ultrasound catheters

are between 10 MHz and 30 MHz [78]. The sound waves are generated by a transducer generally composed of piezoelectric elements that convert electrical energy (fluctuating voltage) to acoustical energy (vibrations), and vice-versa to capture the reflected signal[83]. The pressure waves propagate in human tissues with a local compression and stretching of the tissues. Frequency dependent phenomena occur such as absorption and scattering, and both reflection and scattering provide information used in Doppler and imaging techniques, respectively.

A difference in tissue impedance at surface interfaces or at small wave diffusers (red blood cells) permits reflection or scattering of a part of the incident wave to the transducer. The magnitude of this difference determines the size of the echo, therefore, a water bath or specialized gel is used in clinical practice to allow the ultrasound to propagate from the transducer to the tissues and, consequently, to minimize intensity loss[83].

A focus of the transmission-reception beam is produced electronically in some transducers which gives the ability to increase structural details in the ultrasonic image, or to increase the resolution. This is produced, using multi-element transducers, by phasing the transmission of the ultrasound, exciting the outer elements ahead of the inner ones. The position of the focus is changed by altering the delays of the signals. The reception zone is also focused and the greatest sensitivity of detection is at the focus. Furthermore, a fundamental fact is that the higher the transducer frequency, the better the resolution, however, attenuation in tissue increases with frequency. The temporal resolution, i.e. the separation of events in time, depends on the frame rate of the scanner[83]. It is determined by the time required to process and display the received ultrasound signal by the instrument.

2.3.2 Doppler Effect

Echoes received from moving structures experience a slight alteration in frequency. This concept allows blood flow to be identified and provides information about the velocities of the red cells, therefore, Doppler instruments essentially measure velocity[83].

For an arrangement of blood particles flowing along a tube at a uniform speed, u, if a continuous beam of ultrasound at a frequency, f_1, intersects the flow at an angle θ

(see Figure 12, page 38), some of the energy is scattered in all directions by the moving blood cells. The ultrasound sent back toward the transmitter has a shifted frequency, f_2. The difference in the frequencies, or the Doppler shift (f_D) (Eq.17), is negative ($f_1 > f_2$) for an object moving away from the transducer (source), and positive ($f_2 > f_1$) for an object moving towards the transducer. The Doppler shift is small and in the audible range, and the greater the frequency of sound, the higher the pitch heard. High-pitched components are related to high flow speeds, and signals of high intensity correspond to strong echoes.

$$\text{Doppler shift } (f_D) = f_1 - f_2 = f_1 \frac{2u \cos\theta}{c}, \qquad (17)$$

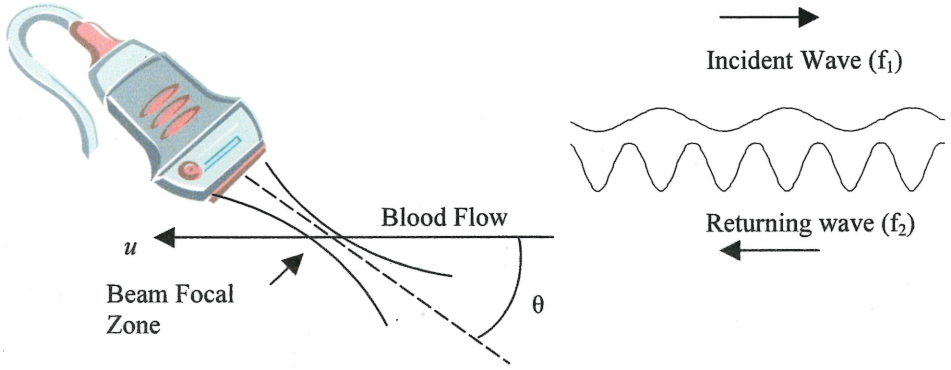

Figure 12. The Doppler shift on an incident ultrasound wave pointed towards flowing blood.

However, it must be kept in mind that:

1) The Doppler shift depends on the component of the velocity along the ultrasonic beam (u*cosθ). If the actual blood velocity has components that are not parallel to the artery, errors will be made in estimating the velocities.

2) In practice, in a volume of interest (the sample volume of the ultrasound instrument), the cells move with many velocities each giving rise to a Doppler shift. The output is then a spectrum whose width depends on the flow characteristics such as the velocity profile and turbulence[83]. This phenomenon is related to the Doppler spectral broadening effect mentioned earlier and used as diagnostic criteria for vascular disease.

3) The velocity of ultrasound in blood is 1570 m/s, and is 1540 m/s in soft tissues, causing underestimation errors in the flow speed of up to 5% because most ultrasound instruments use a sound velocity of 1540 m/s in the computation of the Doppler shift[42].

Echoes produced by scattering are much weaker than those generated by reflection[83]. Scattering, however, provides echo data from rough surfaces and blood particles. The signal from blood is determined by the non-uniform distribution of the cells creating scattering centers which fluctuate in position. Hematocrit (volume of red blood cells/volume of whole blood), normally ranges between 40% to 45% in humans, and rouleau formation of the red blood cells in patients with cardiovascular diseases may modify the nature of the signal back-scattered to the transducer[26].

2.3.3 Ultrasound Modalities

Ultrasound techniques are noninvasive, viewed in real-time, repeatable, non-toxic, and inexpensive compared to other radiological imaging techniques. Moreover, the systems are portable and relatively easy to manipulate[85]. In B-mode, representations of anatomic sections are viewed in two dimensions. To create such images, the ultrasonic beam sweeps a plane section through the body. A one-dimensional signal (A-mode) is sent in the tissues and part is reflected at each tissue interface towards the transducer. The detected echo intensities are represented as grey-levels which are transferred to a pixel on the screen. Sweeping the ultrasonic beam allows many lines of echoes to be obtained which combine to delineate the internal structures of the body[83]. The image acquisition process is very fast and allows an image renewal rate (frame rate) in the order of 5 to 70 images/s or more, depending on the line density and the size of the area being investigated.

Pulsed-Wave (PW) Doppler is based on the Doppler effect and, to the advantage of Continuous-Wave (CW) Doppler, allows the analysis of a small region of particles within the ultrasound beam. In CW Doppler, the beam field is fully investigated, making a measurement at a precise vessel difficult due to dynamically moving surfaces and neighboring vessels. In PW Doppler, a non-harmonic pulsed voltage is sent to the transducer typically in a series of eight cycles at a time (train of pulses). Each cycle has

the characteristic frequency of the transducer and a certain number of trains are sent per second (Pulse-Repetition-Frequency or PRF). The reflected signal is listened to between each train, the time waited for the transmission of the signal into the tissues allowing the sampling depth to be adjusted (range gating)[83].

Variations in blood velocity with time are viewed at various positions within a vessel by moving and varying the size of the range-gate, or sample-volume[67]. Only the sampled frequencies are viewed at a given moment, and the velocities are calculated from the shift in position of the diffusers (red blood cells)[83] by Fourier transformation of the received demodulated Doppler signal.

Duplex Doppler (see Figure 13, page 40) combines B-mode imaging and PW Doppler. The advent of array transducers allowed the division of acquisition time between the two techniques. The images are superimposed, the B-mode image of the vessel serving as a guide to position the PW sample-volume within the artery. This technique rendered noninvasive diagnosis a clinical reality[88] though its spatial resolution is limited and other problems are associated with the technique[52].

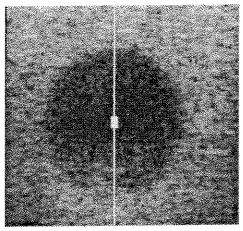

Figure 13. a) A duplex cross-sectional image as seen on screen with the B-mode image in the background. The PW Doppler sample volume is placed within the vessel at the position of maximum velocity, for this example.

Color Doppler systems (see Figure 14, page 41) are an extension of the duplex concept, however, multiple range-gates are used and a color image is superimposed on the B-mode image. The average velocity in each range-gate is estimated, and this value is represented on screen by the color intensity, the actual color palette indicating the flow direction. Red (warm colors) generally represent blood traveling towards the transducer and blue (cold colors) represent blood moving away from the transducer[67]. Green may be used to represent turbulence based on the variance of the velocity signal.

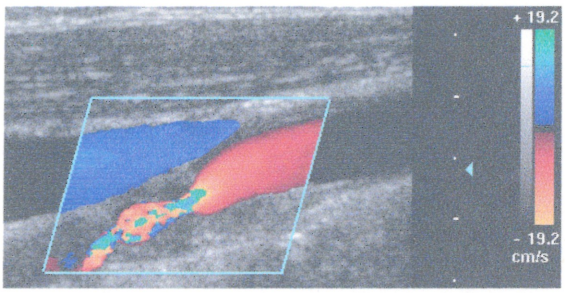

Figure 14. A color duplex image of the carotid artery along the longitudinal axis of the vessel. (from http//www.atl.com/ref_lib/imglib/vascular/vascular.html.)

Color Doppler imaging is a widely accepted tool for assessing the presence of blood flow and it works well for many clinical applications. However, it remains largely qualitative as analyzing the approximate color brightness and the layout takes precedence over quantifying the precise spatial dependence of velocities. If quantitative analysis is needed, duplex PW Doppler must be used[113].

2.3.4 Image Processing and Parameter Selection on the Ultrasound Instrument

Image processing is used to display the imaging signals received from the structures and the Doppler signals scattered by the blood. It is aimed typically at reducing speckle noise to improve the detection of small contrast changes or to sharpen the edges in an image.

The quality of an image depends on the equipment used and the adjustment of many controls on the ultrasound instrument. First, the appropriate transducer must be chosen as lower frequencies increase the penetration in the tissues, although the details in the image decrease. A general working rule is to use the highest frequency for the necessary penetration, and to only reduce frequency when gain and intensity controls are at their maximum. Next, the Doppler angle must be chosen, keeping in mind that blood flow measurement error increases with angle. Finally, the mode of operation (ex. B-mode, color, or duplex) of the machine must be determined. Other modes of operation not discussed here are the M-mode, power mode, harmonic mode, and pulse inversion mode.

Parameters to be adjusted during an examination are transmitted output power or intensity which affect the magnitude of echo, and the overall gain, since echoes received

are small (μV and mV) and amplification is necessary. When amplifier gain is too high, the displayed image is uninterpretable as large echoes saturate the image and small echoes are overemphasized. Conversely, too low a gain may result in very few echoes being displayed. The Time-Gain Compensation (TGC) corrects for attenuation as depth increases, since echoes received from superficial structures are much stronger than those from deep interfaces[83]. Persistence in color velocity mode (averaging of the signal over several frames) is very useful if a signal is almost obscured by noise, as clinical measurements often have a low signal-to-noise ratio.

During blood flow measurements by Doppler, estimation of the Doppler angle and the vessel diameter are essential since they are the main sources of error, though errors also arise in sampling the flow velocities. Vessel diameter is usually measured using electronic calipers on the B-mode image, resulting in possibly large flow rate measurement errors. Accordingly, the average velocity may be evaluated more accurately than the flow rate[42,67]. The Doppler angle is also normally measured in B-mode by aligning a cursor along the vessel axis in a longitudinal scan plane, and the angle value is indicated on the monitor. The accuracy becomes critical as the angle approaches 90°, when the cosine function varies rapidly. To limit this source of error, the insonation angle is normally kept below 60°, and preferably below 45° [42]. However, a precise measurement is often difficult due to factors such as anatomy, inadequate image resolution, depth, and the fact that high velocity jets are often not axially oriented[69]. The assumption that the blood stream is moving parallel to the vessel axis is thus a limitation of the procedure used to estimate the Doppler angle.

Aliasing, abnormal spots on the color image of the vessel or wrapping of the PW Doppler sonogram, is obtained when the Nyquist limit (one half the PRF) is exceeded[127]. Said otherwise, it is a phenomenon that occurs when the range of frequencies or velocities being looked at is smaller than that present in the flow. This is explained from the following relationship:

$$v_{\max} = \frac{c}{2 f_1 \cos(\theta)} \frac{PRF}{2}, \qquad (18)$$

where v_{max} is the maximum velocity able to be detected without aliasing, c is the speed of sound in the tissue, PRF is the pulse-repetition frequency selected on the instrument, f_1 is the transducer frequency, and θ is the Doppler angle. The velocity range displayed automatically affects the maximum possible PRF allowed. On a pulsed Doppler reading, velocity peaks that should go beyond the maximum defined velocity appear on the negative side of the spectrum (wrapping effect). To avoid aliasing, a large velocity range must be used to verify the coherence of the results, and then the maximum velocity measurable may be reduced. However, it must be kept in mind that a large velocity range is associated with a high PRF, and thus, a small depth of measurement within the tissue.

The wall filter is a variable threshold high-pass filter that removes low frequency Doppler signals from slowly moving structures such as the vessel walls. The cutoff frequency for peripheral vascular applications is normally selected around 200 Hz for a transmitted frequency around 5-7 MHz, but it may be adjusted on most instruments, from 40-1000 Hz. In general, it should be left at a low level since small frequency echoes often contain valuable information[127]. In some situations, however, it should be increased in frequency to remove phenomena such as "flash artifacts" that hide important flow information.

In PW Doppler, as briefly mentioned above, the distance within the tissue of the sample volume is limited by the PRF as follows: $d \leq d_{\max} = \frac{c}{2PRF}$, where d is the distance of the sample volume, and d_{max} is the largest allowable distance. The size of the sample volume can also be adjusted. A large size is chosen to locate desired signals, and shorter sizes are chosen to exclude unwanted contributions from the signal[127]. If the sample size is small, the frequency spectrum becomes perturbed due to statistical fluctuations (isolated spots on the sonogram). Therefore, an appropriate size must be chosen as a compromise between spatial accuracy and statistical validity. When attention is brought to the measurement parameters mentioned in this section, the chances of obtaining reasonable measurements are improved.

2.3.5 Clinical Applications for the Lower Limb Arteries

The clinical goal of Doppler ultrasound systems is to view blood flow (velocity profiles, pulsatility, and blood perfusion) noninvasively, and in real-time for the diagnosis[67]. In itself, however, the ultrasound diagnosis is generally based on a clinical index instead of a visual interpretation of the displayed image or spectrum (PSV, VR, Pulsatility index, Spectral Broadening index, Resistance index, etc.)[88]. Typically, the Doppler signal is analyzed and an instantaneous spectrum of frequencies is obtained. The spectrum corresponds to a histogram of velocities within the sample volume. This histogram is often coded in grey-level and juxtaposed in time to create a sonogram (frequencies as a function of time). The maximum frequency sampled, for example, at the greatest lumen area reduction of a stenosis, is proportional to the maximum velocity and is related to the stenosis severity. The mean frequency is proportional to the mean velocity and is related to the flow rate in the sample volume[88]. If the ultrasound beam insonates the vessel with a uniform power, the mean velocity is then a measure of the mean flow rate.

Studies have shown that only PSV is related to the severity of a stenosis[71], and furthermore, the PSV is the most accurate parameter in evaluating carotid artery stenoses $\geq 70\%$ [63]. However, as blood flow increases, the severity is increasingly overestimated with this parameter[132]. Nevertheless, in a clinical situation, the flow is of greater interest than the velocity. The simplest way to obtain the best flow measurement accuracy (assuming uniform insonification of the vessel and a parabolic velocity profile) is to measure the flow rate by duplex and to determine the Doppler angle and vessel diameter on the monitor. This method is at least as accurate as angiography in evaluating carotid artery stenoses[70], is accurate in identifying stenoses $\geq 60\%$ [20] or $\geq 70\%$ [62]. If quality of insonification is assured to minimize measurement variability[6,30], duplex is reliable for vessels with diameters of 4-8 mm (medium-sized vessels)[67]. Finally, quantifying the PW spectrum is reliable if the sample volume is large and positioned at or near the maximum area reduction of the lumen and at an appropriate radial position[71].

Although certain parameters are preferred, no single Doppler measurement can accurately quantify the severity of a stenosis. Bascom et al.[10] found that one of the only noninvasive techniques able to discriminate between the major stages of stenosis

severity was duplex combined with spectral broadening. However, spectral broadening is influenced by the size of the sample volume, the variations in the characteristics of the flow velocities within the cardiac cycle, certain transducer characteristics, the spectral analyzer, and the velocity profile[8,11,27]. Moreover, the quantification of a stenosis based on spectral broadening is subjective[70]. In light of such arguments, it is of interest to further investigate additional parameters and to evaluate the accuracy of the current parameters under probable physiological conditions. Therefore, the following section will discuss the pressure gradient parameter in the lower limb arteries and will refer to the few studies found in the literature.

2.3.6 Estimation of the Pressure Gradients with Ultrasound

In terms of hemodynamic assessments of stenosis severity based on measuring the pressure gradient, *in vivo* studies have been conducted comparing duplex, color duplex, and catheter measurements. Doppler maximum pressure gradients (mmHg) are obtained by blindly measuring the PSV (m/s) within the arterial constriction or in the jet of the stenosis and inserting this value into the Simplified Bernoulli equation ($\Delta P_{max} = 4*PSV^2$). Doppler mean pressure gradients are determined by subjecting the flow velocity profile to planimetry and by applying the Simplified Bernoulli equation point by point to calculate the maximum instantaneous gradients at each point, and averaging them over a whole cardiac cycle. Table I (page 46) shows a summary of some of the findings.

Conversely, *in vitro*, experiments were performed by Weber et al.[137] on a square model stenosis in a tube having an inner diameter (D) of 10 mm (iliac size). Stenosis severities investigated were 64%, 84%, 91%, and 96% area reduction. The blood hematocrit varied between 25 to 60% and pulsatile flow rates ranged from 300 to 2000 mL/min. Lateral (wall tap) and axial (endhole catheter) pressures were measured at four positions; P1 situated 1D pre-stenotically, and P2, P3, P4 situated post-stenotically at 1D, 4D, and 40D, respectively. A plot comparing manometric and Doppler pressure gradients, for all stenoses, flow rates, and hematocrits, showed that the mean pressure gradients between the two methods correlated better than peak pressure gradients. The

Study Type/ Reference	Stenosis model	Mean duplex ΔP (mmHg)	Mean Catheter ΔP (mmHg)	Correlation	Maximum duplex ΔP (mmHg)	Maximum Catheter ΔP (mmHg)	Correlation	Peak to Peak duplex (mmHg)
in vivo /Strauss (1993a)	1) Duplex: Single short (<20mm) common or external iliac stenosis	3-36 (mean = 14±7)	2-31 (mean = 16±7)	r = 0.84	15-114 (mean = 52±21)	10-87 (mean = 53±16)	r = 0.86	-
	2) Color duplex: Single short (<20mm) common or external iliac stenosis	0-35 (mean =17)	0-43 (mean = 18)	r = 0.86	10-104 (mean = 61)	12-95 (mean = 56)	r = 0.83	-
in vivo /Strauss (1993b)	Duplex: Single short (<20mm) common or external iliac stenosis	5-36 (mean= 14±7)	4-31 (mean = 16±7)	r = 0.77	22-114 (mean = 53 ± 21)	25-85 (mean = 54±17)	r = 0.80	13-73 (mean = 46±18)

Table I. Mean and maximum pressure gradients across a single stenosis in the common or external iliac arteries of patients, as measured by color duplex and by catheter. The flow rates across the stenoses were physiological[117,118].

Doppler mean gradients were 13% higher than the corresponding catheter mean gradients, whereas the Doppler instantaneous peak gradients exceeded the catheter peak-to-peak gradient by 10% to 150%. In the 84% stenosis model, lateral pressure dropped 60% but axial pressure dropped only 10% across the obstruction. Furthermore, the peak pressure gradient represented only maximum instantaneous measurements within the flow cycle, whereas mean pressure gradients yielded information over the entire stroke cycle. The Doppler mean gradient probably accurately reflects the manometric mean pressure gradient, however, it does not take into account the pressure recovery that occurs in the relaminarized flow region[137].

Pressures measured further downstream showed that most of the high kinetic energy at the throat was lost as flow passed through the turbulent region, but some of it was transformed back into lateral pressure energy by 4D downstream. With relaminarization, lateral and axial pressures again became relatively equal, as they were pre-stenotically[137].

The overestimation of the peak pressure gradient by Doppler method is due to the fact that Doppler measures an instantaneous peak gradient that is both different and higher than the manometric peak-to-peak gradient. Doppler spectral broadening can also affect the measurement because it produces an overestimation of the PSV. Furthermore, the peak-to-peak gradient can not be measured by Doppler since the peak systolic pre-stenotic and post-stenotic pressures occur at different times and at different places. As a result of the simplicity of the measurements, the Doppler instantaneous peak gradient is widely used for hemodynamic examinations, although it is not a sound application of hydraulic principles. The pressure gradient measurements that include post-stenotic energy changes assess significance of stenosis better than those pressure gradients across the tunnel only[137].

The duplex scan can be used to quantify reliably and noninvasively the hemodynamic significance of iliac artery stenoses in patients with peripheral artery occlusive disease. Although the peak-to-peak catheter pressure gradient is easily obtained and commonly used in catheterization laboratories, it cannot be equated with the maximum instantaneous pressure gradient determined by duplex scanning or catheter, as the peak systolic pre- and post-stenotic pressures are asynchronous. The

peak-to-peak catheter gradient across iliac stenoses can be estimated only approximately from the maximum duplex-derived gradient using regression equations, the former being significantly lower than the latter. Hemodynamically, the mean pressure gradient is a better expression of the severity of a stenosis in the peripheral circulation, as it considers the pressure drop in diastole as well, having direct impact on the driving pressure distal to the stenosis[120,137].

The static pressures in the vessel model for the present study were obtained from pressure taps along the SOI. Since the experiments were conducted under steady flow conditions and that all tap positions were measured simultaneously, the difference in the pressures were approximately equal to the instantaneous mean pressure gradients across the SOI. These gradients will be compared in the Discussion to those found *in vivo* in the various experiments previously mentioned, though the experimental conditions are not necessarily equivalent.

CHAPTER 3.
Materials and Methods

3.1 Purpose, Problem, and Scope

The manifestation of PVD in patients indicates the presence of coexistant disease in other vascular beds, namely cerebrovascular and coronary artery disease [d]. The relative predictive power of PVD for further ischemic events, however, is not well recognized. Patients with PVD that may be at significant cardiovascular risk yet appear asymptomatic from this perspective. Thus, patients with PVD receive less intense medical therapies to prevent cardiovascular ischemic events. However, based on the CAPRIE database, PVD may delineate a population of individuals with a markedly increased risk of ischemic events. Furthermore, based on this study, the effective global management of ischemic risk required, in part, the identification of patients with PVD [e].

The diagnosis of PVD at an early stage of development requires an accurate technology which is cost-effective and which minimizes the examination time required. The superficial femoral artery is straight, has a relatively simple flow field, and its superficial position in the thigh allows easy access for ultrasound imaging. Therefore, from a general perspective, such examinations would be quick to perform and would give insight on the overall health of the patient from a cardiovascular point of view.

This project is mainly concerned with the application of ultrasound technology for the diagnosis of PVD as determined using a clinical index of stenosis severity, the Velocity Ratio (VR), and furthermore, the effect of stenoses on pressure drop in the artery. In a clinical situation, however, diagnosis is complicated by the presence of multiple stenoses in a single arterial segment, such as is often found in the superficial

---

[d] Medscape presentation of Michael H. Criqui MD, PhD, University of California, San Diego, La Jolla California, USA: data from: Aronow WS, Ahn C; Am J Cardiology, 1994, 74:64.

[e] Medscape course: Alan T. Hirsch, MD, Minessota Vascular Diseases Center, U of Minnesota Medical School, Minneapolis, USA.

femoral artery. The VR is a validated indicator of stenosis severity in the presence of single arterial stenoses, however, few studies (*in vivo* and *in vitro*) have been performed to evaluate its accuracy in the presence of multiple stenoses, and the results were conflicting[2,4,110]. Furthermore, no stand alone apparatus exists which will allow a hemodynamic assessment of an arterial stenosis.

In the *in vitro* experiments, the accuracy of the VR is influenced by the correctness of the PSV measurement, by the flow conditions, and possibly by the geometrical arrangement of the stenoses. The pressure gradient accuracy measured by ultrasound will depend on the duplex instrument employed and on the validity of the implicit assumptions made when using the Simplified Bernoulli equation. On the other hand, the accuracy of the pressure gradient determined by catheter will depend on the integrity of the taps and the local flow conditions. Therefore, the purpose of this study in a peripheral artery model is: a) to evaluate the validity of the velocity ratio (VR) index for a stenosis of interest (SOI) alone, and in the presence of an adjacent stenosis, using color duplex ultrasound and finite element simulations, and b) to study the local hemodynamic effects of single and double arterial stenoses through the determination of the pressure drop across the SOI using color duplex ultrasound (Simplified Bernoulli) and catheter measurements, and by FE simulations.

3.2 Velocity Ratio Index

The Velocity Ratio (VR) is a clinical index to help estimate the morphological severity of an arterial constriction. The theory was developed under steady flow conditions for a single stenosis in a uniform arterial segment. The flow rate is assumed constant along the entire arterial segment with an absence of bifurcations or losses of flow through the arterial wall, and is calculated as the average spatial velocity multiplied by the corresponding cross-sectional area of the artery. The actual index is the ratio of the mean velocity within the stenosis ($\overline{v_2}$) to that proximal to the stenosis ($\overline{v_1}$). Mathematically, it is obtained by equating the flow rates (Q) at these positions (Eq. 19, page 51) based on the equation of continuity. By the rationale of equivalent flow rates, this is equal to the ratio of the cross-sectional area proximal to the stenosis (A_1) to that

within the stenosis (A_2) (Eq. 20), thereby indicating the severity of the stenosis from a morphological perspective. This straightforward premise is written as follows:

$$Q_1 = \overline{v_1} A_1 = \overline{v_2} A_2 = Q_2, \tag{19}$$

$$VR = \frac{\overline{v_2}}{\overline{v_1}} = \frac{A_1}{A_2}, \qquad \begin{array}{ll} < 2.0 & \rightarrow \text{Stenosis} < 50\% \text{ lumen area reduction,} \\ \geq 2.0 & \rightarrow \text{Stenosis} \geq 50\% \text{ lumen area reduction.} \end{array} \tag{20}$$

Considering that the stenosis cross-sectional area reduction is $A_2/A_1 * 100\% = 1/VR * 100\%$, where A_1 is the size of the normal section, it follows that the percent area reduction of the lumen is:

$$\% \text{ Stenosis} = 100(1 - \frac{1}{VR}). \tag{21}$$

Clinically, however, velocity measurements with duplex ultrasound are not necessarily taken in concordance with the theoretical conditions. Three main issues arise when comparing practice and theory:

1. *The actual value measured is neither the cross sectional area, nor the mean spatial velocity.* Firstly, the calculation of the cross-sectional area requires measuring either the diameter of the artery on a longitudinal scan and assuming a circular cross-section of the artery, or the surface on a perpendicular scan. These measurements are difficult to obtain with precision, especially when dealing with non-echogenic plaque, and consequently, are not used in this project. Secondly, *in vivo*, maximum velocities are measured more accurately than average velocities. This has worked in favor of replacing the mean blood velocity in the calculation of VR by the Peak Systolic Velocity (PSV), which is the maximum velocity at peak systole. The analysis of the Doppler signal received by the transducer, however, requires the inference of a given velocity profile. In order for the substitution of the PSV for $\overline{v}$ to be valid in the computation of VR, the ratio of the two values must be the same at both measurement positions, which requires equivalent velocity profiles. However, it

is noted in the literature that the velocity profile of a fluid passing through an arterial constriction flattens, and more so as the severity of the constriction increases, as discussed in the Chapter 2: Fluid Dynamics (page 19). In theory, such a phenomenon would compromise the accuracy of VR based on PSVs.

2. *The measurement position for position 1 is not necessarily chosen proximal to the stenosis.* An arterial stenosis may be found in a location that renders impossible the measurement of the PSV proximally. That is, it may be too difficult for the clinician to obtain a proper ultrasound image for the reading. Such circumstances include the presence of multiple stenoses or of an arterial bifurcation just proximal to the SOI. In such cases, the clinician is inclined to choose a distal measurement position for PSV_1 as an alternative to its theoretical proximal position. This may not favor an accurate VR since turbulence may arise distal to a severe stenosis for Reynold numbers as low as 200 to 300, as may be found in the femoral and iliac arteries[140].

3. *In the case of multiple stenoses, the clinical symptoms are not necessarily associated with the more severe obstructions.* In practice, therefore, the clinician is faced with a second problem which relates to multiple stenoses in the peripheral arterial system: that of determining which stenosis in the arterial tree is the main factor causing the patients clinical symptoms. It should be noted that the main goal of the clinician is to alleviate the symptoms of the patients to improve their quality of life, regardless of stenosis severity. That is, assuming all stenoses are circumferential and symmetrical within the artery, a patient presenting with a 70% diameter reduction (91% area reduction) stenosis will be treated if clinical symptoms are present. A patient may even be treated for a stenosis of 50-60% reduction in diameter (75-84% area reduction) if symptoms are present. This indicates how actual blood flow to the distal vascular bed is not simply related to the morphology of the stenosis but to its overall hemodynamic effects, which requires consideration of the influence of the neighboring stenoses and arteries. Blood flow to the peripheral vascular bed was described by Young[140] as follows:

$$Q_p = \frac{(p_a - p_v) - \Delta p_s}{R_p} \quad (22)$$

where Q_p is the blood flow in a peripheral artery, p_a is the arterial pressure, p_v is the venous pressure (p_a-p_v is the driving pressure), R_p is the peripheral resistance to flow, and Δp_s is the pressure gradient measured across the constriction. Inversely, a given stenosis may produce different pressure gradients depending on the resistance, the flow, and the driving pressure within the artery. Therefore, the pressure gradient alone would probably not be the same from one patient to the next for a given stenosis morphological severity.

If many morphologically "severe" stenoses are present, which one must the clinician chose to dilate? Furthermore, geometrically, most stenoses are neither circumferential nor symmetrical and the severity is calculated based on a measurement where the lumen diameter is the smallest. Due to such limitations of the VR, clinicians also base their diagnoses on additional factors such as the stenosis unicity and oldness, and collateral blood flow availability. Selecting the appropriate stenosis to treat either by angioplasty or other techniques is postulated based on such findings. The key is to determine what hemodynamic phenomena creates the symptoms and what stenosis characteristic(s) create the hemodynamic effects so as to develop a related clinical index and to correctly chose the stenosis for treatment.

To gain increased insight into the clinical problem of diagnosing a stenosis, the aspects relating to measurement position of the PSV and the presence of an adjacent stenosis were studied in this project in relation to their effect on the measurement accuracy of the VR index. The pressure gradients induced by the SOI were also studied to give additional insight into the actual consequences of a stenosis configuration on the distal blood flow. These conditions were verified using computer simulations and *in vitro* experiments.

3.3 Geometrical Representation of PVD

Computer simulations and *in vitro* experiments were performed using the following general vessel and fluid characteristics for a peripheral artery. An artery with a diameter (D) of 7.9 mm was chosen. The vessel was a straight circular cylinder having either single or double stenoses. The transition from the unstenosed arterial diameter to the maximum reduction of a stenosis was concentric and cosine shaped based on the following equation:

$$r = R - e * (1/2 * \sin (2\pi/L_s * (z - Z) + \pi/2) + 1/2) \qquad (23)$$

where r is the radial coordinate of the artery, R is the non-constricted vessel radius (D/2), $e = R * (1 - (1 - p/100)^{1/2})$ is the maximum reduction of the artery radius at the stenosis, p is the percent area reduction of the lumen, $L_s = 20$ mm is the stenosis length, Z is the axial position of the center of the stenosis from the beginning of the vessel, and z is the axial position along the curvature of the stenosis ($Z - L_s/2 \leq z \leq Z + L_s/2$) from the beginning of the vessel segment (see Figure 15, page 54). All values of length are in millimeters.

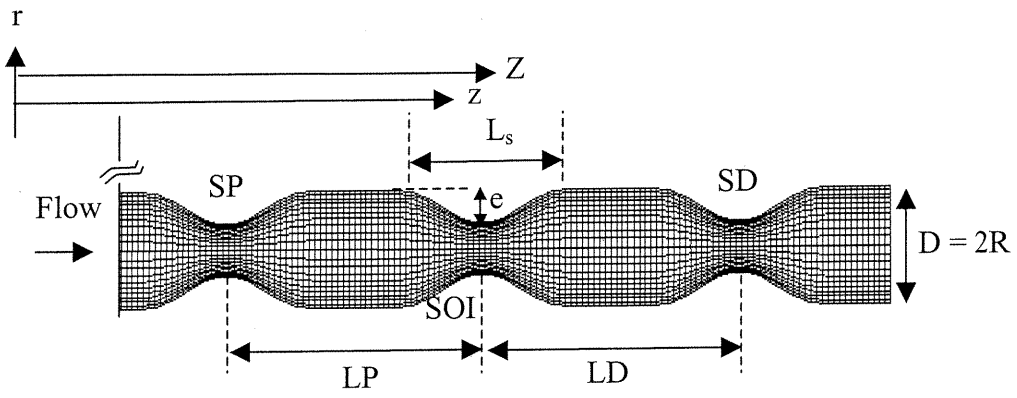

Figure 15. Representation of the geometrical arrangement of the stenoses. Either SP and SOI, or SOI and SD, are present in a given experiment. LP and LD are the interstenotic distances. The formula describing the shape of the stenoses is given in Equation 23.

The severity (p) of the stenosis of interest (SOI) varied from mild to severe (30, 50, 70, 80, and 90% area reduction) in each set of experiments. An adjacent proximal

(SP) or distal (SD) stenosis, when present, was placed at a distance of 3, 6, 10, or 20 arterial diameters from the SOI, center to center (see Figure 15, page 54). These interstenotic distances for either the proximal or distal adjacent stenosis are termed LP or LD, respectively. The severity of the adjacent stenosis was chosen to represent a critical stenosis with a 75% lumen area reduction (see Table II).

Stenosis Configuration	Proximal Stenosis (SP) *	Stenosis of Interest (SOI) *	Distal Stenosis (SD) *
SOI	-	30,50,70,80,90	-
SP and SOI : LP = 3, 6, 10, and 20D	75	30,50,70,80,90	-
SOI and SD : LD = 3, 6, 10, and 20D	-	30,50,70,80,90	75

*A percentage of the lumen area reduction.

Table II. Summary of the geometrical descriptions of PVD used in the simulations and in the *in vitro* experiments, where SOI, SP, and SD are the stenosis of interest, proximal stenosis, and distal stenosis, respectively. LP and LD represent the interstenotic distances between the SOI and the SP or SD, respectively.

3.4 Finite Element Simulations

Finite element simulations were performed under steady flow conditions using Fidap 8.0 (Fluent Inc. USA). In all simulations, the fluid was Newtonian with a constant viscosity of 3.5×10^{-3} N·s/m^2 and a constant density of 1050 kg/m^3, such values being well within the physiological range for blood[84,140]. These values are the two most important material properties in almost all fluid dynamics problems as they define the Reynold's number.

In these simulations, the degrees of freedom are velocity and pressure. For the boundary conditions, a null velocity was imposed at the wall. The radial component of the velocity was fixed at zero along the central axis of the vessel since the problem is axi-symmetric, necessitating such a supposition for continuity of the fluid at the axis (no

void of fluid). The outlet boundary condition was not constrained since, by default, it is considered to be "free" and its value is computed in the analysis. The flow at the inlet was assumed to be fully developed, with a velocity profile (see Figure 16) of the following parabolic form:

$$V_z(r) = 2\frac{Q}{\pi R^2}\left[1-\left(\frac{r}{R}\right)^2\right], \tag{24}$$

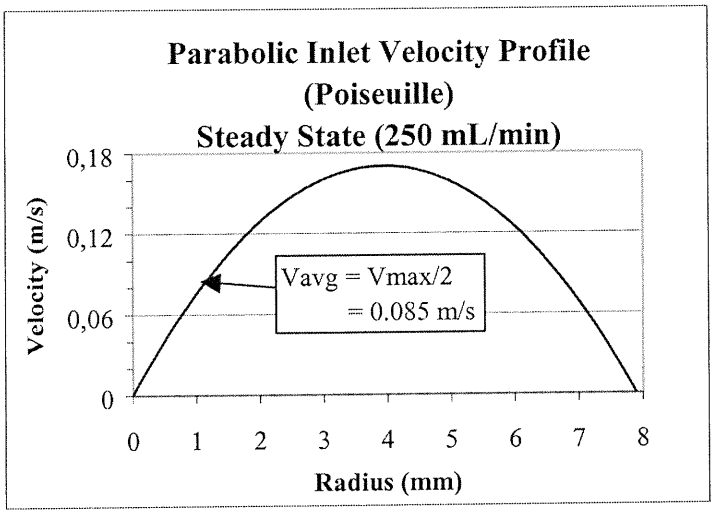

Figure 16. A graphic representation of the parabolic velocity profile at the inlet for the simulations with a flow rate of 250 mL/min. The shape of the velocity profile at the inlet was the same in all simulations. V_{avg} is the mean spatial velocity, and V_{max} is the maximum centerline velocity.

where V_z is the axial velocity as a function of the radial coordinate r (m), $0 \leq r \leq R$, R is the non-constricted vessel radius (m), z is the axial coordinate (m), and Q is the constant flow rate (m^3/s).

Flow rates of 250, 500, and 750 mL/min were simulated, corresponding to Reynold's numbers of 201, 403, and 604, respectively. For flow through arterial constrictions, typical *Re* numbers found in the large arteries (> 1mm in diameter) are moderate, and range from a few hundred to several thousand[140].

3.5 *In Vitro* Experiments

In vitro experiments were performed under conditions as close as possible to the simulations. The Velocity Ratios and the pressure gradients for the SOI were measured for the various geometrical configurations specified in section 3.4 (page 55).

3.5.1 Experimental Setup

The experimental setup comprised a steady flow roller pump, a damping reservoir to eliminate any unsteadiness in the flow, a 25 mm internal circumference (D = 7.96 mm) cannulating probe to measure blood flow (Model SF625) coupled to an electromagnetic flowmeter (Cliniflow II, Model FM701D, Carolina Medical Electronics, King, NC, USA), and an agar-based wall-less flow phantom with five pressure taps. The pressure measurements were performed with disposable medical transducers (Namic Angiographic Systems Division, Boston Scientific, Glen Falls, NY, USA) coupled to a 16-channel portable Power Lab (ADInstruments, Castle Hill, Australia) physiological monitoring system via an eight channel bridge amplifier (ADInstruments). As shown in Figure 17 (page 58), the flow phantom also comprised a distal resistance and a return reservoir, all of which were connected in a circuit using TYGON® Food and Beverage Tubing and various valves and connectors. The level of fluid in the return reservoir was kept constant to maintain the same hydrostatic pressure at the outlet of the vessel model. A distal resistance was added in the experimental setup by adding a valve to pinch the tube just distal to the artery model. The distal resistance was kept constant in all experiments. This procedure increased the operating static pressure within the vessel so as to amplify the pressure readings and minimize the measurement errors by the Power Lab.

3.5.2 Arterial Stenosis Model

The artery models were made of an agar gel. This concept is commonly used to form a wall-less artery to avoid diffraction of the ultrasound beam caused by the wall when using tube-like artery models. The agar gel is also known as a tissue mimic as it has similar acoustic properties (velocity of sound, attenuation) as human tissues[104].

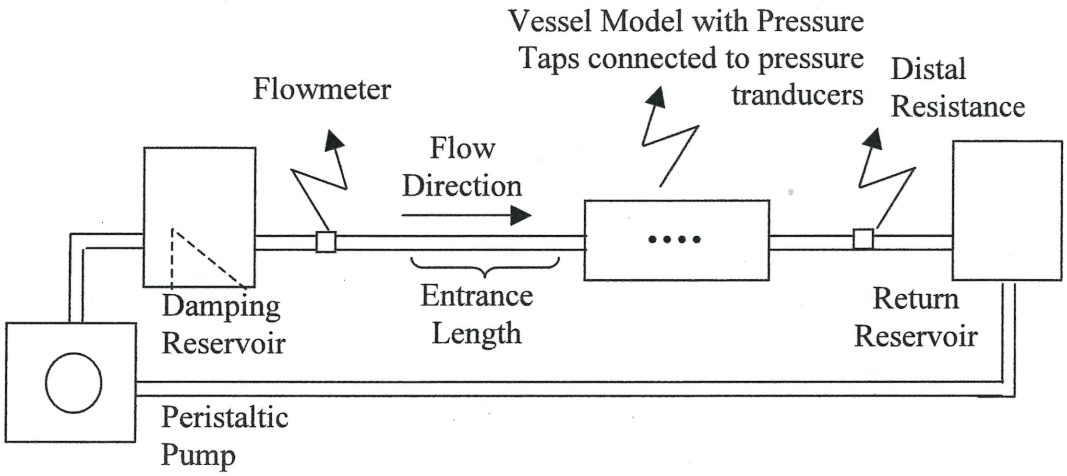

a)

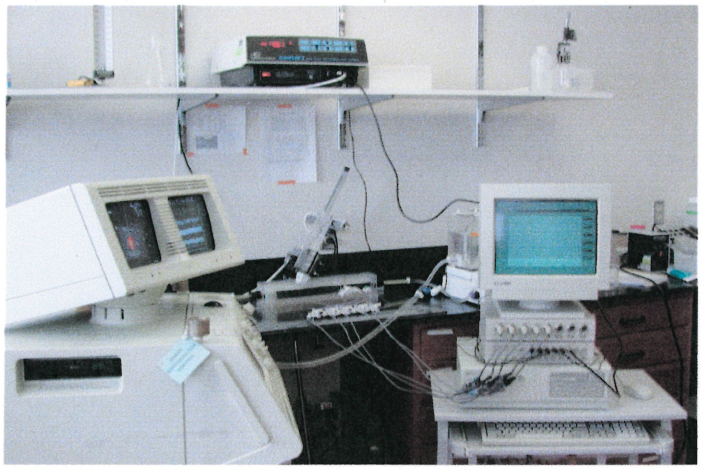

b)

Figure 17. *In vitro* experimental setup for steady flow through the vessel model a) schematic representation, and b) visual representation.

The vessel phantom was created in several steps, each of which is detailed further on in the text: 1) An artery having single or double stenoses was molded out of a bismuth alloy (cerrolow). 2) The artery (cerrolow rod) was fitted at both ends into rigid fiber-glass tubes (with internal diameters equivalent to that of the unstenosed sections of the artery) and secured in an acrylic rectangular container. The needles (pressure taps) were aligned with the mid horizontal plane of the artery along the SOI and positioned so as to make contact with the artery, and the container was hermetically sealed. 3) An agar solution was poured, at a temperature of approximately 45˚C, through a hole at the extremity of the acrylic container so as to surround the cerrolow rod. During this process, the container was placed vertically to avoid softening and bending of the cerrolow rod with gravity due to the heat of the agar solution. 4) Once the agar solution cooled to room temperature and solidified into a gel (approximately one hour and a half), the hermetic seal of the container was removed. The entire container was then immersed vertically into a hot water bath ($65^{\circ}C < T_{bath} < 70^{\circ}C$) for approximately two and a half hours. This liquefied the cerrolow alloy forming the artery causing it to flow out of the gel and the acrylic container via the fiber-glass tube, and was collected in a beaker for reuse. 5) Hot water was injected into the fiber-glass tube to assure that the remaining cerrolow material was properly evacuated, leaving only the wall-less artery formed by a solid agar gel. The arterial phantom, formed using a tissue-like material, was then placed into the circulation model.

The bismuth alloy used is a non-ferrous metal composed of 49% bismuth (Bi), 21% indium (In), 18% lead (Pb), and 12% tin (Sn). The point of fusion is 136˚F = 57.7˚C, which makes it a eutectic (low melting point) alloy. When creating the phantom, the alloy was kept in an oven at approximately 65°C (see Figure 18a, page 60). The mould was placed in the same oven, before injection, for two (single stenosis moulds) or three (double stenosis moulds) hours to avoid hardening of the alloy upon contact with the cold aluminum surface. The cerrolow was injected into the hot mould using a syringe, while the other extremity of the mould was placed in a shallow bath of cold water to avoid leaking of the alloy through the fissures. That is, upon contact of the cerrolow with the water, it would harden, and could no longer leak out of the mould. While the cerrolow was injected, the mould was placed at an angle of approximately

45° to allow any air to escape. The mould was then placed vertically in a vice until it reached room temperature, at which point the arterial cast was removed from the mould. The arterial cast was then barely scraped using a scalpel to remove any protrusions from the molding process. Figure 18b (page 60) shows an example of a cerrolow rod used to create an artery having double stenoses.

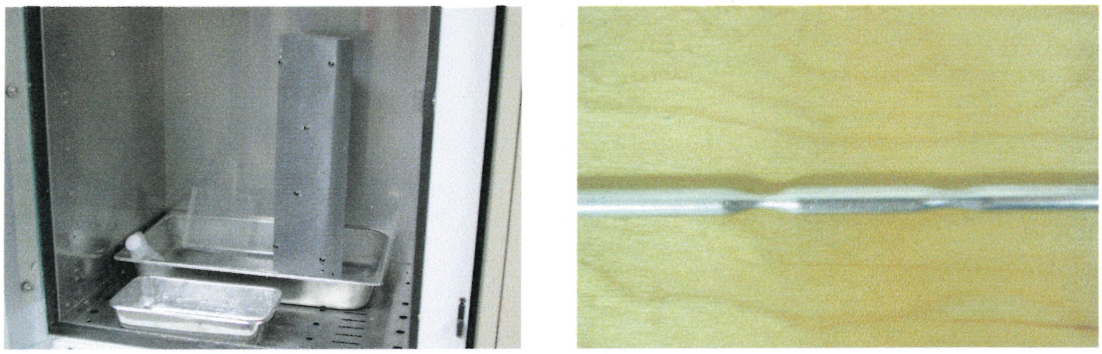

a) b)

Figure 18. a) To mould the arterial model, the cerrolow, the aluminum mould and the syringe were placed in an oven at approximately 65°. b) The final arterial model obtained after scraping the minor imperfections.

The agar gel was made in several steps. A solution was made composed of 3% agar (Sigma Chemical, #A-6924, high gel strength), 8% glycerol (ACP Chemicals, #G3730, $HOCH_2CHOHCH_2OH$, density at 20°C = 1.25 g /cm^3), and 89% distilled water. The solution was heated for approximately 16 minutes in a microwave oven at maximum power until it begins to boil, after which the power level of the microwave was reduced to 70% for four minutes to maintain the boiling temperature. The solution was then stirred constantly and allowed to cool down to the defined pouring temperature of 45°C to avoid melting the bismuth alloy, after which the agar was poured into the acrylic container and kept vertically positioned until the solution solidified. An example of the agar phantom, removed from the acrylic box and cut longitudinally, is shown in Figure 19 (page 61).

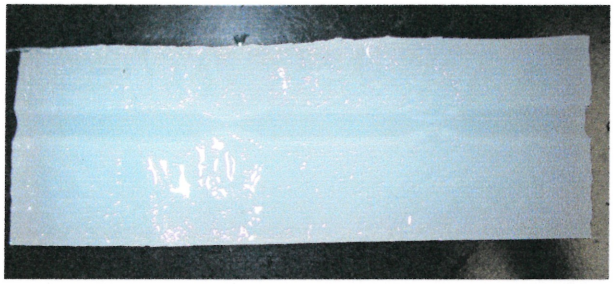

Figure 19. Longitudinal cut of the arterial stenosis model (double stenoses at an interstenotic distance of 10D) formed out of an agar tissue mimic.

3.5.3 Blood Mimic

The fluid used in the experiments (blood mimic) was composed of approximately 40% glycerol, 60% distilled water, 9 g salt/L of solution for the detection of the flowrate by the electromagnetic flowmeter, and 1 g/L of solution of superfine Sephadex particles (Sigma Chemical, #G2550) to provide ultrasound scatterers. The fluid density was similar to that of human blood, as calculated from the following equation:

$$\rho_{blood\_mimic}=\frac{\rho_{glycerol}\times V_{glycerol}+\rho_{DW}\times V_{DW}}{V_{glycerol}+V_{DW}} \tag{25}$$

where ρ is the density, V is the volume, and DW is distilled water. The density of the solution obtained was approximately 1.09 g/cm^3, for a volume of 1.2 L of glycerol, and 2.2 L of DW. The viscosity of the solution was approximately 3.5 mPa·s (3.5 cP), which is within the range of normal human blood at high shear stresses and a normal hematocrit (3-5 mPa·s) [16]. The actual viscosity of the fluid was measured before each experiment using a cone-plate type viscometer (Brookfield Engineering Laboratories Inc., Stoughton, Massachusetts, USA, model LVDVIII-CP-42). Should the viscosity have been other than 3.5 mPa·s, either additional distilled water or glycerol were added to the solution before the experiment to reach the required viscosity.

3.5.4 Protocol for Physiological and Ultrasound Measurements

The vessel phantom was placed in the experimental circuit. The blood mimic was poured into the fluid reservoir and began circulating, by gravity and using the pump,

towards the damping reservoir. The air bubbles in the circuit were eliminated by buoyancy in the fluid reservoir. The needles were cleaned or changed if blocked with agar gel, and the catheters were allowed to fill with the blood mimic. The flow in the catheters and the circuit were then stopped using valves, and the flowmeter and the pressure transducers were zeroed to eliminate any offsets in the measurements.

The flow phantom was covered with a layer of distilled water for coupling with the ultrasound transducer. As shown in Figure 20 (page 62), the transducer (B) was fixed at an angle of $\theta = 60°$ with the axis of the vessel, and its horizontal position along the vessel was adjusted by sliding the arm (C), to which the transducer was fixed, along its base (D). The positions of the arm were indicated on a ruler on the base.

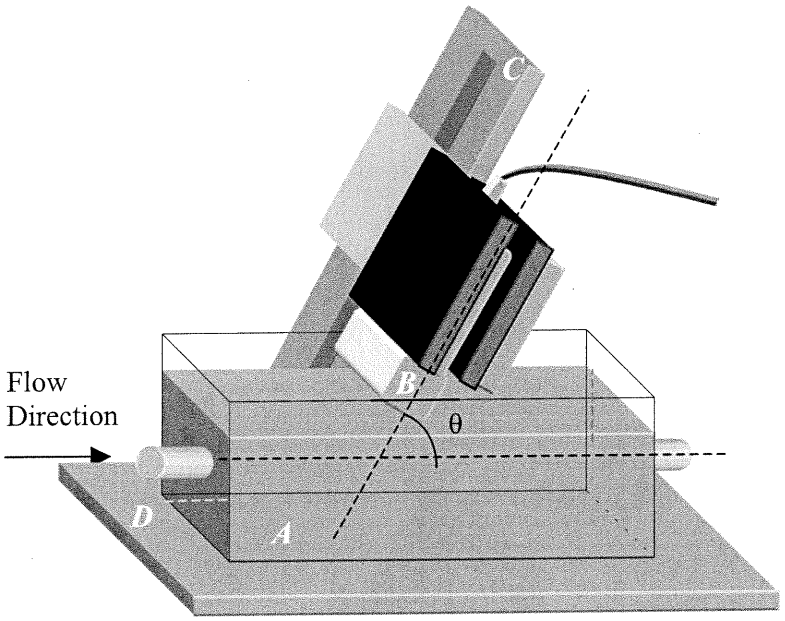

Figure 20. Setup and coupling (distilled water) of the ultrasound transducer (B) with the phantom model (A). The Doppler angle (θ) was fixed by adjusting the angle of arm (C), and the transducer was positioned along the vessel by sliding arm (C) along the base (D).

The ultrasound settings, on the ATL Ultramark 9 HDI system, were adjusted in B-mode (1 Focal Zone positioned at or as near the center of the artery as possible, Zoom magnification 3x), in color Doppler (Filter type = D0, Color Map = 1, Steering Angle = 0°), and in Pulsed-Wave Doppler (Angle Correction = 60°). To assure the integrity of the vessel model, B-mode images were visualized along the entire artery, and at several

positions (proximal to, distal to, and at the maximum area reduction of the SOI, at the maximum area reduction of the adjacent stenosis, and at the beginning and end of the artery). The cross-sectional areas were measured, using an elliptical approximation on the monitor (because the vessel was viewed at an angle), and compared against the theoretical vessel area. The positions of the needles were simultaneously verified in B-mode and in color Doppler to assure that the pressure tap needles were at the wall and did not perturb the flow. To align the ultrasound transducer with the needle positions, the transducer was slid along the arm until the needle appeared in B-mode with its greatest intensity, at which time the transducer position was noted.

3.5.5 Velocity and Pressure Measurements

Velocities (PSV_1 and PSV_2) were measured using the Ultramark HDI system and a 4 MHz (L7-4) linear-array transducer. The flow rate was adjusted using the roller pump. The transducer was then positioned at the first recording site 2D proximal to the SOI. The ultrasound machine was set in color mode and the velocity range adjusted to the smallest value possible while avoiding aliasing. The values for the wall filter and the PRF were automatically adjusted based on the velocity range. These values and a qualitative description of the color image were noted for future reference. The ultrasound system was then set in duplex mode for the measurement of the PSV. The sample volume position was adjusted by both the audio and spectral signal to record the highest blood flow velocity with the cleanest spectral envelope obtainable, as in Strauss[118]. The maximum frequency was measured with a cursor from the displayed Doppler frequency spectrum and the corresponding velocity was displayed on the monitor screen. All values were noted and the transducer was then moved to the next fixed position along the artery to repeat the same procedures. Once all the measurement positions were obtained (2D proximal to the SOI, at the maximum reduction of the SOI, and 2D and 10D distal to the SOI), the maximum and minimum PSVs along the artery were located "blindly" as would be done in a clinical situation. The duplex pressure gradients ($\Delta P_{MAX} = 4*PSV^2$) were noted at the maximum area reduction of the SOI for comparison with the pressure tap values. These procedures were repeated for flow rates of 250, 500, and 750 mL/min.

The static pressures along the SOI (2D proximal to the SOI, at the maximum reduction of the SOI, and 2D, 5D, and 10D distal to the SOI) at each flow rate were measured through pressure taps (needles, 21 gage, 1 ½ in. long) inserted horizontally from the side of the acrylic container through the agar gel, and fixed flush with and perpendicular to the vessel wall as shown in Figure 21 (page 64). The needles were connected to rigid fluid-filled tubes leading to pressure transducers (Namic Angiographic Systems Division, Boston Scientific, Glen Falls, New York, USA). The transducers convert the fluid pressures into voltages filtered and amplified using a Bridge Amp (ADInstruments) in series with the PowerLAB instrument (ADInstruments) (see Figure 22, page 65).

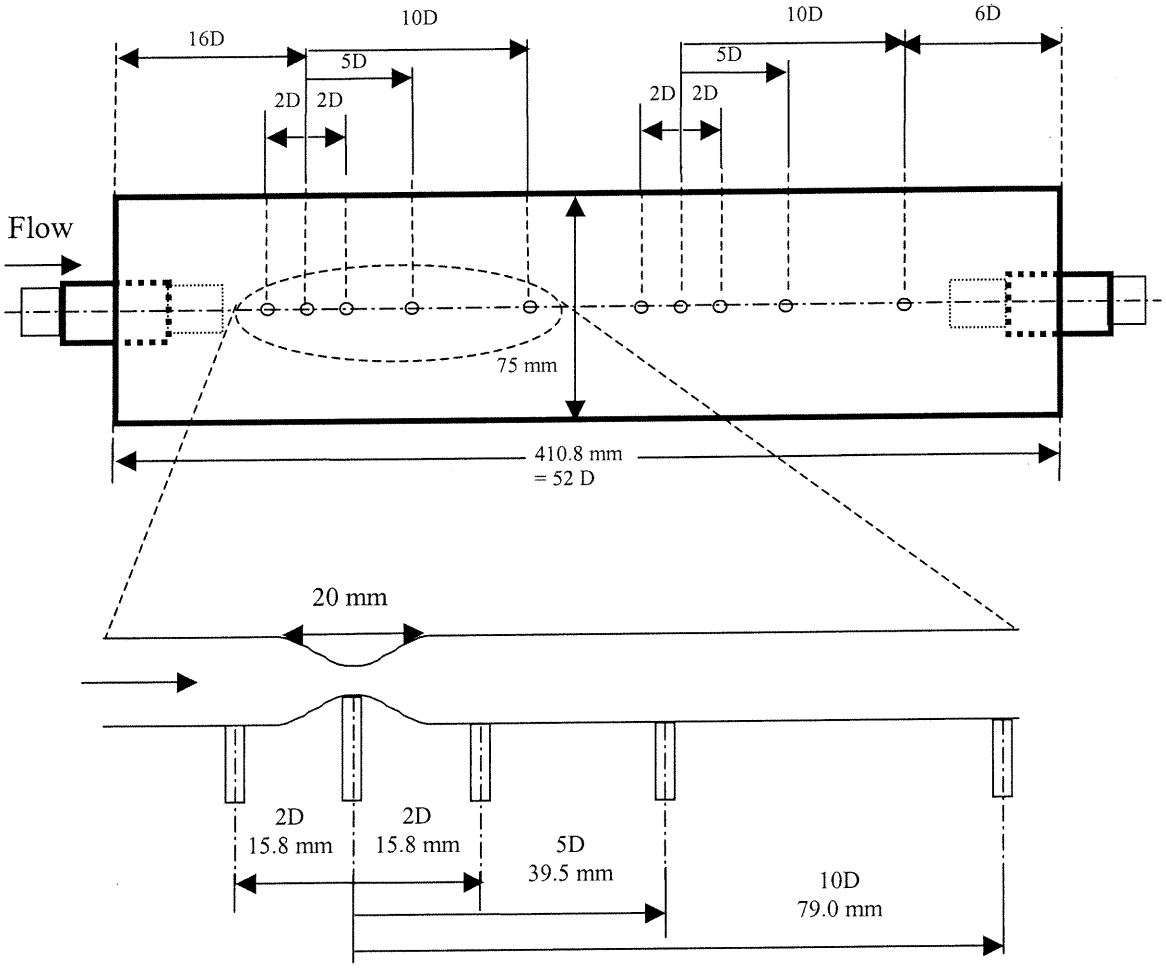

Figure 21. Vessel model dimensions and pressure tap (needle) positions relative to the maximum area reduction of the stenosis of interest. The needles are Becton Dickinson 21G11/2 *PrecisionGlide*®, and the tips of the needles were cut square and placed flush with the fluid/vessel interface.

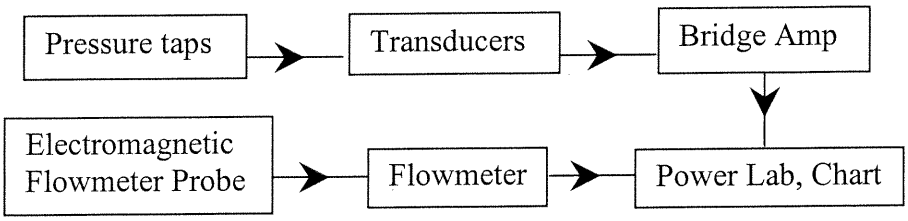

Figure 22. A flow chart representing the recording of the static pressure values in the artery and the flow rate.

The flow and pressure values were recorded in mV for approximately a 15 second interval using the Chart software (version 3.4.6, ADInstruments) in a Windows environment, and converted in flow (mL/min) and pressure (mmHg) units in Excel based on calibration curves. With Chart, the number of recording channels may be selected. In our case, six channels were used of which five were to record the pressures along the SOI, whether as a single stenosis, or proximal or distal to an adjacent stenosis. The sixth channel allowed the numerical acquisition of the flowmeter readings.

As shown in Figure 21 (page 64), the positions of the pressure taps were chosen so as to avoid the transition areas of the stenosis where the artery wall is not perpendicular to the taps. At these positions, the needles ideally measure pure static pressure and not the kinetic energy of the fluid.

Calibration of the flowmeter was obtained by collecting a volume of fluid flowing from a reservoir, timing the collection with a digital stopwatch, and dividing the two values. The voltage outputs of the flowmeter were recorded in parallel with the actual flow rates. This was done for flow rates from 100 mL/min to 1000 mL/min.

The pressure transducers were calibrated using the vessel model. The flow outlet of the phantom was closed while the pressure furnished by the pump was increased. Static pressures read by the transducers were recorded in parallel with that using a mercury filled manometer (Omega HHP-102D), and a calibration equation was obtained for each transducer (see the pressure calibration curves in Appendix I).

3.5.6 VR and ΔP Calculations

The PSVs measured in duplex mode were used to calculate the VRs. PSV_2 was always taken as that velocity measured at the maximum area reduction of the stenosis, however, PSV_1 was taken as either the PSV measured 2D proximal, or 2D, 5D, or 10D distal to the SOI. The actual ratios were calculated using the frequency shifts measured in duplex, this ratio being equivalent to the ratio of velocities.

The duplex pressure drops were calculated automatically by the ultrasound system using the Simplified Bernoulli equation ($\Delta P_{MAX} = 4*PSV^2$). The catheter pressure drops were calculated from the static pressure values measured at the pressure taps in Chart. These pressure files were imported into Microsoft ® Excel 97 SR-2 and the average pressure (in mV) was calculated at each position for each flow rate. The pressures were then converted into mmHg units and the gradients calculated. The reference pressure was 2D proximal to the SOI, and this was the value from which were subtracted the SOI maximum reduction pressure, and the distal pressures.

The simulation and *in vitro* curves of the VR or the pressure gradients versus the actual percentage area reduction of the SOI, were plotted at all flow rates and may be found in Appendix II. The *in vitro* experiments performed did not include all the geometrical configurations of the simulations. Only the configurations that appeared to affect the measurement of the VR or the ΔP in the simulations, were considered *in vitro*.

CHAPTER 4.

Results and Discussion

Before introducing the structure and content of this chapter, it is judicious to highlight the following important observation: the diagnosis of the severity of arterial stenoses, currently based on the functional aspects of the stenosis with the VR ratio, may be inaccurate due to non-ideal physiological or measurement conditions relative to those under which the index theory was developed. The theoretical curve for the VR index as a function of the stenosis area reduction, VR = 100 / (100 - % stenosis), has an exponential form with a value of 1 in the absence of a stenosis, a value of 10 for a 90% area reduction stenosis, and tends to infinity as the stenosis severity progresses to a complete obstruction of the artery. This tendency is represented on each VR graph found in Appendix II (Figs AII-1-AII-6, graphs a-f) up to a value of approximately 6, below which are contained most of the author's results from the simulation and *in vitro* experiments.

The results of the *in vitro* experiments are based on a single set of experimental values obtained by the author of the present thesis. However, three sets of additional experiments were performed by a research assistant of the Laboratory of Biomedical Engineering of the IRCM (Ms Zhao Qin) for the cases of a single stenosis and for SP at 3D proximal to the SOI. This data is represented on separate graphs also found in Appendix II (Figs AII-1 and AII-2, graphs g-i) and are compared to the author's experiments after an initial examination of these last.

Before studying the results for the double stenoses, the error in diagnosing a single arterial stenosis by VR is initially established as a point of comparison from the theoretical case. Afterward, the results for the SOI in the presence of an adjacent stenosis are studied to eventually establish the worst stenosis configurations, of those considered, for the evaluation of SOI by the VR ratio. The pressure gradients are studied following each discussion of the VRs for a given stenosis configuration. Finally,

a summary of these results is discussed and the results are compared to those available in the literature.

In the simulations and *in vitro* experiments, at all PSV_1 measurement positions and flow rates, the calculated VR curves generally show an underestimation of the theoretical value of VR at a specific stenosis severity (Figs AII-1-AII-6). The only few exceptions are observed for some of the *in vitro* studies performed for moderate lumen area reductions (50 and 70% AR). Clinically, an underestimated VR measurement could lead to an inappropriate diagnosis and treatment approach for the patient.

As concerns the pressure gradient results also found in Appendix II (Figs AII-7-AII-12), the *in vitro* values are generally inferior to those obtained by simulation. The possible reasons for such discrepancies between the simulations and *in vitro* experiments will be discussed, when necessary, for each stenosis configuration. The extent of the VR errors and the pressure gradients measured are looked at in detail in the following section. Each graph in Appendix II contains the results of a single flow rate, and each curve represents one of the various measurement positions relative to the SOI.

4.1 Velocity Ratios

In the experiments, the VR was calculated from the PSVs obtained at the various measurement positions. From this VR, an estimation of stenosis severity was obtained from the theoretical curve. The severity estimation error for a stenosis of say 70% estimated as being 50%, based on its VR obtained experimentally, will hereafter be referred to as a 20% underestimation error. The results will be discussed as a function of the stenosis configuration, treating the proximal PSV_1 measurement positions first, followed by the distal measurement positions, and including the effects of flow rate on the respective measurement positions.

4.1.1 Single Stenosis

For a single stenosis, the *2D proximal* PSV_1 measurement position yields comparable shapes for the VR curves in the simulations and *in vitro* experiments, at all flow rates (Figs AII-1a-i), yet are shifted downwards to lower VR values than in theory. For the

simulations (Figs AII-1a, c, e) and PSV_1 at *2D proximal*, the largest underestimation errors are for the 50% and 70% stenoses, and are approximately 20% at all flow rates. However, *in vitro* (Figs AII-1b, d, f), the error is greatest for the 50% stenosis at a flow rate of 250 mL/min (approximately a 40% underestimation), the error decreasing as the flow rate increases. At 750 mL/min, the largest error is for the 70% stenosis (approximately a 25% underestimation). In the experiments performed by Qin (Figs AII-1g-i), the largest errors are consistently found for the 70% stenosis, with an error of 25% at all flow rates. This finding is comparable to the author's results.

For *PSV_1 measured distally*, the *simulation* curves (Figs AII-1a, c, e) are flat with a value of approximately 1 (no stenosis estimated) at both measurement positions except for a flow rate of 250 mL/min and PSV_1 at 10D distal (Fig AII-1a). Here, the VR increases slowly to a value of almost 2 for an 80% stenosis (35% error), and decreases to approximately 1.7 (50% error) for a 90% stenosis. The flat VR curves may be due to the absence of turbulence in the simulations, thereby, prolonging the distance over which the high jet velocities are maintained, and consequently, PSV_1 and PSV_2 are similar and their ratio is approximately 1. At the lower flow rate of 250 mL/min, however, the jet may have dissipated before the very distal PSV_1 measurement position, and the flow partially redeveloped. Thus, the lower velocities distal to SOI allow the VR value to increase, approaching that for the 2D proximal measurement position, and this for stenosis severities of up to 80%. The negative slope after the 80% stenosis possibly indicates that the length of the flow jet is longer for a 90% stenosis and the flow has not yet redeveloped at 10D distal. *In vitro* (Figs AII-1b, d, f), the 10D distal measurement curve has a similar trend to the 2D proximal position at all flow rates, whereas the 2D distal curves are flat with a value of approximately 1 (no stenosis estimated) as they were in the simulations. The improved results for 10D distal *in vitro*, relative to the simulations, may be due to the presence of turbulence in the *in vitro* flow allowing the dissipation of the jet post-stenotically, thus increasing the VR. In the experiments by Qin (Figs AII-1g-i), the 2D distal position also results in flat curves. The 10D distal position gives lower VRs at 250 mL/min for 80 and 90% severities, relative to the same curve in the author's experiments, and higher values at 500 mL/min for the 70% stenosis and at 750 mL/min for the 90% stenosis. The author's

experimental curves, however, appear approximately within the error bars of the experiments by Qin.

The *blinded in vitro* measurements of the VR appear to give slightly improved estimates of stenosis severity, especially for severities inferior to 80%. This could be due to more appropriate choices of measurement positions for PSV_1 and PSV_2 that may not necessarily be found at systematically placed measurement positions.

4.1.2 SP at 3D Proximal to the SOI

When SP is located 3D proximal to the SOI (SPSOI(3D)), the *PSV_1 measurement position 2D proximal to the SOI* is located 1D distal to SP. Therefore, perturbations in the flow due to SP (75% area reduction) should affect the PSV_1 values recorded at this position. The resulting VR curves for PSV_1 at 2D proximal are similar in the simulations and the *in vitro* experiments (Figs AII-2a-f), to the exception of the values at 90% AR of the SOI which have greater underestimation errors *in vitro* than in the simulations. Similar *in vitro* results were found by Qin (Figs AII-2g-i). The 2D proximal curves (Figs AII-2a-i) are shifted down from both the theoretical situation and the single stenosis data despite the fact that it is the position used in the theoretical case. At all flow rates considered, underestimation errors for 2D proximal range from 30 to 55% in the simulations, and from 40 to 70% *in vitro*, the errors being greatest and equivalent at flow rates of 500 and 750 mL/min. The lower VR values for this stenosis configuration should be due to the creation of a jet distal to SP, especially at high flow rates, increasing the value of the PSV_1 measured proximal to SOI and, consequently, decreasing the VR.

The *measurement positions distal to the SOI* are distal to both stenoses. The VR curves are generally flat in the *simulations* (Figs AII-2a, c, e) with a value of approximately 1 (no stenosis estimated). However, as for the single stenosis, the 10D distal position at a flow rate of 250 mL/min is shifted to slightly greater VR values at all stenosis severities. The curve is flat with a value of approximately 2 up to an 80% stenosis, and decreases to approximately 1.5 for a 90% stenosis. At the low SOI severities, the VR of 2 may be explained by a relatively larger PSV_2 created by the severe proximal stenosis. The curve tendency at greater SOI severities is due to PSV_1 at

10D distal which increases rapidly when the SOI increases to 90% severity, possibly due to the lack of dissipation in the simulations, whereas PSV_2 increases more regularly as stenosis severity increases. Therefore, the severity is overestimated by 20% for the 30% stenosis and underestimated increasingly so for stenoses greater than 50% (20, 30, and 50% errors for 70, 80, and 90% stenoses, respectively). As the flow rate increases, the curve shifts down and flattens to a value of approximately 1. Again, this may be due to the lack of dissipation of the jet in the simulations which encourages the propagation of the jet distally causing PSV_1 and PSV_2 to be similar, and more so as the flow rate increases. *In vitro* (Figs AII-2b, d, f), the VR values tend to increase with stenosis severity, however, the 2D and 10D distal curves differ from one another, unlike in the simulations. The 10D curve is shifted upwards and resembles more the theoretical curve whereas the 2D distal position resembles the curve 2D proximal to the SOI (1D distal to SP), especially at 70% severity of SOI. This may be because the severity of the adjacent stenosis is almost the same as the SOI, and the 2D proximal position is in the jet of SP just as the 2D distal position is in the jet of SOI. These results are confirmed by the experiments of Qin (Figs AII-2g-i), where the 2D distal curves are flat, the 10D curves are shifted to greater values, and the 2D distal and 2D proximal curves are alike at 70% and 80% severity. As could be expected when SOI is more severe (90%) than SP, the VR values for 2D proximal are greater than those for 2D distal, since PSV_1 in the jet of SP is less than in the jet of SOI. At 10D distal, the author's experiments (Figs AII-2b, d, f) have comparable results to Qin (Figs AII-2g-i). Since the velocity in the jet of SP is dependent on its severity, the VR will depend on SP. Therefore, it appears preferable to use a very distal measurement position to SOI, such as 10D distal, where the effect of the jet of SOI is reduced. This could lead to greater consistency in the velocity measurements, because measurements closer to SOI may result in a VR that approaches 1 when the jet velocity is similar to that within the SOI. The results obtained (Figs AII-2b, d, f) appear to confirm such reasoning. At a 2D distal measurement position, errors range from 20-80% at 250 mL/min, from 15-75% at 500 mL/min, and from 30-70% at 750 mL/min. Whereas at 10D distal, the underestimation errors are much smaller and range from 5-25% at 250 mL/min, from 0-15% at 500 mL/min, and from 5-15% at 750 mL/min.

The *blinded* curves are comparable to those where the measurements were taken systematically 10D distal to the SOI, and may serve as an alternative.

4.1.3 SP at 6D Proximal to the SOI

When SP is located 6D proximal to the SOI (SPSOI(6D)), the *2D proximal PSV_1 measurement position* is 4D distal to SP. In the *simulations* (Figs AII-3a, c, e), the curves at this measurement position are equivalent to those for SPSOI(3D) (Figs AII-2a, c, e). However, at 250 mL/min, the VR value at 90% is slightly higher, with a value of approximately 2.8 (25% underestimation error), versus approximately 2.5 (30% underestimation error) for an interstenotic distance of 3D. *In vitro* (Figs AII-2b, d, f and Figs AII-3b, d, f), this tendency, where the VR values at the 90% stenosis are slightly greater for SPSOI(6D) (the larger interstenotic distance) than for SPSOI(3D), is seen at all flow rates. This may be due to the dissipation of the turbulence following SP, resulting in lower PSV_1 values, and consequently, greater VRs.

For the *distal measurement positions*, in general, the *simulation* curves (Figs AII-3a, c, e) greatly resemble those for SPSOI(3D) (Figs AII-2a, c, e), being relatively flat at around a value of 1, to the exception of the 10D distal curve at 250 mL/min, as for SPSOI(3D). This curve is like that for SPSOI(3D) except for the VR values at 30 and 50% stenosis which are slightly less than 2. The curve, therefore, increases slightly up to the 80% stenosis, and slopes downward at 90% stenosis to a value of approximately 1.5. *In vitro*, as for SPSOI(3D), the curves 2D proximal and 2D distal are equivalent to the exception of the 90% stenosis at 250 mL/min in which case, at 6D interstenotic distance, the 2D proximal curve increases, and the 2D distal curve remains around 1. At 500 and 750 mL/min (Figs AII-2d, f and Figs AII-3d, f), these curves follow closely and increase more than SPSOI(3D), showing less errors in the approximations than when SP is closer to SOI. The 10D distal curves are once again closer to the theoretical curve than the 2D distal position. The VR values for the 10D distal measurement, however, only increase to values between 4 and 5 at 90% severity, and around 4 for SPSOI(3D), whereas they increased to between 5 and 6 for the single stenosis. Therefore, SP seems to show less influence on the diagnosis of SOI when they

are further apart, yet the VR values still have large errors relative to the single stenosis or to the theoretical curve.

The *blinded* estimations appear closer to the theoretical curve, more so than for the 10D distal measurement position, and differ more from 10D distal at 6D than at 3D interstenotic distance. The better VR estimates may be due to more appropriately placed measurement positions for PSV_1 and PSV_2. The values of VR above the theoretical curve may be due to experimental errors.

4.1.4 SP at 10D Proximal to the SOI

When SP is located 10D proximal to the SOI, the *2D proximal PSV_1 measurement position* is 8D distal to SP. At this measurement position in the *simulations*, the VR at 90% severity and 250 mL/min (Fig AII-4a) is approximately 3.8, resulting in an underestimation error of approximately 15%. This is the best estimation observed for the 2D proximal position at all flow rates and all interstenotic distances for SOI in the presence of a proximal stenosis. The combination of the large distance between SP and SOI and the lower flow rate may contribute to this improved VR. *In vitro* (Figs AII-4b, d, f), the VR estimates are greater at 2D proximal, at equivalent flow rates, than at 3D or 6D interstenotic distances (Figs AII-2b, d, f and Figs AII-3b, d, f). An increase in the VRs was also seen when the interstenotic distance increased from 3D to 6D. Furthermore, as the flow rate increases, the 2D proximal curve appears to approach the same curve as for the single stenosis, with the underestimation errors ranging between approximately 10-30% at 750 mL/min.

The *simulation* curves for the *distal measurement positions* (Figs AII-4a, c, e) are similar to those for interstenotic distances of 3D (Figs AII-2a, c, e) and 6D (Figs AII-3a, c, e). However, for the 10D distal position at 250 mL/min, the curve increases from 1.5 up to almost 2 at 80% severity and decreases to 1.5 for the 90% stenosis. For the 3D interstenotic distance, the curve is almost flat up to 80% and decreases at 90%, and at 6D interstenotic distance the curve is intermediate to the 3D and 10D curves. Therefore, a progressive increase in the slope of this curve is observed as the interstenotic distance increases. Overall, however, the severity estimations are not much improved with interstenotic distance. At 10D interstenotic distance and 250 mL/min,

this measurement position provides better results than the 2D proximal position for severities of approximately 80% or less, yet the 2D proximal position provides better estimates for greater severities. Aside from the curves at 10D distal and 250 mL/min, generally, the distal measurement curves at all interstenotic distances (Figs AII-2a, c, e, Figs AII-3a, c, e, and Figs AII-4a, c, e) are almost flat and the severity estimation errors are very large. *In vitro* (Figs AII-4b, d, f), the curves generally increase exponentially, and the 10D distal measurement position gives results closer to theory than the 2D distal or 2D proximal positions. However, some fluctuations are noted in the severity estimation curves, suggesting the need to repeat such experiments.

The *blinded* VR estimates are the best at a flow rate of 250 mL/min (Fig AII-4b), and are approximately equivalent to those of the 10D distal position as the flow rate increases to 750 mL/min.

4.1.5 Summary for SP Proximal to the SOI

In the simulations, the 10D distal measurement position is best at a flow rate of 250 mL/min for severities up to approximately 80% area reduction of the SOI. In all other cases, the 2D proximal position appears best. *In vitro*, the 10D distal measurement position is best for a fixed position, however, the blinded measurements appear better or equivalent to these last.

4.1.6 SD at 3D Distal to the SOI

When the SOI is followed by a distal stenosis, the distal PSV_1 measurement positions may either be between the two stenoses, or beyond the distal stenosis. An asterisk in the legend of the graphs indicates those positions that are beyond SD.

For the *2D proximal PSV_1 measurement position*, the curves in the *simulations* (Figs AII-5a, c, e) are equivalent to those for the single stenosis (Figs AII-1a, c, e), revealing no effect of SD on the measurement proximal to the SOI, at an interstenotic distance of 3D. On the other hand, i*n vitro* (Figs AII-5b, d, f), SD seems to affect the proximal measurement curve when compared to the single stenosis (Figs AII-1b, d, f), by lowering the VR values at 90% stenosis severities. However, for the other stenosis

severities, the underestimation errors for the single stenosis and SOISD(3D) are approximately equivalent at 30-40%.

For the *distal measurement positions*, in the *simulations* (Figs AII-5a, c, e), the curves are relatively flat with values in the region of 1 at all flow rates, generating large estimation errors. The two distal curves are fairly similar despite the fact that the 2D distal position is situated between the SOI and SD, and the 10D distal position is situated seven diameters beyond SD. *In vitro* (Figs AII-5b, d, f), the 2D distal measurement curve is again approximately flat at all flow rates, leading to large estimation errors of the SOI severity, as in the simulations. This measurement position may be situated within a post-stenotic jet, having little time to dissipate, possibly explaining the flat VR curve. At 10D distal, however, the curves tend to rise and resemble more the 2D proximal curves than the 2D distal curves. This is unlike in the simulations (Figs AII-5a, c, e) where the lack of turbulence does not allow dissipation of the high velocities, distal to SD, by the 10D distal measurement position. The estimation errors at 10D distal appear to be greatest for a flow rate of 250 mL/min, and stenoses in the range of 50 to 80% AR. The best estimations for this measurement position occur at flow rates of 500 mL/min, with errors ranging from 5 to 20% for stenoses of 70 to 90% AR, respectively. The curve is approximately exponential at 250 mL/min, has two points of inflection at 70 and 80% stenosis severities at 500 mL/min, and has 1 point of inflection at 80% severity and 750 mL/min. No explanation seems evident for such a phenomenon, however, the 10D position is situated distal to SD, which may contribute to the variable behaviour of the VR index. Among the fixed measurement positions, the 10D distal position gives the best estimation results, at flow rates of 500 and 750 mL/min and high stenosis severities, otherwise, the 2D proximal measurement position is best.

For the *blinded* measurements, the curve at 250 mL/min clearly gives the best VR estimations. At 500 mL/min, the 10D distal and blinded measurements appear equivalent overall, each position alternately giving the best estimation. At 750 mL/min, the blinded option appears best up to 80% stenosis, after which the curve for the 10D position appears best.

4.1.7 SD at 6D Distal to the SOI

At the *2D proximal PSV_1 measurement position*, the curves in the *simulations* (Figs AII-6a, c, e) are very similar to those for the single stenosis (Figs AII-1a, c, e), as they were for the SOISD(3D) configuration (Figs AII-5a, c, e). *In vitro* (Figs AII-6b, d, f), the SOI 50% AR experiments were not performed due to a lack of time. For the experiments performed, the 2D proximal measurement curve is similar to that of the simulations with an exponential shape, however, the VR values at 90% severity are less than in the simulations at 250 and 500 mL/min. The same trend was observed for SOISD(3D) at all flow rates.

For the *distal measurement positions*, the 2D distal position is situated between the SOI and SD, and the 10D measurement position is distal to SD. In the *simulations* (Figs AII-6a, c, e), the 2D distal curve is flat with a value of approximately 1, and the 10D distal curve increases slightly while crossing the 2D distal curve, as for SOISD(3D). Above 75% AR, the severity estimation at 10D distal (distal to SD) is slightly superior to that at 2D distal (between SOI and SD) for flow rates of 250 and 500 mL/min. The errors in the estimations increase for 10D distal as the flow rate increases. At both interstenotic distances, for SOI in the presence of a distal stenosis, the distal measurement positions are very poor indicators of SOI severity. Consequently, the best fixed measurement position is proximal to SOI. *In vitro*, the 2D distal PSV_1 measurement position has a relatively flat curve. At 10D distal, however, the curve is improved and similar to the proximal measurement position at 500 and 750 mL/min, with errors up to 30% and 35%, respectively. At 250 mL/min, the curve is shifted down relative to the other positions with underestimation errors up to 70%.

The *blinded* measurements show curves that, overall, give the best results with maximum errors of 15-20% at all flow rates.

4.1.8 Summary for SD Distal to the SOI

In this configuration, the 2D proximal PSV_1 measurement position is clearly the best in the simulations. *In vitro*, this position is also best for a flow rate of 250 mL/min, among the fixed positions tested. However, at 500 and 750 mL/min, the 10D distal or the 2D proximal positions appear interchangeable. The blinded measurements, however, result

in better severity estimations under the majority of experimental conditions and stenosis severities.

4.2 Pressure Gradients

In this study, several different pressure measurement positions were considered to observe the behaviour of the pressures as stenosis severity increases, and to evaluate the effect of the pressure recovery on the measured gradient. An example of the pressure curves obtained at different flow rates in the *in vitro* experiments, and showing the pressure loss and recovery taking place along the stenosis, is seen in Figure 23 (page 78) for an 80% AR stenosis. This is useful clinically in understanding the differences between catheter and Doppler pressure gradient measurements. The pressure tap measurements allowed a measurement of the static pressures along the SOI ideally without interfering with the flow. However, the duplex Doppler gradient was also measured using the ATL ultrasound machine by placing the sample volume to measure the PSV within the maximum area reduction of the stenosis to obtain the Simplified Bernoulli estimation of the maximum pressure gradient caused by the SOI. This estimation value is automatically calculated based on the maximum frequency value designated by the technician on the monitor of the instrument. This estimation was noted for future comparisons since, theoretically, the pressure gradient measured at the maximum reduction by catheter is generally the maximum pressure gradient and it corresponds to that measured clinically by duplex Doppler using the Simplified Bernoulli Equation, $\Delta P_{max} = 4*PSV^2$. The minimum, or effective, pressure gradient of the stenosis would be equivalent to that measured clinically by catheter downstream to the stenosis, assuming no stenoses or branching of the artery follow the SOI.

The results for the Bernoulli pressure gradients are omitted to promote clarity in the results, however, it was generally found that these estimations were at least twice as great as the maximum pressure gradients measured using the pressure taps, and in a few cases the gradients were comparable. These discrepancies may be due to the assumptions used in developing the Simplified Bernoulli equation not coinciding with

the actual conditions of the flow in the experiments. Such assumptions are discussed in section 2.1.2. (page 20) of this study.

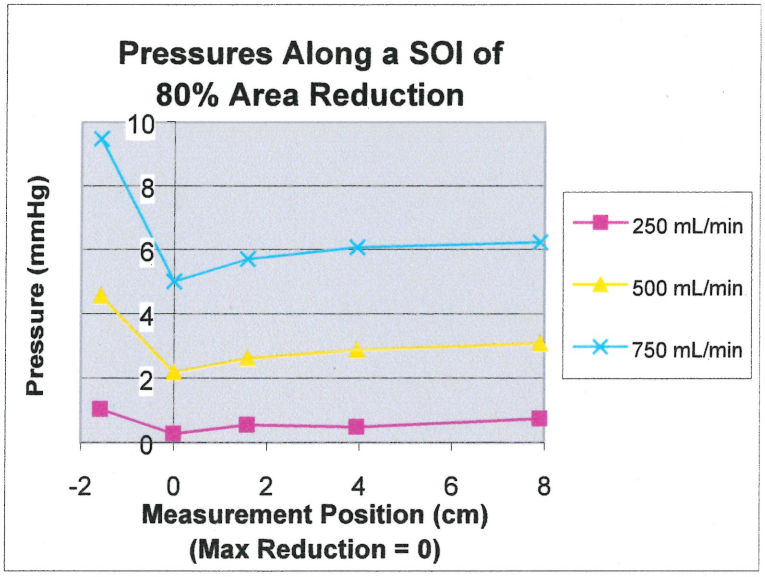

Figure 23. Pressures along a single SOI of 80% AR, showing the pressure drop at the SOI (position 0) and the recovery taking place distal to the SOI. Note how the pressure drop is greatest for the largest flow rate.

4.2.1 Single Stenosis

In the *simulations*, the pressure gradient curves for a single stenosis (Figs AII-7a, c, e) are exponential for all measurement positions, and increase with flow rate. Furthermore, at a given flow rate, the curves at all measurement positions are equivalent. However, the curves diverge slightly and progressively with stenosis severity. That is, at 90% stenosis, there is a slightly larger range in ΔP values with measurement position than at other stenosis severities. The range in values at 90% severity, between all measurement positions, is less than 1 mmHg for a maximum gradient of approximately 3.8 mmHg at 250 mL/min, approximately 1.5 mmHg for a maximum gradient of approximately 13.5 mmHg at 500 mL/min, and approximately 3 mmHg for a maximum gradient of approximately 28 mmHg at 750 mL/min. In the simulations, for all flow rates, the maximum pressure drop calculated relative to the pressure at 2D proximal to the SOI, is found at the maximum reduction of the stenosis. The minimum pressure gradient is found for the furthest measurement position downstream, that is, 10D and even 5D

distal to the stenosis. As could be expected, this minimum pressure drop may reflect the effect of the energy dissipation downstream to the stenosis.

In vitro, the curves are generally exponential (Figs AII-7b, d, f), as in the simulations, however, the pressure gradients are lower than in the simulations. More specifically, the ΔP values at 90% stenosis severity are approximately halved relative to the simulation values. Surprisingly, at 250 mL/min (Fig AII-7b), the pressure gradients corresponding to the maximum reduction seem to have a linear relation with stenosis severity. This may be due to an experimental measurement problem, since these results are unlike those of Qin (Fig AII-7g), which are discussed further in this section. At 90% stenosis, for all flow rates (Figs AII-7b, d, f), the range of values is approximately 1 mmHg for a maximum gradient of approximately 2 mmHg at 250 mL/min, approximately 1 mmHg for a maximum gradient of approximately 7 mmHg at 500 mL/min, and approximately 6 mmHg for a maximum gradient of approximately 19 mmHg at 750 mL/min. Therefore, the curves are slightly more divergent than in the simulations.

In the results of Qin (Figs AII-7g-i), all the curves are exponential, and the curves for the different measurement positions diverge slightly at all flow rates. The gradient values at 90% stenosis severity, however, are slightly greater than in the author's experiments. Furthermore, Qin's results show that the maximum gradients correspond consistently to the measurement position 2D distal to the SOI, rather than at the maximum reduction. This is similar to the author's experiments (Figs AII-7b, d, f) at 250 mL/min, though the two positions are equivalent at 500 mL/min, and at 750 mL/min the maximum gradient is at the maximum reduction. The minimum gradients for Qin are obtained at 5D or 10D distal, as in the author's experiments. Furthermore, the pressure gradients at 90% stenosis are greater than in the author's experiments (Figs AII-7b, d, f). Consequently, the pressure gradient values obtained by Qin are closer to the simulations (Figs AII-7a, c, e) than the author's experiments, although the maximum pressure drop is found at 2D distal rather than at the SOI. More specifically, at 90% stenosis (Figs AII-7g-i), the range of values is approximately 2 mmHg for a maximum gradient of approximately 4.5 mmHg at 250 mL/min, approximately 4 mmHg for a maximum gradient of approximately 14 mmHg at 500 mL/min, and

approximately 9 mmHg for a maximum gradient of approximately 27 mmHg at 750 mL/min.

4.2.2 SP at 3D Proximal to the SOI

In the *simulations* (Figs AII-8a, c, e), the curves are equivalent at all measurement positions, and have an exponential shape. At 90% stenosis severity, the range of values between measurement positions is less than 1 mmHg for a maximum gradient of approximately 3.5 mmHg at 250 mL/min, and is almost the same as for the single stenosis, is approximately 2 mmHg for a maximum gradient of approximately 12 mmHg at 500 mL/min, which is 2 mmHg less than for the single stenosis, and approximately 3 mmHg for a maximum gradient of approximately 25 mmHg at 750 mL/min, again which is 2 mmHg less than for the single stenosis. Therefore, the ΔP values at 90% severity are slightly lower than for the single stenosis simulations. Consequently, the presence of SP seems to have little effect on the pressure drop at SOI relative to the single stenosis pressure drops.

In vitro, the curves at all flow rates (Figs AII-8b, d, f) are equivalent, to the exception of that obtained at the maximum reduction, where the ΔP values are much greater than at the other measurement positions. The curves have an exponential shape at 250 and 500 mL/min (Figs AII-8b, d). However, at 750 mL/min (Fig AII-8c) they have a point of inflection at 80% severity, after which the curves slope downward to generally attain negative gradient values, to the exception of the maximum reduction position. This is an unexpected behaviour that may be due to various experimental problems (pressure tap positioning or angle, curvature of the artery, etc.) since such phenomena are in disagreement with the more in depth results of Qin (see below), which agree with the simulation results. Furthermore, the pressure gradients at SOI generally increase with flow rate, although, again at a flow rate of 750 mL/min, the gradients drop suddenly for a 90% SOI. For this configuration, on the curve of pressure vs. flow rate (not shown), the pressure measured at the 2D proximal measurement position (the reference pressure) was found to be abnormally low for the 90% stenosis at 750 mL/min, consequently reducing all the pressure gradients. Experimental errors may explain this variation, since the results of Qin (Fig AII-8i) show that the gradients

increase with flow rate. Therefore, the gradients at 90% severity and 750 mL/min are ignored. At 250 and 500 mL/min (Figs AII-8b, d), the gradients at 90% severity are only slightly less relative to the single stenosis (Figs AII-7b, d), to the exception of the maximum reduction position. Based on the original curves of pressure at the SOI vs. flow rate, the pressures at the maximum reduction position for the 90% AR appear low relative to the other measurement positions, decreasing as flow rate increases. Therefore, the difference in the pressures at the maximum reduction relative to the reference pressure (2D proximal) will result in greater gradients than for the other positions. This could serve as an explanation for the previous observation, however, it is not clear since this pattern is also seen, though to a lesser degree, for a SOI severity of 80% AR, for which a separate experimental setup was used. Whether these divergences are due to experimental or systematic errors or are valid measurements is unknown and further investigation is necessary. However, the results of Qin (Figs AII-8g-i) show that the curves at all measurement positions converge more or less, are exponential, and that the gradients obtained for a SOI of 90% severity are very similar to the simulations (Figs AII-8a, c, e). Furthermore, the results of Qin show that the measurement position at which the maximum gradients are obtained is 2D distal to the SOI, as for the single stenosis curves obtained by Qin (Figs AII-7g-i), whereas it is found at the maximum reduction in the author's results. The differences in the curves of the author's experiments and those of Qin are remarkable in this stenosis configuration.

4.2.3 SP at 6D Proximal to the SOI

In the *simulations* (Figs AII-9a, c, e), the curves are essentially the same at all measurement positions and at all flow rates. The pressure gradients are the same as when the interstenotic distance is 3D (Figs AII-8a, c, e). The maximum pressure gradient at all flow rates is found at the maximum reduction, and the minimum value is at 5D or 10D distal to the SOI. The divergence of the pressure gradients at 90% severity is less than 1 mmHg at 250 mL/min (Fig AII-9a) for a maximum value of approximately 3.7 mmHg, of approximately 1.5 mmHg at 500 mL/min (Fig AII-9c) for a maximum of approximately 12.5 mmHg, and of approximately 3 mmHg at 750 mL/min (Fig AII-9e) for a maximum of approximately 26 mmHg.

In vitro (Figs AII-9b, d, f), the curves are exponential at all measurement positions, to the exception of the maximum reduction. At this position, the curve appears to have a parabolic tendency, decreasing for stenoses up to 70% reduction, that is, for the 50% stenosis experiment, and then joining the curves of the other measurement positions. This is unlike the interstenotic distances of 3D or 10D, and it occurred most significantly at 500 mL/min. When the interstenotic distance was 3D (Figs AII-8b, d, f), the maximum reduction position diverged rather for stenoses superior to 70%. Therefore, since this parabolic tendency in the curves seems quite isolated, it is believed to be due to experimental errors. The pressure gradients at 90% severity, for all flow rates, are inferior to those in the simulations at LP = 3D or 6D, and superior to those for LP = 3D (Figs AII-8b, d, f). This last is probably because the pressure has a greater distance to recover following SP when LP = 6D. The divergence of the pressure gradients at 250 mL/min is approximately 1 mmHg, for a maximum gradient of approximately 2.9 mmHg, at 500 mL/min is approximately 2.5 mmHg, for a maximum gradient of approximately 9.5 mmHg, at 750 mL/min is approximately 5 mmHg, for a maximum gradient of approximately 22 mmHg.

4.2.4 SP at 10D Proximal to the SOI

In the *simulations* (Figs AII-10a, c, e), the curves are equivalent to those at interstenotic distances of 3D and 6D. Therefore, the additional interstenotic distance of 4D between the stenoses, seems to have no effect on the pressure gradients in the simulations.

In vitro (Figs AII-10b, d, f), the curves are comparable to those in the simulations at all interstenotic distances (Figs AII-8a, c, e, AII-9a, c, e, and AII-10a, c, e). However, at 250 and 750 mL/min, the pressure gradients at 90% severity are slightly higher, and slightly lower, respectively, than in the simulations. At 500 mL/min, these pressure gradients are the same as in the simulations. The *in vitro* pressure gradients are greater at 10D than at 3D or 6D interstenotic distances (Figs AII-8b, d, f, and AII-9b, d, f).

At a given flow rate, the *in vitro* curves are superimposed at all measurement positions, as for the single stenosis (Figs AII-7b, d, f). The gradients, however, are doubled at 250 and 500 mL/min (Figs AII-10b, d), and slightly greater at 750 mL/min

(Fig AII-10f) relative to the author's single stenosis experiments, yet are in the same range of values as the single stenosis results of Qin (Figs AII-7g-i). Therefore, it is believed that the discrepancies between the SPSOI(10D) pressure gradients and the author's single stenosis values are due to a lack of experimental data which could in fact bring the values closer together with the averaging out of certain experimental errors.

4.2.5 Summary for SP Proximal to the SOI

The presence of SP proximal to SOI (Figs AII-8a, c, e, AII-9a, c, e, and AII-10a, c, e) does not appear to affect the pressure gradients in the *simulations*, relative to the single stenosis (Figs AII-7a, c, e). *In vitro*, however, the pressure gradients taken at the majority of positions seem to increase with interstenotic distance at 250 and 500 mL/min (Figs AII-8b, d, AII-9b, d, and AII-10b, d). Put aside the results that appear erroneous, the pressure gradients at SOI generally increase with interstenotic distance and with flow rate, though apparently more at flow rates of 250 and 500mL/min.

4.2.6 SD at 3D Distal to the SOI

When a distal stenosis is in the presence of the SOI, the distal pressure measurement positions may either be between the two stenoses, or beyond the distal stenosis. When the measurement is beyond SD, an asterisk marks the position in the legend of the graphics (Figs AII-11 and AII-12). These measurement positions are investigated assuming that, in a clinical situation, the presence of SD is unknown, though this may not necessarily be the case. It is also useful to verify the combined effect of the stenoses on the pressure drop.

In the *simulations* (Figs AII-11a, c, e), the curves are all exponential, though there appears to be a divergence in those where the pressure is measured distal to SD and those proximal to SD. The maximum reduction and 2D distal curves are very similar, as are the 5D and 10D distal curves. Both sets of curves cross over at a stenosis severity just below 80%, perhaps indicating at which point the SOI becomes more severe than the distal stenosis. It is interesting to notice that the pressure gradient 2D distal to the SOI and 5D distal to the SOI (2D distal to SD) are equivalent when the severities of SOI and SD are the same (75%). Once the SOI becomes more severe than

SD, the pressure gradients at SOI (Max Red or 2D distal to SOI) become greater than those across the two stenoses combined (5D or 10D distal to SOI). Whether this is significant is still unknown. The possible existence of turbulence is not considered in these simulations. This is evident since the second stenosis, so closely placed to the SOI, should have the effect of partially breaking the flow or jet from the SOI, and that the pressure should re-establish much earlier on than in the absence of a distal stenosis, that is, for a single stenosis. However, when comparing the simulation curves for the single stenosis (Figs AII-7a, c, e) and SOISD(3D) (Figs AII-11a, c, e), only the 5D and 10D distal measurement positions seem affected by the presence of SD. All flow phenomena that occur proximal to SD, appear unaffected by SD, despite the fact that it is a critical stenosis. These simulations may, therefore, be limited in establishing the effects of the complex flow on the pressure gradients.

In vitro (Figs AII-11b, d, f), the curves do not resemble those in the simulations (Figs AII-11a, c, e), and they are not exponential. Apart from the maximum reduction curve, the curves increase up to 70% stenosis where there is a point of inflection. Then, a second point of inflection is observed at 80% severity. Beyond 80% severity, the curves increase once again. The maximum reduction curve decreases for stenosis severities up to approximately 75%, and then increases along with the other measurement positions, having an almost parabolic shape. The pressure gradients increase globally with stenosis severity. The gradients *in vitro* (Figs AII-11b, d, f), however, are generally much lower than in the simulations (Figs AII-11a, c, e). The fact that SD had no important effect on the gradient at SOI in the simulations, therefore, does not seem very realistic, and further, more complex simulations taking into account the effect of turbulence should be performed to obtain more realistic flow conditions.

4.2.7 SD at 6D Distal to the SOI

In the *simulations* (Figs AII-12a, c, e), the curves are all exponential, as for SOISD(3D). At a given flow rate, the curves for the different measurement positions follow one another, except for 10D distal which, once again, is positioned distal to SD. This was also seen for the 5D and 10D measurement positions for SOISD(3D) (Figs AII-11a, c, e). As the flow rate increases from 250 to 500 and to 750 mL/min, the pressure

gradients at 90% stenosis severity for 2D and 5D distal increase from approximately 3.5 mmHg to 12 mmHg and to 26.5 mmHg, respectively. These curves are equivalent to those for the single stenosis (Figs AII-7a, c, e), and to that at 2D distal for SOISD(3D). The pressure gradients for 5D distal at 90% severity, are greater for SOISD(6D) than for SOISD(3D).

In vitro (Figs AII-12b, d, f), the curves for the different measurement positions are very similar for all flow rates. At 250 mL/min, the curves appear to be slightly parabolic, whereas at 500 and 750 mL/min, they are exponential. Though the pressure gradient values at 90% stenosis (Figs AII-12b, d, f) are inferior to those in the simulations (Figs AII-12a, c, e), they are greater than for the *in vitro* single stenosis (Figs AII-7b, d, f). Therefore, relative to a single stenosis, a stenosis 6D distal to SOI would appear to increase the pressure gradient measured across SOI, and this, much more than for a 3D distal stenosis (Figs AII-11b, d, f). This would not appear to be the case based on the simulations, and further investigations are necessary.

4.2.8 Summary for SD Distal to the SOI

In the simulations, the pressure gradients are exponential at both interstenotic distances. Furthermore, the curves are equivalent at all measurement positions to the exception of those beyond SD, where the gradients diverge from the other measurement positions. That is, the gradients are higher for severities inferior to 80%, and lower for severities greater than 80%. This was also found by Tranulis et al.[130] in similarly conducted simulations. *In vitro*, the curves are difficult to interpret for an interstenotic distance of 3D, and are exponential at an interstenotic distance of 6D, though the values are lower than in the simulations. Therefore, there appears to be a greater effect on the pressure gradients as SD approaches the SOI.

4.3 Results Summary

The single stenosis 2D proximal and 10D distal VR curves resemble most closely the theoretical curve of VR relative to those for the other stenosis configurations (Figs AII-

2-AII-6). No theoretical curve, based on the Navier-Stoke equations, was developed in this thesis.

4.3.1 Proximal Stenosis

In the simulations for the 2D proximal measurement position (a proximal position as assumed in developing the VR theory), the presence of a proximal stenosis decreases the VR values measured at the SOI, relative to the single stenosis. The lower VRs calculated may be due to increased PSV_1 values created by the presence of the proximal critical stenosis. However, as LP increases, the VR appears to increase mostly at 250 mL/min, less at 500 mL/min, and negligibly at 750 mL/min. At LP = 10D, the VR was inferior by at least 2 at all flow rates. *In vitro,* the author's experiments also show that the proximal stenosis decreases the VR, and this is confirmed by the results of Qin. However, as LP increases from 3D to 10D, the VR increases at all flow rates. At LP = 10D, the VR curves are more comparable to the single stenosis curves than in the simulations. Indeed, in the simulations they remain inferior at all interstenotic distances, probably due to the absence of turbulence in the model.

For the distal measurement positions, the simulations show that SP globally appears to have little effect on the VR relative to the single stenosis, and under all interstenotic and flow conditions. *In vitro*, the author's and Qin's results show that the 2D distal measurement position does not allow the detection of SOI as the curve remains at a value of approximately 1 under all conditions, as for the single stenosis. At the 10D distal measurement position and all flow rates, there is a small decrease in VR upon the introduction of SP at 3D proximal for the author's experiments. The results of Qin show a similar tendency. As LP increases, the VRs globally appear to slightly increase, and resemble the curves for the single stenosis. Therefore, in the presence of a proximal stenosis at a somewhat large interstenotic distance, the very distal PSV_1 measurements provide among the best VR values. The blinded measurements, however, appear best under most experimental conditions. This is probably due to a more precise positioning of PSV_1 and PSV_2 to obtain the actual maximum velocities along the artery, as this position may vary with stenosis configuration and severities. However, these

measurements are more subjective than at the fixed measurement positions, and may not always obtain better severity estimates.

For the pressure gradients at SOI in the simulations, the addition of SP at LP = 3D has little effect at 250 mL/min, and slightly reduces the gradients at 90% stenosis for flow rates of 500 and 750 mL/min relative to the single stenosis. The curves all remain exponential. As LP increases to 10D, the gradients increase and finally return to similar values as for the single stenosis. Under any given conditions, the different PSV_1 measurement positions appear to give approximately the same pressure drop curves, the maximum reduction position giving slightly greater pressure gradients than the other positions.

In vitro, the addition of SP at LP = 3D tends to decrease the recorded pressure drop across SOI. The effect is almost negligible at 250 mL/min for the majority of PSV_1 measurement positions, but is accentuated as the flow rate increases. At 750 mL/min and SP at LP = 3D, the author's results appear erroneous, as they slope downwards whereas the results of Qin show exponential curves and the average gradients are slightly lower only at 500 mL/min and otherwise remain the same. However, the range of the error bars for SPSOI(3D) are visibly lower at all flow rates than for the single stenosis. As the interstenotic distance increases, the pressure gradients increase and surpass those for the single stenosis at equivalent flow rates. At 250 and 500 mL/min and LP = 10D, the pressure gradients have doubled relative to the single stenosis. At 750 mL/min, the pressure gradients are moderately greater than for the single stenosis. Overall, there is much greater variability in the pressure drop curves in this configuration than are shown in the simulations. The pressure recovery distal to SOI, for LP = 3D and 6D, appears to affect the gradient measured, to a degree which depends on the measurement position chosen. Furthermore, the interstenotic distance appears to be an important factor in the pressure gradient measured across SOI. SP creates perturbations in the flow proximal to SOI, and the flow conditions that are found near SOI will depend on whether the entrance length to SOI is great enough for the flow to redevelop.

4.3.2 Distal Stenosis

In the simulations, the addition of a stenosis distal to the SOI appears to have no effect on the VRs for the 2D proximal measurement position. Recall that a proximal position for the measurement of PSV_1 is specified in the development of the VR theory. Therefore, the addition of SD does not affect the VR, relative to a single stenosis, when PSV_1 is measured as in the theory. The 2D distal position shows no change in the VR relative to the single stenosis, though the curves are flat and are very poor indicators of stenosis severity. The 10D distal position occasionally results in VRs which are better than at 2D distal, however, the stenosis estimation errors remain great. On the other hand, the VRs at 2D proximal in the *in vitro* experiments decrease considerably at 90% stenosis upon the addition of SD at LD = 3D. As the interstenotic distance increases to 6D, the VRs increase once again, though have not yet attained those for the single stenosis. The single stenosis results of Qin show comparable VRs to the author's. Experiments with the addition of a distal stenosis, however, were not performed by Qin.

For the distal measurement positions, the simulations show that SD has no effect on VR relative to the single stenosis when the PSV_1 measurement is taken at 2D distal to SOI. However, no stenosis is estimated since the curve remains flat with a value of approximately 1 under all conditions. At the 10D distal measurement position, the curves change slightly with the addition of SD, but very little with interstenotic distance or flow rate, and the underestimation errors remain very large. *In vitro*, the 2D distal measurement position is more or less the same as for the single stenosis. The 10D distal position, however, gives inferior VR values relative to the single stenosis, upon the addition of SD at 3D, especially for severities greater than 80%. Aside from the 2D distal measurement position, the VRs appear to improve as LD increases, especially for severities greater than 80%, though do not yet return to the values for the single stenosis when LD = 6D. It is interesting to note that the 10D distal curves are relatively flat in the simulations for the single stenosis, and for all cases of SPSOI and SOISD, but exponential *in vitro*. The *in vitro* results of Qin for the single stenosis also show an exponential shape for the 10D distal VR curve. This is most likely since the jet created for the high stenosis severities distally is dissipated *in vitro* at 10D distal to SOI. Consequently, the VRs increase. At lower stenosis severities, the lack of turbulence in

the simulations appears less essential for the VR. The blinded measurements appear best under all conditions, though the VR values are also reduced when SD is present. However, these measurements appear to return to values comparable to the single stenosis at an interstenotic distance of 6D. Therefore, either a proximal or a very distal PSV_1 measurement position seems acceptable. Otherwise, the blinded measurements consistently provide the best results. As mentioned previously, the blinded measurements may allow more precise localization of the peak systolic velocities along the artery, especially since the positioning of the PSVs may change with the stenosis configuration.

For the pressure gradients, the simulations show little variation relative to the single stenosis, with interstenotic distance or measurement position, and a large increase in gradients with flow rate, as could be expected. The only variations in the curves arise when the measurement position distal to SOI is also beyond SD, that is, the measurement includes both SOI and SD. The gradients measured as such, when SOI is less than 80% severity, have similar values to those measured for the single stenosis at approximately 75% severity. This statement is valid for SOISD (LD = 3D and 6D), when SOI is between 30% and 80% and SD is 75%. For SOI greater than 80% severity, the pressure gradients are inferior to those measured for an equivalent single stenosis. This suggests that the presence of SD may help in breaking the jet distal to a severe SOI allowing the pressure to recover more rapidly and, consequently, reduces the gradient. The greater distal stenosis, therefore, appears to take precedence on the gradient in the simulations where the distal pressure measurement (P2) is beyond SD. The gradients obtained when P2 is between SOI and SD, however, are similar to the gradients for SOI as a single stenosis. This would suggest that the gradient for SOI must be measured by including only SOI, resulting in values as though SOI were the only stenosis present. *In vitro*, however, the situation is not as simple since certain flow phenomena come into play to create much different pressure gradients across SOI when SD is present, particularly when the stenoses are at a distance of 3D. Compared to the *in vitro* gradients at 3D, the *in vitro* gradients at LD = 6D are much closer to the simulations for interstenotic distances of 3D and 6D, and to the *in vitro* and simulation curves for the single stenosis.

CHAPTER 5.

Conclusion

In reference to the simulation and *in vitro* experiments performed, the VRs at all measurement positions for the single stenosis are inferior to the theoretical values. For the multiple stenoses, the VRs appear more influenced by the measurement position of PSV_1 than by the interstenotic distance. In addition, at a given measurement position, the VR seems fairly independent of flow rate in all stenosis configurations. However, the interstenotic distance appears to come into play a little more than the flow rate, whether the adjacent stenosis is proximal or distal. Overall, the greatest interstenotic distances considered show *in vitro* curves most similar to those for the single stenosis. However, for a proximal stenosis, a PSV_1 measurement position very distal to SOI seems most appropriate. For a distal stenosis, the proximal measurement position seems best, as in the theoretical situation. Otherwise, obtaining PSV_1 and PSV_2 blindly appears to consistently result in among the most acceptable VR curves for all stenosis configurations, as this probably allows the best positioning along the artery for the measurement of the peak systolic velocities.

Based on the simulations, the pressure gradients at SOI appear most influenced by flow rate. *In vitro*, the pressure gradients seem most affected, and are reduced, when the proximal or distal stenosis is at the shortest interstenotic distance considered, i.e. 3D. As the interstenotic distance increases, this effect becomes almost negligible since the gradients increase. Furthermore, at large interstenotic distances, the pressure gradients vary less with measurement position and are most similar to the simulations. In the author's results, the pressure gradients appear most consistent when the second pressure measurement is taken distal to the SOI, and not at the maximum reduction. However, the results of Qin show that all measurement positions are approximately equivalent.

In the literature[117,118] mentioned in section 2.3 (page 36), the ΔP values quoted correspond to single short stenoses in the common or external iliac arteries of patients with occlusive artery disease. Assuming the stenoses are severe, these gradients may be compared to those obtained experimentally in the present study. Furthermore, it is assumed that physiological flow rates and vessel sizes are comparable to those used in the present study. Referring to Table I (page 46), it is clear that the pressure gradients obtained experimentally for the severe stenoses in the present study correspond to the ranges of mean pressure gradients obtained from the patients. However, the maximum pressure gradients in Table I (page 46) are greater than those obtained in the present study. Therefore, the results for the pressure gradients appear reasonable, and discrepancies in these values could be due to factors such as the arterial size, peripheral resistance[140], flow rate[25], and variability in the stenosis severities, as well as other factors. Consequently, pressure gradients should not be the only criteria on which is based the evaluation of a stenosis[25].

For the multiple stenoses, few studies have been performed for measuring the pressure gradients across a stenosis of interest. Young[140] remarked that whether or not the effect of multiple stenoses can be treated as merely the sum of their individual effects depends on the severity of the stenosis, the Reynolds number, and the spacing. However, Young concluded that no simple criteria can be given for assessing the effect of multiple stenoses, though the effects are additive in some sense so that several non-critical stenoses can combine to give a critical stenosis[140]. The *in vitro* results from the present study show that no significant effect is observed on the pressure gradients upon the addition of a stenosis 3D or 6D distal to the SOI, whether the gradients are measured simply across SOI or across both SOI and SD. For SOI in the presence of a proximal stenosis, the gradients across both stenoses were not investigated. Furthermore, in all experiments, the adjacent stenosis considered was always critical at 75% area reduction and further investigations are necessary to establish the cumulative effect of two non-critical stenoses.

Typically, it has been found that under resting flow conditions, a lumen area reduced by approximately 80% or more may have a significant effect on flow[3,140]. As the flow rate across the stenosis decreases, the pressure gradients will also decrease, as

could be seen in the present study by comparing the pressure gradients at the three different flow rates. The effect of a reduced flow rate may also explain the lower pressure gradients recorded for severe SOIs when following a severe proximal stenosis. More precisely, instead of ΔP increasing exponentially as for the single stenosis, the curves appear much more linear. McWilliams et al.[86] noted that pressure gradients alone were not necessarily accurate indicators of stenosis severity, especially in low flow conditions created across a severely constricted artery. Furthermore, not only does this affect the pressure gradients, but also the VR. Allard et al.[3] found that such low flow conditions caused a SOI to be detected with lower sensitivity, using the VR, when following a severe or an almost occluded stenosis, than if the SOI was in the presence of a distal stenosis. Indeed, our results have shown lower VR values for the SOI when in the presence of a severe proximal stenosis than if alone or in the presence of a distal stenosis.

The discrepancies in the pressure gradient results obtained in the author's experiments and those of Qin may be explained by systematic errors induced by the experimental setup. As the author's experiments progressed, the plexiglass container in which the agar solution was poured, bowed little by little due to the heat of the solution and due to the melting process of the cerrolow arterial cast. This occasionally caused the solidified gel to separate from the container and could cause leaks in the model. For the experiments of Qin, new containers were fabricated, which could have led to the different experimental values obtained. Discrepancies between the simulations and the *in vitro* experiments may have arisen due to the non-ideal conditions in the *in vitro* experiments. The simulations were highly idealized, factors such as turbulence being ignored. Furthermore, inexact vessel sizes or stenosis area reductions in the *in vitro* model, as well as possible slight curvatures in the vessel due to minor bending of the cerrolow arterial cast when the tissue mimic solution was poured into the model occurred occasionally, and may have contributed to experimental errors. Such errors would be masked by repeating the experiments and averaging the results such as in the experiments of Qin. Generally, however, the author's results fall within the range of the error bars on the graphs of Qin. Errors may have also arisen due to slight variations in the fluid viscosity, density, or flow rate from one experiment to the next, and from those

values specified in the simulations. Also, the flow in the *in vitro* experiments may have been perturbed before entering the first stenosis due to difficulties in fabricating the phantom, or due to the pressure taps along the SOI. Therefore, various factors come into play in the success of such experiments.

Given that clinical diagnoses of PVD are only practiced upon the presence of clinical symptoms, which in turn are usually present once the stenoses are severe (>75% area reduction), the results of this study are most pertinent for stenoses greater than 75%, as discussed in Chapter 4. However, two non-critical stenoses in the same arterial segment can create symptoms as though a critical stenosis was present[140]. Such conditions should be verified, that is, the same studies with SP and SD as sub-critical stenoses should be performed to verify the accuracy of VR under such conditions. Pulsatile flow conditions should also be examined, as the hemodynamics involved may change quite dramatically. Cassanova et al.[23] found that significant flow disorder was created by mild stenoses in pulsatile flow when none was present in steady flow. The use of a non-Newtonian fluid, such as blood, should also be investigated as it has been shown that this blood property may influence the hemodynamic behaviour of the fluid, namely by reducing the pressure gradients and the flow reversal zones[126]. Furthermore, Young[140] remarked that which hemodynamic criteria best reflect the importance of a stenosis is difficult to obtain, especially in the context of serial stenoses. Though the indices used in the present study appear reasonable when the proper measurement positions are chosen, further studies should be performed under different geometrical conditions to assure that such indices obtain consistent results. Furthermore, the combination of two indices such as the VR and the pressure gradient may give further insight into the severities of the stenoses that are difficult to diagnose. However, more experimental data and statistical analysis is required to justify such a conclusion. Finally, since the accuracy of Doppler US may be impaired due to flow phenomenon, angle malcompensation[118], and depending on the measurement position chosen, the presence of turbulence should also be investigated under various stenosis configurations and various Reynold's numbers, by simulation and *in vitro* experiments.

In conclusion, this study has shown that the presence of a severe stenosis proximal or distal to a stenosis of interest may affect the accuracy of the VR value

relative to the theoretical case, and with respect to an isolated stenosis. This was supported by the VR values obtained *in vitro* for the single stenosis that were lower than in the theoretical situation. In consequence, large estimation errors may arise when calculating the stenosis severity corresponding to the VR, and improper diagnoses could be established. Consequently, clinicians should attempt to verify the presence of an adjacent stenosis and adjust the PSV_1 measurement location accordingly. That is, when a proximal stenosis is present, PSV_1 should be measured at a site blindly located as distal to the stenosis of interest as possible, while remaining within the same arterial segment. When a distal stenosis is present, a blindly located proximal PSV_1 measurement appears most accurate, as for the case of a single stenosis. If this is not possible, the measurement should be taken as distal to the stenosis of interest as possible to reduce the effects of the post-stenotic phenomena on the measurement. Notwithstanding, stenosis severity estimation errors may remain large and a second clinical index such as the pressure gradient could be of use to ensure the diagnosis. The pressure gradient appears to be a consistent index under the experimental conditions studied. However, more complex conditions should be studied, by simulation and *in vitro*, to closer resemble the blood flow conditions present in patients attained by Peripheral Vascular Disease.

BIBLIOGRAPHY

[1] Ahmed, S. A. and Giddens, D. P., "Pulsatile poststenotic flow studies with laser Doppler anemometry," *Journal of Biomechanics*, vol. 17, no. 9, pp. 695-705, 1984.

[2] Allard, L., Cloutier, G., and Durand, L. G., "Doppler velocity ratio measurements evaluated in a phantom model of multiple arterial disease," *Ultrasound in Medicine & Biology*, vol. 21, no. 4, pp. 471-480, 1995.

[3] Allard, L., Cloutier, G., Guo, Z., and Durand, L. G., "Review of the assessment of single level and multilevel arterial occlusive disease in the lower limbs by duplex ultrasound," *Ultrasound in Medicine & Biology*, vol. 25, no. 4, pp. 495-502, 1999.

[4] Aly, S., Jenkins, M. P., Zaidi, F. H., Coleridge Smith, P. D., and Bishop, C. C., "Duplex scanning and the effect of multisegmental arterial disease on its accuracy in lower limb arteries," *European Journal of Vascular & Endovascular Surgery*, vol. 16 pp. 345-349, 1998.

[5] Archie, J. P. J., "Analysis and comparison of pressure gradients and ratios for predicting iliac stenosis," *Annals of Vascular Surgery*, vol. 8 pp. 271-280, 1994.

[6] Arnold, J. A., Modaresi, K. B., Thomas, N., Taylor, P. R., and Padayachee, T. S., "Carotid plaque characterization by duplex scanning: Observer error may undermine current clinical trials," *Stroke*, vol. 30, no. 1, pp. 61-65, 1999.

[7] Aronow, W. S. and Ahn, C., "Prevalence of coexistence of coronary artery disease, peripheral arterial disease, and atherothrombotic brain infarction in men and women greater-than-or-equal-to 62 years of age," *American Journal of Cardiology*, vol. 74, no. 1, pp. 65-65, 1994.

[8] Bascom, P. A. J., Cobbold, R. S. C., Law, Y. F., and Johnston, K. W. Problems in the quantitative assessment of pulsed Doppler spectra. Ann Inter Conf IEEE Eng Med Biol Soc 12[2], 557-559. 1990.

[9] Bascom, P. A. J., Cobbold, R. S. C., and Roelofs, B. H. M., "Influence of spectral broadening on continuous wave Doppler ultrasound spectra: A geometric approach," *Ultrasound in Medicine & Biology*, vol. 12, no. 5, pp. 387-395, 1986.

[10] Bascom, P. A. J., Johnston, K. W., Cobbold, R. S. C., and Ojha, M., "Defining the limitations of measurements from Doppler spectral recordings," *Journal of Vascular Surgery*, vol. 24 pp. 34-45, 1996.

[11] Beach, K. W., "The evaluation of velocity and frequency accuracy in ultrasound duplex scanners," *Journal of Vascular Technology*, vol. 14, no. 5, pp. 214-220, 1990.

[12] Bergqvist, D. and Karacagil, S., "Femoral artery disease," *Lancet*, vol. 343 pp. 773-778, 1994.

[13] Berguer, R. and Hwang, N. H. C., "Critical arterial stenosis: A theoretical and experimental solution," *Annals of Surgery*, vol. 180 pp. 39-50, 1974.

[14] Brewster, D. C., "Clinical and anatomical considerations for surgery in aortoiliac disease and results of surgical treatment," *Circulation*, vol. 83, no. suppl. I, pp. I-42-I-52, 1991.

[15] Bronzino, J., *The biomedical Engineering handbook* CRC Press, 1998.

[16] Brooks, D. E., Goodwin, J. W., and Seaman, G. V. F., "Interactions among erythrocytes under shear," *Journal of Applied Physiology*, vol. 28, no. 2, pp. 172-177, 1970.

[17] Brown, A. L. and Juergens, J. L., "Arteriosclerosis and atherosclerosis," in Allen, E. V. (ed.) *Peripheral vascular disease* Philadelphia: Saunders, 1972, pp. 57-66.

[18] Burton, A. C., "Kinetic energy in the circulation; streamline flow and turbulence; measurement of arterial pressure," *Physiology and biophysics of the circulation* 2 ed. Chicago: Year Book Medical Publishers, 1972, pp. 104-114.

[19] Caro, C. G., Fitz-Gerald, J. M., and Schroter, R. C. Atheroma and arterial wall shear observation, correlation and proposal of a shear dependent mass transfer mechanism for atherogenesis. Proceeding Royal Society London 177, Ser. B, 109-159. 1971.

[20] Carpenter, J. P., Lexa, F. J., and Davis, J. T., "Determination of sixty percent or greater carotid artery stenosis by duplex Doppler ultrasonography," *Journal of Vascular Surgery*, vol. 22 pp. 697-705, 1995.

[21] Carroll, B. A., "Carotid sonography," *Radiology*, vol. 178 pp. 303-313, 1991.

[22] Carter, S. A., "Response of ankle systolic pressure to leg exercises in mild or questionable arterial disease," *New England Journal of Medicine*, vol. 287 pp. 578-582, 1972.

[23] Cassanova, R. A. and Giddens, D. P., "Disorder distal to modeled stenoses in steady and pulsatile flow," *Journal of Biomechanics*, vol. 11 pp. 441-453, 1978.

[24] Cezeaux, J. L., Austin, V., Hoseinipour, M. C., Ward, K. A., and Zimmer, S., "The effects of shear stress and metastatic phenotype on the detachment of transformed cells," *Biorheology*, vol. 28 pp. 195-205, 1991.

[25] Chiang, H. T., Lin, S. L., Hwang, D. Y., Wang, S. P., and Chang, M. S. Different pressure gradients can be produced in a fixed stenosis-an in vitro study. Clinical Cardiology 16, 797-800. 1993.

[26] Cloutier, G. and Qin, Z., "Ultrasound backscattering from non-aggregating and aggregating erythrocytes - A review," *Biorheology*, vol. 34, no. 6, pp. 443-470, 1997.

[27] Cloutier, G., Shung, K. K., and Durand, L. G., "Experimental evaluation of intrinsic and nonstationary ultrasonic Doppler spectral broadening in steady and pulsatile flow loop models," *IEEE Transactions on Ultrasonics, Ferroelectrics, & Frequency Control*, vol. 40, no. 6, pp. 786-795, 1993.

[28] Comolet, R., *Biomécanique circulatoire* Paris: Masson, 1984.

[29] Criqui, M. H., Fronek, A., Barett-Conner, E., Klauber, M. R., Gabriel, S., and Goodman, D., "The prevalence of peripheral arterial disease in a defined population," *Circulation*, vol. 71 pp. 510-515, 1985.

[30] Criswell, B. K., Langsfeld, M., Tullis, M. J., and Marek, J., "Evaluating institutional variability of duplex scanning in the detection of carotid artery stenosis," *American Journal of Surgery*, vol. 176, no. 6, pp. 591-597, 1998.

[31] Cronenwett, J. L., Warner, K. G., Zelenock, G. B., Whitehouse, W. M. Jr., Graham, L. M., Lindenaur, M., and Stanley, J. C., "Internittent claudication: current results of nonoperative management," *Archives of Surgery*, vol. 119 pp. 430-436, 1984.

[32] Crouse, J. R. and Thompson, C. J., "An evaluation of methods for imaging and quantifying coronary and carotid lumen stenosis and atherosclerosis," *Circulation*, vol. 87, no. Suppl II, pp. II-17-II-33, 1993.

[33] Das, B., Johnson, P. C., and Popel, A. S., "Computational fluid dynamic studies of leukocyte adhesion effects on non-Newtonian blood flow through microvessels," *Biorheology*, vol. 37, no. 3, pp. 239-258, 2000.

[34] Davies, P. F., Barbee, K. A., Volin, M. V., Rotewshyj, A., Chen, J., Joseph, L., Griem, M. L., Wernick, M. N., Jacobs, E., Polacek, D. C., DePaola, N., and Barakat, A. I., "Spatial relationships in early signaling events of flow-mediated endothelial mechanotransduction," *Annual Review of Physiology*, vol. 59 pp. 527-549, 1997.

[35] Davies, P. F., Dewey, C. F., Jr., Bussolari, S. R., Gordon, E. J., and Gimbrone, M. A. Jr., "Influence of hemodynamic forces on vascular endothelial function: *in vitro* studies of shear stress and pinocytosis in bovine aortic cells," *Journal of Clinical Investigation*, vol. 73 pp. 1121-1129, 1984.

[36] Deshpande, M. D., Giddens, D. P., and Mabon, R. F., "Steady laminar flow through modeled vascular stenoses," *Journal of Biomechanics*, vol. 9, no. 4-A, pp. 165-174, 1976.

[37] Dewey, C. F., Jr., Bussolari, S. R., Gimbrone, M. A. Jr., and Davies, P. F., "The dynamic response of vascular endothelial cells to fluid shear stress," *Journal of Biomechanical Engineering*, vol. 103 pp. 177-185, 1981.

[38] Douville, Y., Johnston, K. W., Kassam, M., Zuech, P., Cobbold, R. S. C., and Jares, A., "An *in vitro* model and its application for the study of carotid Doppler spectral broadening," *Ultrasound in Medicine & Biology*, vol. 9, no. 4, pp. 347-356, 1983.

[39] Drenckhahn, D. and Ness, W., "The endothelial contractils cytoskeleton," in Born, G. V. R. and Schwartz, G. (eds.) *Vascular endothelium, Physiology, Pathology and Therapeutic Opportunities* Germany: Schattauer, stuttgart, 1997, pp. 1-25.

[40] Drumel, M. and Kuiken, G. D. C., "Steady flow through a double converging and diverging tube model for mild coronary stenosis," *Transactions ASME Biomechanical Engineering*, vol. 111 pp. 212, 1989.

[41] Eskin, S. G., Ives, C. L., McIntire, L. V., and Navarro, L. T., "Response of cultured endothelial cells to steady flow," *Microvascular Research*, vol. 28 pp. 87-94, 1984.

[42] Evans, D. H., McDicken, W. N., Skidmore, R., and Woodcock, J. P., *Doppler Ultrasound. Physics, Instrumentation, and Clinical Applications*, 1 ed. Chichester, New York, Brisbane, Toronto, Singapore: John Wiley & Sons, 1989, pp. 1-287.

[43] Faccenda, F., Usui, Y., and Spencer, M. P., "Doppler measurement of the pressure drop caused by arterial stenosis: An experimental study: A case report," *Angiology*, vol. 36, no. 12, pp. 899-905, 1985.

[44] Falk, E., Shah, P. K., and Fuster, V., "Pathogenesis of plaque disruption," in Fuster, V., Ross, R., and Topol, E. J. (eds.) *Atherosclerosis and coronary artery disease* Philadelphia: Lippincott-Raven, 1996, pp. 592-510.

[45] Farrar, D. J., Green, H. D., and Peterson, D. W., "Noninvasively and invasively measured pulsatile Haemodynamics with graded arterial stenosis," *Cardiovascular Research*, vol. 13 pp. 45-57, 1979.

[46] Forestrom, R. J., Voss, G. O., and Black, P. L., "Fluid dynamics of the particle (Platelets) deposition on filtering wall," *ASME*, vol. 5 pp. 73-W, 1973.

[47] Forrester, J. H. and Young, D. F., "Flow through a converging-diverging tube and its implications in occlusive vascular disease I. Theoretical development," *Journal of Biomechanics*, vol. 3, no. 3, pp. 297-305, 1970.

[48] Forrester, J. H. and Young, D. F., "Flow through a converging-diverging tube and its implications in occlusive vascular disease II. Theoretical and experimental results and their implications," *Journal of Biomechanics*, vol. 3, no. 3, pp. 307-316, 1970.

[49] Fowkes, F. G. R., "Epidemiology of atherosclerotic arterial disease in the lower limbs," *European Journal of Vascular Surgery*, vol. 2 pp. 283-291, 1988.

[50] Fox, J. A. and Hugh, A. E., "Localization of atheroma: A theory based on boundary layer separation," *British Heart Journal*, vol. 28, no. 3, pp. 383-399, 1966.

[51] Fry, D. L., "Acute vascular endothelial changes associated with increased blood velocity gradients," *Circulation Research*, vol. 22, no. 2, pp. 165-197, 1968.

[52] Giddens, D. P., Zarins, C. K., and Glagov, S., "The role of fluid mechanics in the localization and detection of atherosclerosis," *Journal of Biomechanical Engineering*, vol. 115, no. 11, pp. 588-594, 1993.

[53] Glagov, S., Weisenberg, E., Zarins, C. K., Stankunavicius, R., and Lolettis, G. J., "Compensatory enlargement of human atherosclerotic coronary arteries," *New England Journal of Medicine*, vol. 316 pp. 1371-1375, 1987.

[54] Golledge, J., "Lower-limb arterial disease," *Lancet*, vol. 350, no. 9089, pp. 1459-1465, 1997.

[55] Gordon, T. and Kannel, W. B., "Predisposition to atherosclerosis in the head, heart, and legs. The Framingham study," *The Journal of the American Medical Association*, vol. 221, no. 661, pp. 666, 1972.

[56] Gotlieb, A. I. and Langille, B. L., "The role of rheology in atherosclerotic coronary artery disease," in Fuster, V., Ross, R., and Topol, E. J. (eds.) *Atherosclerosis and coronary artery disease* Philadelphia: Lippincott-Raven, 1996.

[57] Haimovici, H., "Patterns of atherosclerotic lesions of the lower extremity," *Archives of Surgery*, vol. 95 pp. 918-933, 1967.

[58] Hatle, L. and Angelsen, B., *Doppler Ultrasound in Cardiology. Physical principles and clinical applications*, 2 ed. Philadelphia: Lea & Febiger, 1985, pp. 1-320.

[59] Hatsukami, T. S., Primozich, J. F., Zierler, R. E., Harley, J. D., and Strandness, D. E., Jr., "Color Doppler imaging of infrainguinal arterial occlusive disease," *Journal of Vascular Surgery*, vol. 16 pp. 527-533, 1992.

[60] Hatsukami, T. S., Primozich, J. F., Zierler, R. E., and Strandness, D. E., Jr., "Color Doppler characteristics in normal lower extremity arteries," *Ultrasound in Medicine & Biology*, vol. 18, no. 2, pp. 167-171, 1992.

[61] Holen, J., Waag, R. C., Gramiak, R., Violante, M. R., and Roe, S. A., "Doppler ultrasound in orifice flow. In vitro studies of the relationship between pressure difference and fluid velocity," *Ultrasound in Medicine & Biology*, vol. 11, no. 2, pp. 261-266, 1985.

[62] Hood, d. B., Mattos, M. A., Mansour, A., Ramsey, D. E., Hodgson, K. J., Barkmeier, L. D., and Summer, D. S., "Prospective evaluation of new duplex criteria to identify 70% internal carotid artery stenosis," *Journal of Vascular Surgery*, vol. 23, no. 2, pp. 254-261, 1996.

[63] Hunink, M. G. M., Polak, J. F., Barlan, M. M., and O'Leary, D. H., "Detection and quantification of carotid artery stenosis: Efficacy of various Doppler velocity parameters," *AJR American Journal of Roentgenology*, vol. 160 pp. 619-625, 1993.

[64] Imparato, A. M., Kim, G. E., Davidson, T., and Crowley, J. G., "Intermittent claudication: It is natural course?," *Surgery*, vol. 78 pp. 795-799, 1975.

[65] Jager, K. A., Phillips, D. J., Martin, R. L., Hanson, C., Roederer, G. O., Langlois, Y. E., Ricketts, H. J., and Strandness, D. E., Jr., "Noninvasive mapping of lower limb arterial lesions," *Ultrasound in Medicine & Biology*, vol. 11, no. 3, pp. 515-521, 1985.

[66] Jelnes, R., Gaardsting, O., Hougaard, J. K., Baekgaard, N., Tonnesen, K. H., and Schroeder, T., "Fate in intermittent claudication: Outcome and risk factors," *British Medical Journal*, vol. 293 pp. 1137-1140, 1986.

[67] Jensen, J. A., *Estimation of blood velocities using ultrasound. A signal processing approach*, 1st ed. New York, Australia: Cambridge University Press, 1996, pp. 1-289.

[68] Kannel, W. B. and McGee, D. L., "Update on some epidemiologic features of intermittent claudication: The Framingham study," *Journal of the American Geriatrics Society*, vol. 33 pp. 13-18, 1985.

[69] Kohler, T. R., Nicholls, S. C., Zierler, R. E., Beach, K. W., Schubart, P. J., and Strandness, D. E., Jr., "Assessment of pressure gradient by Doppler ultrasound: Experimental and clinical observations," *Journal of Vascular Surgery*, vol. 6 pp. 460-469, 1987.

[70] Langlois, Y. E., Roederer, G. O., Chan, A., Phillips, D. J., Beach, K. W., Martin, D., Chikos, P. M., and Strandness, D. E., Jr., "Evaluating carotid artery disease: The concordance between pulsed Doppler/spectrum analysis and angiography," *Ultrasound in Medicine & Biology*, vol. 9, no. 1, pp. 51-63, 1983.

[71] Law, Y. F., Bascom, P. A. J., Johnston, K. W., Vaitkus, P. J., and Cobbold, R. S. C., "Experimental study of the effects of pulsed Doppler sample volume size and position on the Doppler spectrum," *Ultrasonics*, vol. 29, no. 9, pp. 404-410, 1991.

[72] Lee, J. S. and Fung, Y. C., "Flow in a locally constricted tube at low Reynolds numbers," *J.App.Mech.*, vol. 37 pp. 9, 1970.

[73] Legemate, D. A., Teeuwen, C., Hoeneveld, H., Ackerstaff, R. G. A., and Eikelboom, B. C., "Spectral analysis criteria in duplex scanning of aortoiliac and femoropopliteal arterial disease.," *Ultrasound in Medicine & Biology*, vol. 17, no. 8, pp. 769-776, 1991.

[74] Legemate, D. A., Teeuwen, C., Hoeneveld, H., Ackerstaff, R. G. A., and Eikelboom, B. C., "The potential of duplex scanning to replace aorto-iliac and femoropopliteal angiography," *European Journal of Vascular Surgery*, vol. 3 pp. 49-54, 1989.

[75] Leiboff, R., Bren, G., Katz, R., Korkegi, R., and Ross, A., "Determination of trans-stenotic gradients observed during angioplasty: An experimental model," *American Journal of Cardiology*, vol. 52 pp. 1311-1317, 1983.

[76] Leng, G. C. and Fowkes, F. G. R., "The epidemiology of peripheral arterial disease," *Vascular Medicine Review*, vol. 4 pp. 5-18, 1993.

[77] Leng, G. C., Whyman, M. R., Donnan, P. T., Ruckley, C. V., Gillespie, I., Fowkes, G. R., and Allan, P. L., "Accuracy and reproducibility of duplex ultrasonography in grading femoropopliteal stenoses," *Journal of Vascular Surgery*, vol. 17 pp. 510-517, 1993.

[78] Liu, J. B. and Goldberg, B. B., "Endoluminal vascular and nonvascular sonography: Past, Present, and Future," *AJR American Journal of Roentgenology*, vol. 165 pp. 765-774, 1995.

[79] Lowe, G. D. O., "Conservative management of chronic occlusive arterial disease," in Galland, R. B. and Clyne, C. A. C. (eds.) *Clinical problems in vascular surgery* London: Edward Arnold, 1994.

[80] Mavor, G. E., "The pattern of occlusion in atheroma of the lower limb arteries. The correlation of clinical and arteriographic findings," *British Journal of Surgery*, vol. 43 pp. 352-364, 1956.

[81] May, A. G. and DeWeese, D. G., "Hemodynamic effects of arterial stenosis," *Surgery*, vol. 53 pp. 513-524, 1963.

[82] May, A. G., Vandeberg, L., DeWeese, J. A., and Rob, D. G., "Critical arterial stenosis," *Surgery*, vol. 54 pp. 250-259, 1963.

[83] McDicken, W. N., *Diagnostic ultrasonics: Principles and use of instruments*, 3 ed. Edinburgh, London, Melbourne & New York: Churchill Livingstone, 1991, pp. 1-321.

[84] McDonald, D. A., *Blood flow in arteries*, 2 ed. London: Edward Arnold, 1974, pp. 1-458.

[85] McNay, M. B. and Fleming, J. E. E., "Forty years of obstetric ultrasound 1957-1997: From A-scope to three dimension," *Ultrasound in Medicine & Biology*, vol. 25, no. 1, pp. 3-56, 1999.

[86] McWilliams, R. G., Robertson, I., Smye, S. W., Wijesinghe, L., and Kessell, D. L., "Sources of error in intra-arterial pressure measurements across a stenosis," *European Journal of Vascular & Endovascular Surgery*, vol. 15 pp. 535-540, 1998.

[87] Milnor, W. R., *Hemodynamics*, 2 ed. Baltimore, Hong Kong, London, Sydney: Williams & Wilkins, 1989, pp. 1-387.

[88] Mo, L. Y. L., Yun, L. C. M., and Cobbold, R. S. C., "Comparison of four digital maximum frequency estimators for Doppler ultrasound," *Ultrasound in Medicine & Biology*, vol. 14, no. 5, pp. 355-363, 1988.

[89] Moniz, E., Lima, A., and de Lacerda, R., "Hémiplégies par thrombose de la carotide interne," *Presse Médicale*, vol. 45 pp. 977-982, 1937.

[90] Moore, K. L., *Clinically oriented anatomy*, 3rd ed. Baltimore: Williams & Wilkins, 1992.

[91] Munson, B. R., Young, D. F., and Okiishi, T. H., *Fundamentals of fluid mechanics*, 2 ed. 1994, pp. 1-848.

[92] Nakamura, M. and Savada, T. Numerical study on the flow of a non-Newtonian fluid through an axi-symmetric stenosis. Journal of Biomechanical Engineering 110, 137. 1988.

[93] Nicholls, S. C., Kohler, T. R., Martin, R. L., Neff, R., Phillips, D. J., and Strandness, D. E., Jr., "Diastolic flow as a predictor of arterial stenosis," *Journal of Vascular Surgery*, vol. 3, no. 3, pp. 498-501, 1986.

[94] Nichols, W. W. and O'Rourke, M. F., *McDonald's Blood Flow in Arteries: theoretical, experimental and clinical principles* , 3 ed. Philadelphia, London: Lea & Febiger, 1990, pp. 1-437.

[95] Ojha, M., Cobbold, R. S. C., Johnston, K. W., and Hummel, R. L., "Pulsatile flow through constricted tubes: An experimental investigation using photochromic tracer methods," *Journal of Fluid Mechanical*, vol. 203 pp. 173-197, 1989.

[96] Ojha, M., Johnston, K. W., and Cobbold, R. S. C., "Evidence of a possible link between poststenotic dilation and wall shear stress," *Journal of Vascular Surgery*, vol. 11 pp. 127-135, 1990.

[97] Ojha, M., Johnston, K. W., Cobbold, R. S. C., and Hummel, R. L., "Potential limitations of center-line pulsed Doppler recordings: An in vitro flow visualization study.," *Journal of Vascular Surgery*, vol. 9 pp. 515-520, 1989.

[98] Pemberton, M., Nydahi, S., Hartshorne, T., Naylor, A. R., Bell, P. R. F., and London, N. J. M., "Can lower limb vascular reconstruction be based on color duplex imaging alone?," *European Journal of Vascular & Endovascular Surgery*, vol. 12 pp. 452-454, 1996.

[99] Perktold, K., Peter, R., and Rosch, M., "Pulsatile non-Newtonian blood flow through a bifurcation with aneurism," *Biorheology*, vol. 26, no. 6, pp. 1011-1030, 1989.

[100] Pignoli, P., Tremoli, E., Poli, A., Oreste, P., and Paoletti, R., "Intimal plus medial thickness of the arterial wall: a direct measurement with ultrasound imaging," *Circulation*, vol. 74, no. 6, pp. 1399-1406, 1986.

[101] Ranke, C., Creutzig, A., and Alexander, K., "Duplex scanning of the peripheral arteries: Correlation of the peak velocity ratio with angiographic diameter reduction," *Ultrasound in Medicine & Biology*, vol. 18, no. 5, pp. 433-440, 1992.

[102] Resnick, D. and Halliday, D., "Fluid dynamics," *Physics Part I* 1966, pp. 440-463.

[103] Reunanen, A., Takkunen, H., and Aromaa, A., "Prevalence of intermittent claudication and its effect on mortality," *Acta Medica Scandinavica*, vol. 211 pp. 249-256, 1982.

[104] Rickey, D. W., Picot, P. A., Christopher, D. A., and Fenster, A., "A wall-less vessel phantom for Doppler ultrasound studies," *Ultrasound in Medicine & Biology*, vol. 21, no. 9, pp. 1163-1176, 1995.

[105] Roederer, G. O., Langlois, Y. E., Chan, A. W., Primozich, J. F., Lawrence, R. J., Chikos, P. M., and Strandness, D. E., Jr., "Ultrasonic duplex scanning of extracranial carotid arteries: improved accuracy using new features from the common carotid artery," *Journal of Cardiovascular Ultrasonography*, vol. 1, no. 4, pp. 373-380, 1982.

[106] Ross, R., "Atherosclerosis - An inflammatory disease," *New England Journal of Medicine*, vol. 340, no. 2, pp. 115-126, 1999.

[107] Schwachtgen, J. L., Houston, P., Campbell, C., Sukhatme, V., and Braddock, M., "Fluid shear stress activation of EGR-1 transcription in cultured human endothelial and epithelial cells is mediated via the extracellular signal-related kinase 1/2 mitogen-activated protein kinase pathway," *Journal of Clinical Investigation*, vol. 101, no. 11, pp. 2540-2549, 1998.

[108] "Second European Consensus document on chronic critical limb ischemia," *European Journal of Vascular Surgery*, vol. 6, no. Suppl. A, pp. 1-32, 1992.

[109] Seeley, B. D. and Young, D. F., "Effect of geometry on pressure losses across models of arterial stenoses," *Journal of Biomechanics*, vol. 9 pp. 439-448, 1976.

[110] Sensier, Y., Hartshorne, T., Thrush, A., Handford, H., Nydahi, S., and London, N. J. M., "The effect of adjacent segment disease on the accuracy of color duplex scanning for the diagnosis of lower limb arterial disease," *European Journal of Vascular & Endovascular Surgery*, vol. 12 pp. 238-242, 1996.

[111] Shukla, J. B., Parihar, R. S., and Rao, B. R. P., "Effect of stenosis on non-Newtonian flow of blood in an artery," *Bulletin of Mathematical Biology*, vol. 42, no. 3, pp. 283-294, 1982.

[112] Spencer, M. P. Carotid stenoses and the Bernoulli principle. Federation Proceedings 40(3), 444. 1981.

[113] Stewart, S. F. C., "A rotating torus phantom for assessing color Doppler accuracy," *Ultrasound in Medicine & Biology*, vol. 25, no. 8, pp. 1251-1264, 1999.

[114] Stoltz, J. F., Muller, S., Wang, X., Dumas, D., Boisseau, M., Legrand, S., and Labrador, V. Hemorheology and vascular endothelial cells. Xth European Conference on Clinical Hemorheology 20, 127-139. 1999. Lisbon.

[115] Strandness, D. E., Jr., "Hemodynamics of the normal arterial and venous system," in Strandness, D. E., Jr. (ed.) *Duplex scanning in vascular disorders* New York: Raven Press, 1993, pp. 45-79.

[116] Strandness, D. E., Jr., "Peripheral arterial system," in Strandness, D. E., Jr. (ed.) *Duplex scanning in vascular disorders* New York: Raven Press, 1993, pp. 159-195.

[117] Strauss, A. L., Karasch, T. H., and Roth, F. J., "Accuracy of duplex scanning in the prediction of pressure gradients across peripheral artery stenoses," *Bildgebung*, vol. 60 pp. 294-296, 1993.

[118] Strauss, A. L., Roth, F. J., and Rieger, H., "Noninvasive assessment of pressure gradients across iliac artery stenoses: Duplex and catheter correlative study," *Journal of Ultrasound Medicine*, vol. 12 pp. 17-22, 1993.

[119] Strauss, A. L., Schaberle, W., Rieger, H., and Roth, F., "Use of duplex scanning in the diagnosis of arterial profunda femoris stenosis," *Journal of Vascular Surgery*, vol. 13 pp. 698-704, 1991.

[120] Strauss, A. L., Scheffler, A., and Rieger, H., "Doppler ultrasound pressure gradient of peripheral arterial stenoses in a pulsatile in vitro flow model," *VASA*, vol. 19 pp. 207, 1990.

[121] Sutton-Tyrrell, K., Wolfson, S. K., Thompson, T., and Kelsey, S. F., "Measurement variability in duplex scan assessment of carotid atherosclerosis," *Stroke*, vol. 23 pp. 215-220, 1992.

[122] Tandon, P. N. and Agarwal, R. A study of the diffusion phenomenon in a normal and modeled stenotic capillary-tissue exchange system. Proceedings International Conference on Computational Methods in Flow Analysis 2, 1154. 1988.

[123] Tandon, P. N. and Misra, J. K., "Microstructure and peripheral layer viscosity effects on the flow of blood through an artery with mild stenosis," *Annals of the New York Academy of Sciences*, vol. 404 pp. 59-62, 1983.

[124] Tandon, P. N., Nirmala, P., Tewari, M., and Rana, U. V. S. Analysis of nutritional transport through a capillary: Normal and stenosed. International Journal of Computational Mathematical Application 22[12], 3. 1993.

[125] Tandon, P. N., Pal, T. S., and Siddiqui, S. U., "Pulsatile blood flow through an axisymmetric stenotic tube," *Indian Journal of Biomedical Computing*, vol. 24 pp. 190, 1986.

[126] Tandon, P. N., Rana, U. V. S., Kawahara, M., and Katiyar, V. K. A model for blood flow through a stenotic tube. International Journal of Biomedical Computer 32, 61-78. 1993. Elsevier Scientific Publishers Ireland Ltd.

[127] Taylor, K. J. W., Burns, P. N., and Wells, P. N. T., *Clinical applications of Doppler ultrasound*, 1 ed. New York: Raven Press, 1988, pp. 1-361.

[128] Teirstein, P. S., Yock, P. G., and Popp, R. L., "The accuracy of Doppler ultrasound measurement of pressure gradients across irregular, dual, and tunnel like obstructions to blood flow," *Circulation*, vol. 72, no. 3, pp. 577-584, 1985.

[129] Thiele, B. L., Hutchison, K. J., Greene, F. M. Jr., Forster, F. K., and Strandness, D. E., Jr., "Pulsed Doppler waveform patterns produced by smooth stenosis in the dog thoracic aorta," in Taylor, D. E. M. and Stevens, A. L. (eds.) *Blood flow: Theory and practice* London New York: Academic press, 1983, pp. 85-104.

[130] Tranulis, C., Savéry, D., Mongrain, R., Cloutier, G., and Durand, L. G. Modélisation du flux sanguin dans une artère en présence de deux sténoses significatives. XVIII ième Congrès de l'AEGSFM et 37ième Congrès des stagiaires d'été de la faculté de médecine Janvier. 1999.

[131] Udoff, E. J., Barth, K. H., Harrington, D. P., Kaufman, S. L., and White, R. I., "Hemodynamic significance of iliac artery stenosis: Pressure measurements during angiography," *Radiology*, vol. 132 pp. 289-293, 1979.

[132] van Everdingen, K. J., van der Grond, J., and Kapelle, L. J., "Overestimation of a stenosis in the internal carotid artery by duplex sonography caused by an increase in volume flow," *Journal of Vascular Surgery*, vol. 27, no. 3, pp. 479-485, 1998.

[133] Vayssairat, M. and Carpentier, P., *Microcirculation Clinique* Paris, France: Masson Publication, 1996.

[134] Vita, J. A., Treasure, C. B., Nabel, E. G., McLenachan, J. M., Fish, R. D., Yeung, A. C., Vekshtein, V. I., Selwyn, A. P., and Ganz, P., "Coronary vasomotor response to acetylcholine relates to risk factors for coronary artery disease," *Circulation*, vol. 81 pp. 491-497, 1990.

[135] Vogt, M. T., Wolfson, S. K., and Kuller, L. H., "Lower extremity arterial disease and the aging process: A review," *Journal of Clinical Epidemiology*, vol. 45 pp. 529-542, 1992.

[136] Wang, X., Navidbakhsh, M., Skalak, R., Chien, S., and Usami, S., "Morphology of bovine aortic endothelial cells in an oscillatory disturbed flow," *Arch.Physiol.Biochem.*, vol. 104 pp. 581-583, 1996.

[137] Weber, G., Strauss, A. L., Rieger, H., Scheffler, A., and Eisenhoffer, J., "Validation of Doppler measurement of pressure gradients across peripheral model arterial stenosis," *Journal of Vascular Surgery*, vol. 16 pp. 10-16, 1992.

[138] Weitz, J. I., Byrne, J., Clagett, P., Farkouh, M. E., Porter, J. M., Sackett, D. L., Strandness, D. E., Jr., and Taylor, L. M., "Diagnosis and treatment of chronic arterial insufficiency of the lower extremities: A critical review," *Circulation*, vol. 94 pp. 3026-3049, 1996.

[139] Welch, H. J., "Chronic lower extremity ischemia," *Comprehensive Therapy*, vol. 23 pp. 534-538, 1997.

[140] Young, D. F., "Fluid mechanics of arterial stenoses," *Journal of Biomechanical Engineering*, vol. 101, no. 8, pp. 157-175, 1979.

[141] Young, D. F., Cholvin, N. R., and Roth, A. C., "Pressure drop across artificially induced stenoses in the femoral arteries of dogs," *Circulation Research*, vol. 36 pp. 735-743, 1975.

APPENDIX I :

Calibration curves for the transducers that measure the pressures along the artery in the *in vitro* experiments

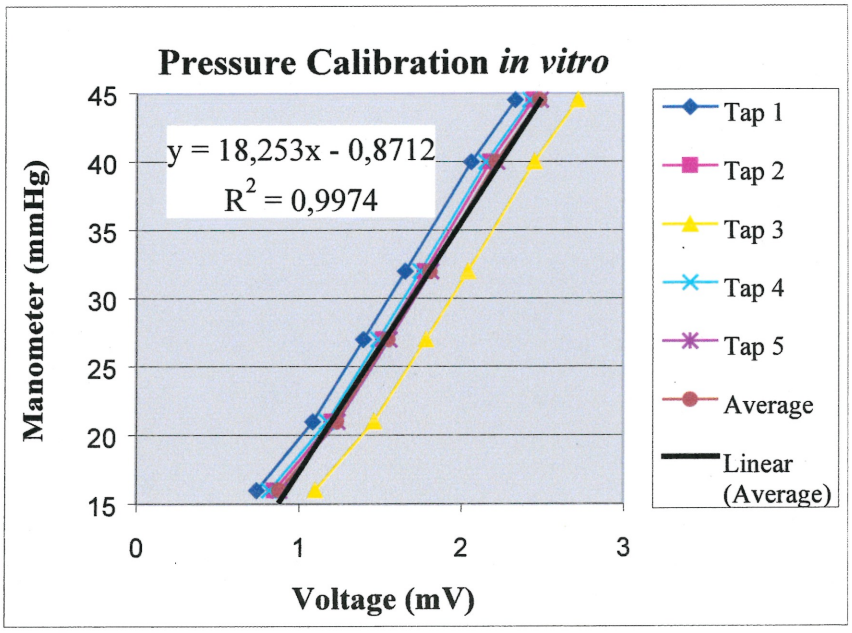

Figure AI-1. Calibration curves for the pressure transducers connected to the pressure taps along the stenosis of interest at positions 2D proximal to the stenosis, at the maximum reduction, and at 2D, 5D, and 10D distal to the stenosis. The linear regression of the average curve of the pressure taps was used as the calibration curve.

APPENDIX II:

VR and pressure gradient curves from the simulations and *in vitro* experiments

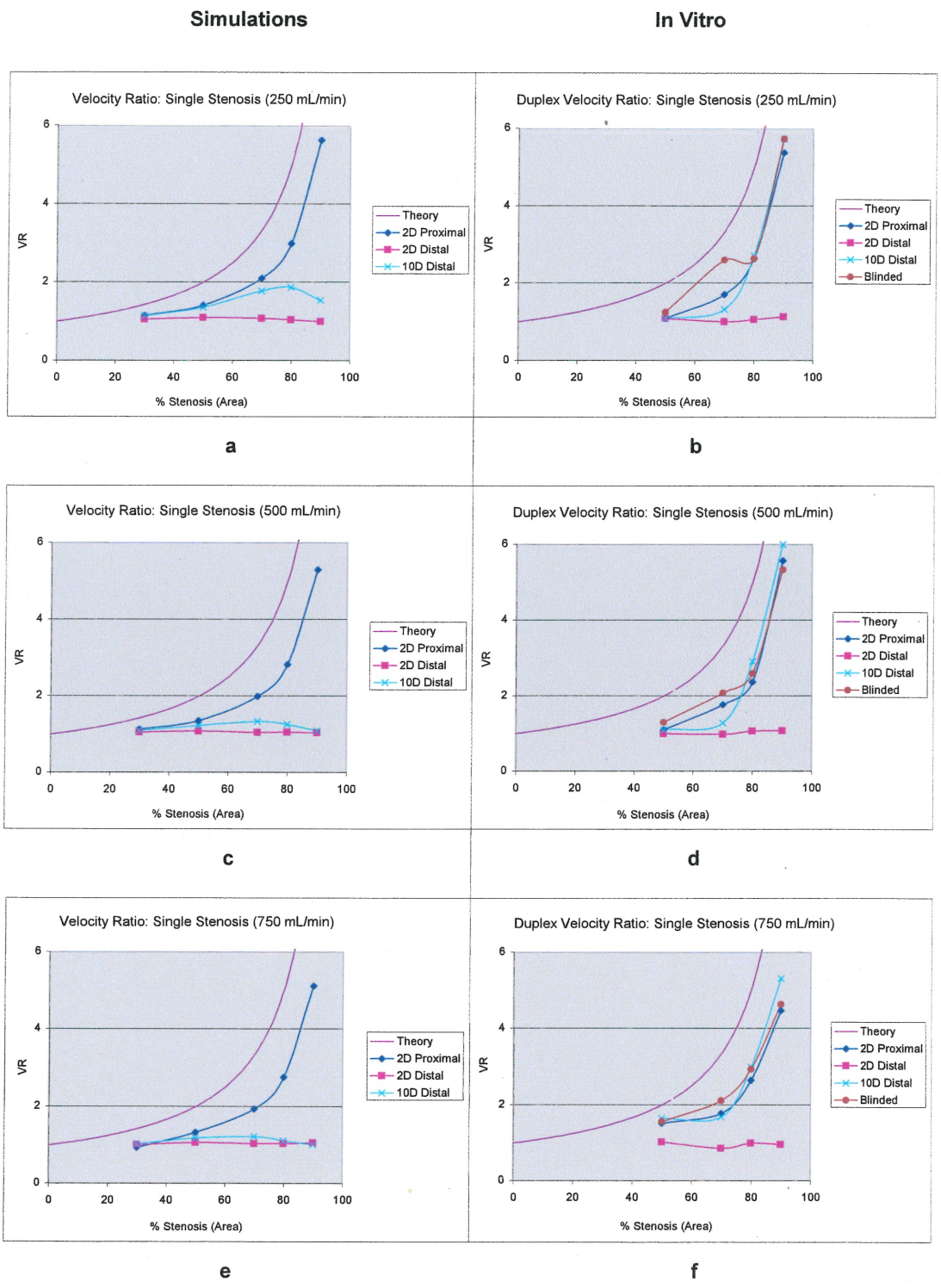

Figure AII-1. Velocity Ratios for a single stenosis from the simulations (left) and *in vitro* experiments (right). Flow rates increase from 250 mL/min (a and b), to 500 mL/min (c and d), and to 750 mL/min (e and f).

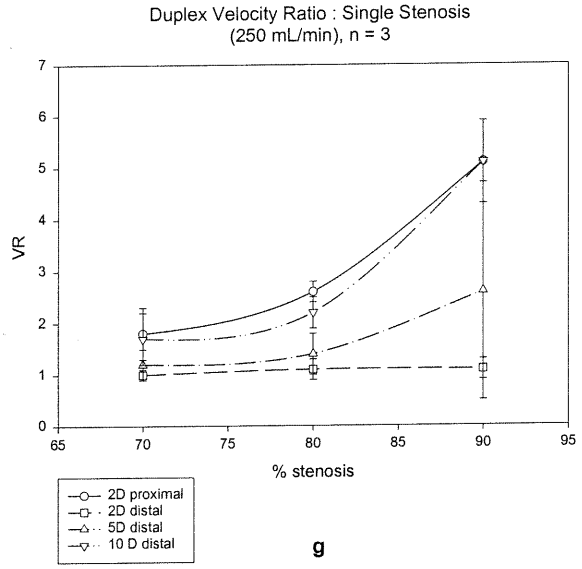

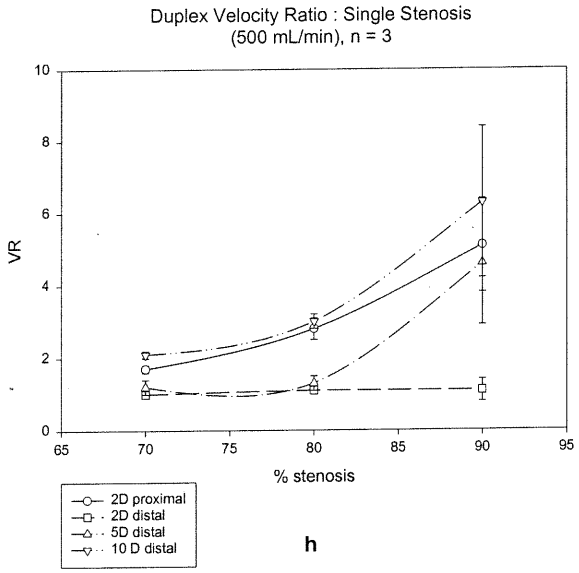

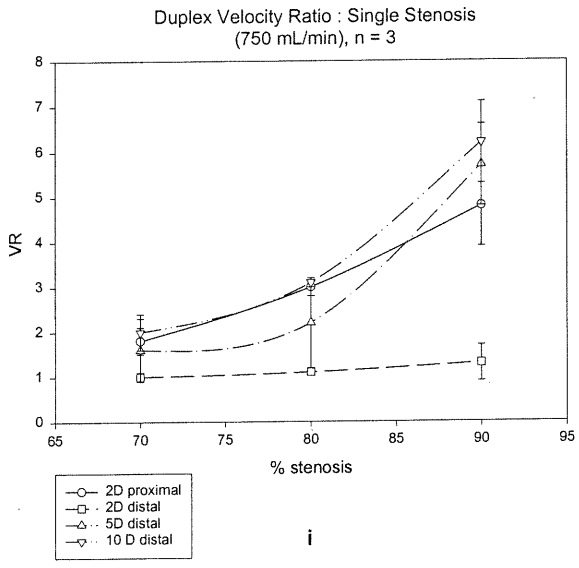

Figure AII-1 (continued). Velocity Ratios for a single stenosis from the *in vitro* experiments of Qin. Flow rates increase from 250 mL/min (g), to 500 mL/min (h), and to 750 mL/min (i).

Simulations **In Vitro**

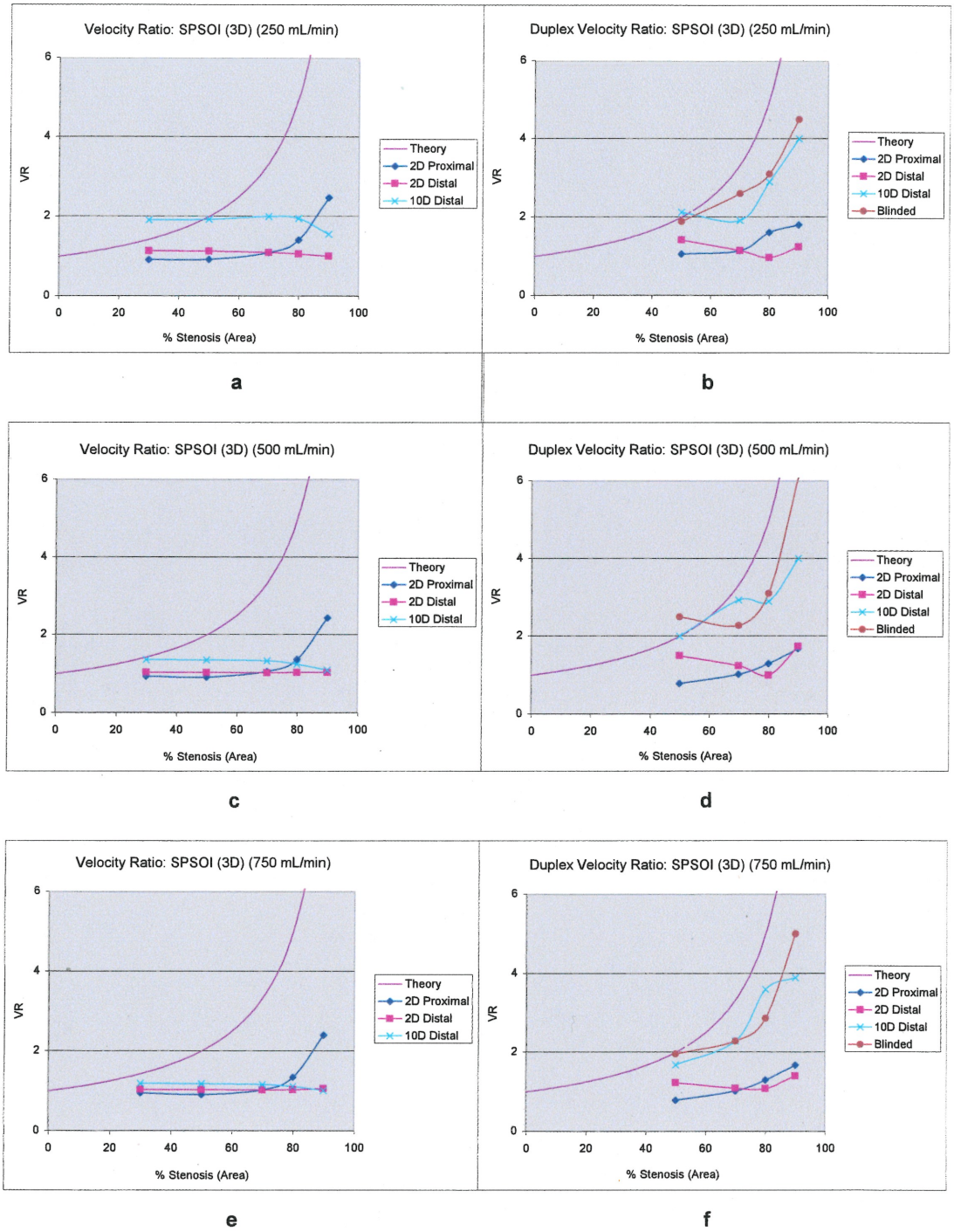

Figure AII-2. Velocity Ratios at SOI, for a stenosis at 3D proximal to the SOI, from the simulations (left) and *in vitro* experiments (right). Flow rates increase from 250 mL/min (a and b), to 500 mL/min (c and d), and to 750 mL/min (e and f).

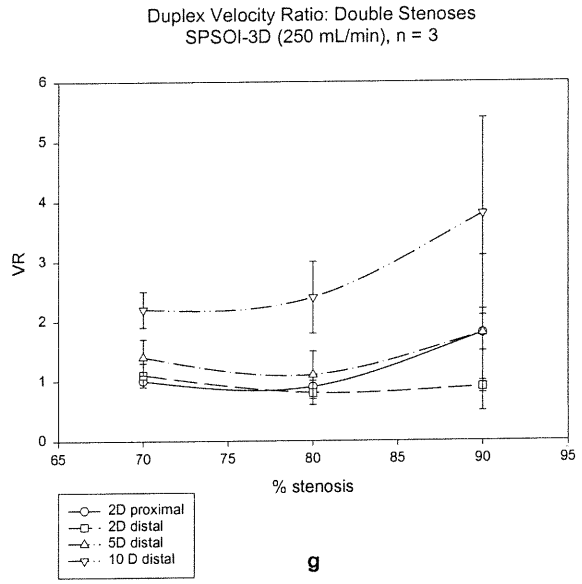

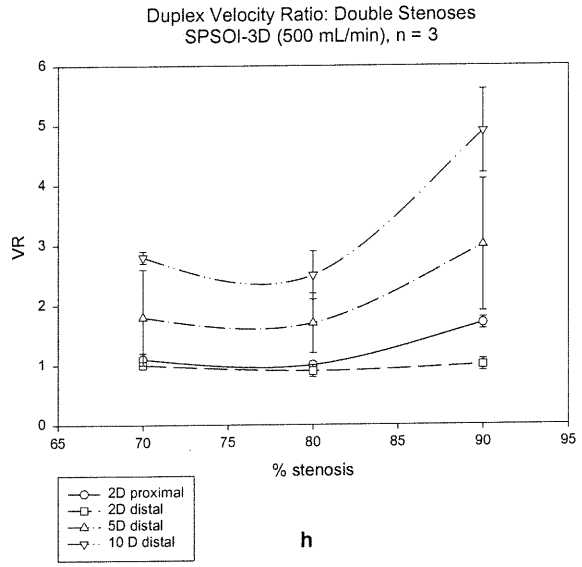

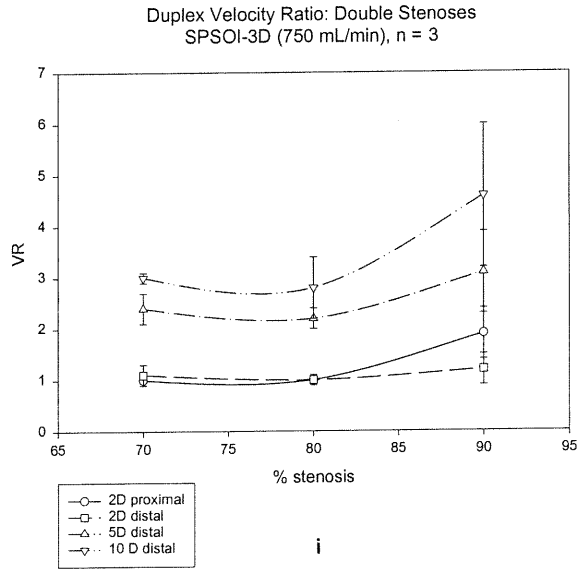

Figure AII-2 (continued). Velocity Ratios at SOI, for a stenosis at 3D proximal to the SOI, from the *in vitro* experiments of Qin. Flow rates increase from 250 mL/min (g), to 500 mL/min (h), and to 750 mL/min (i).

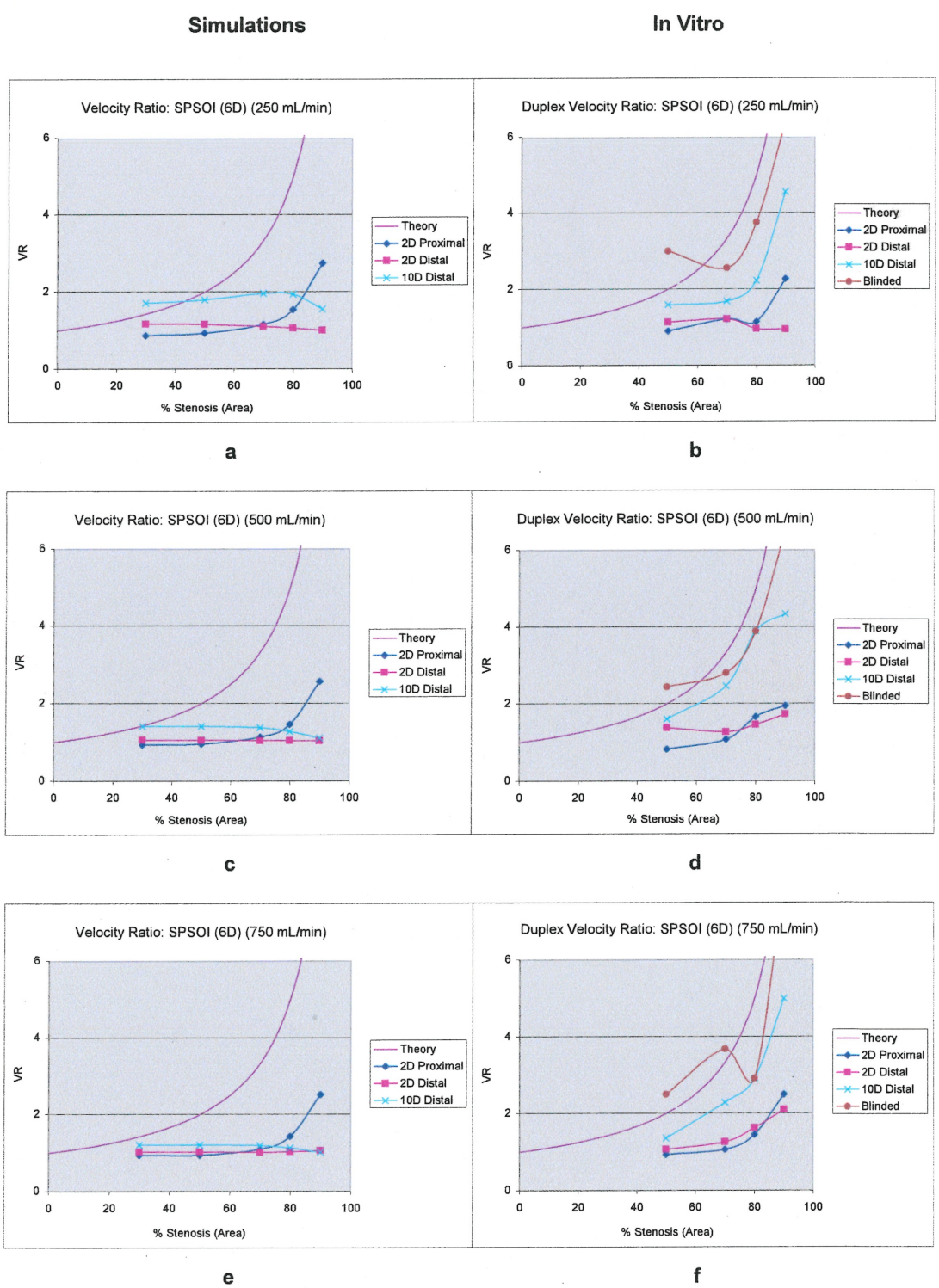

Figure AII-3. Velocity Ratios at SOI, for a stenosis at 6D proximal to the SOI, from the simulations (left) and *in vitro* experiments (right). Flow rates increase from 250 mL/min (a and b), to 500 mL/min (c and d), and to 750 mL/min (e and f).

Simulations **In Vitro**

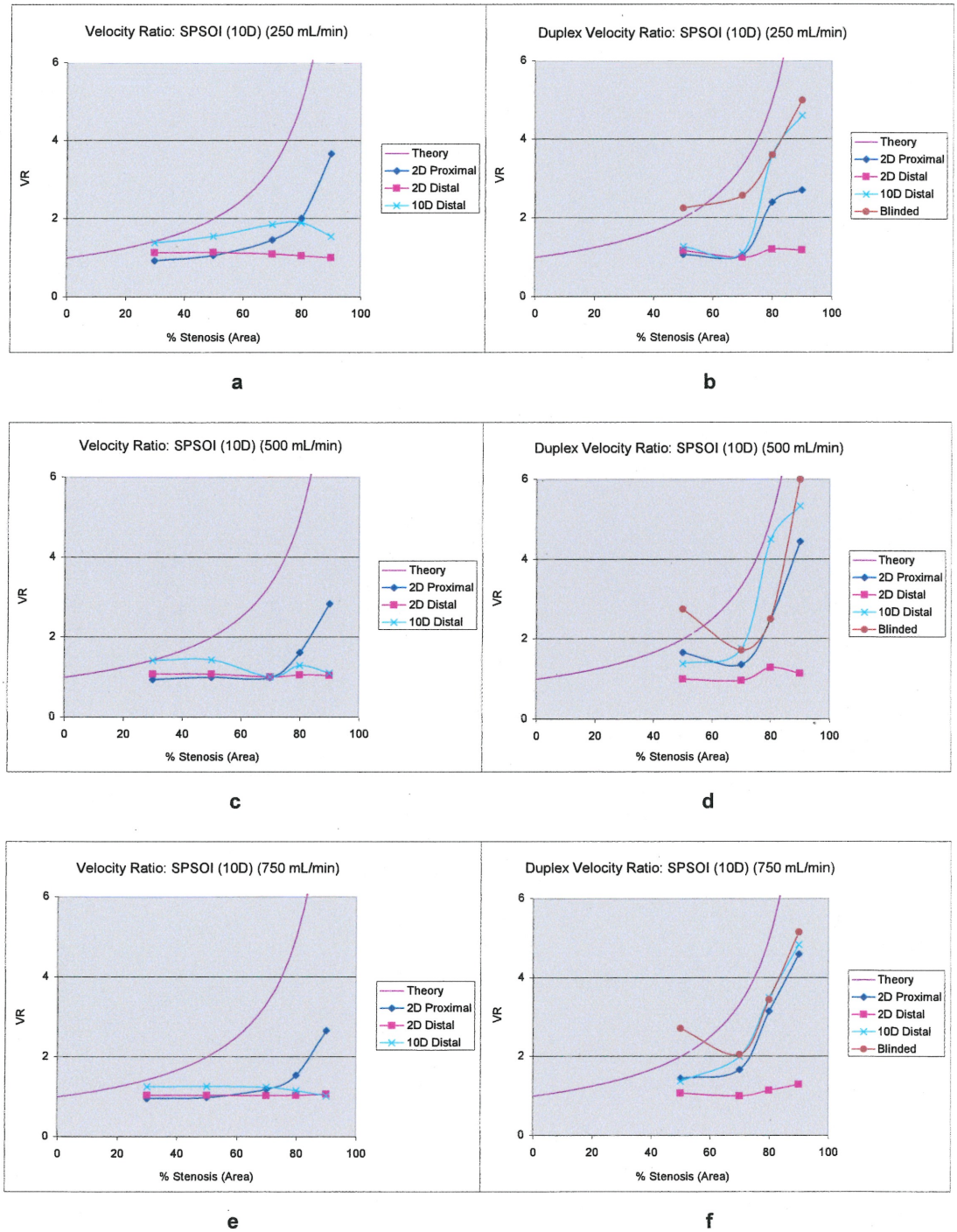

Figure AII-4. Velocity Ratios at SOI, for a stenosis at 10D proximal to the SOI, from the simulations (left) and *in vitro* experiments (right). Flow rates increase from 250 mL/min (a and b), to 500 mL/min (c and d), and to 750 mL/min (e and f).

Simulations **In Vitro**

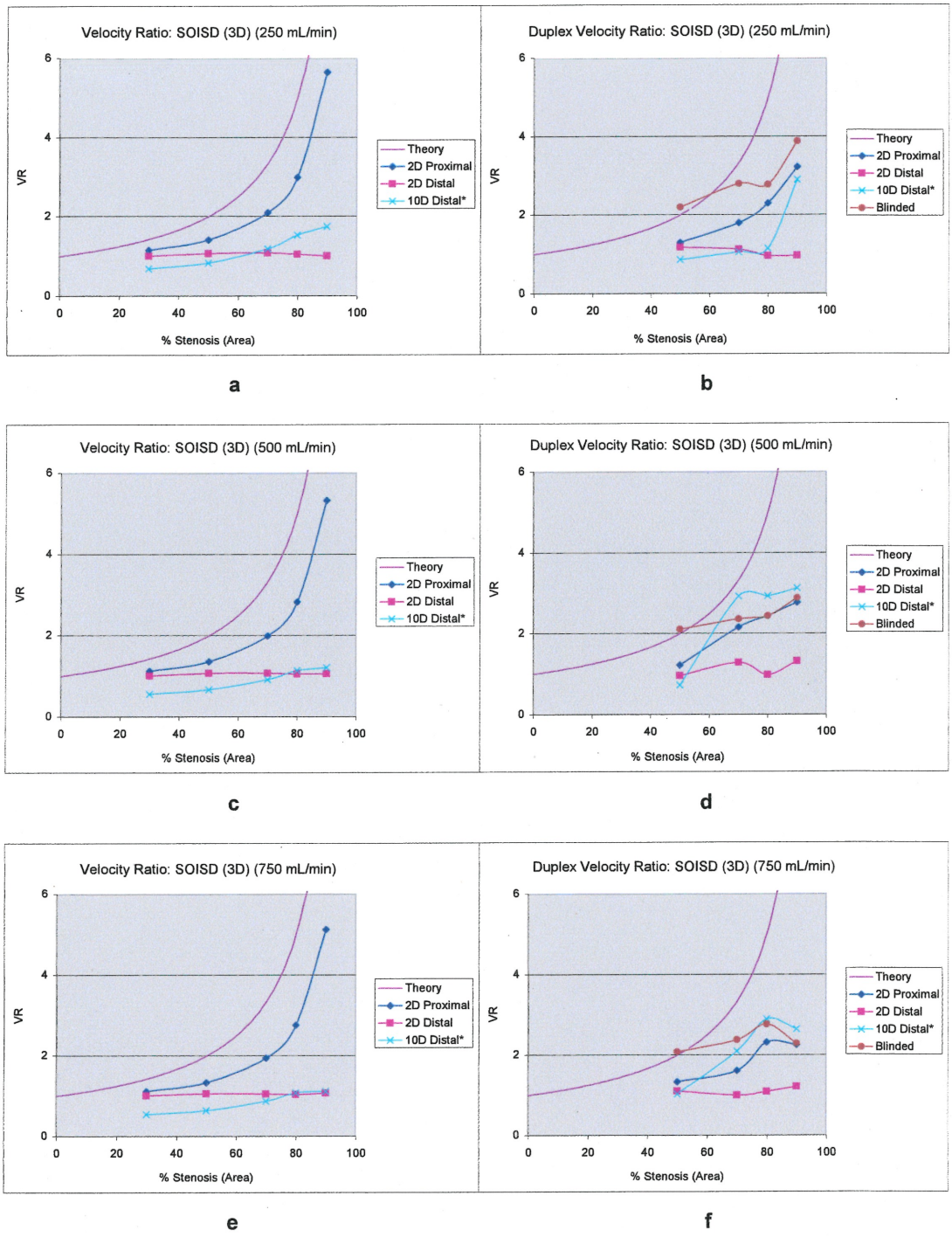

Figure AII-5. Velocity Ratios at SOI, for a stenosis at 3D distal to the SOI, from the simulations (left) and *in vitro* experiments (right). Flow rates increase from 250 mL/min (a and b), to 500 mL/min (c and d), and to 750 mL/min (e and f).

Simulations **In Vitro**

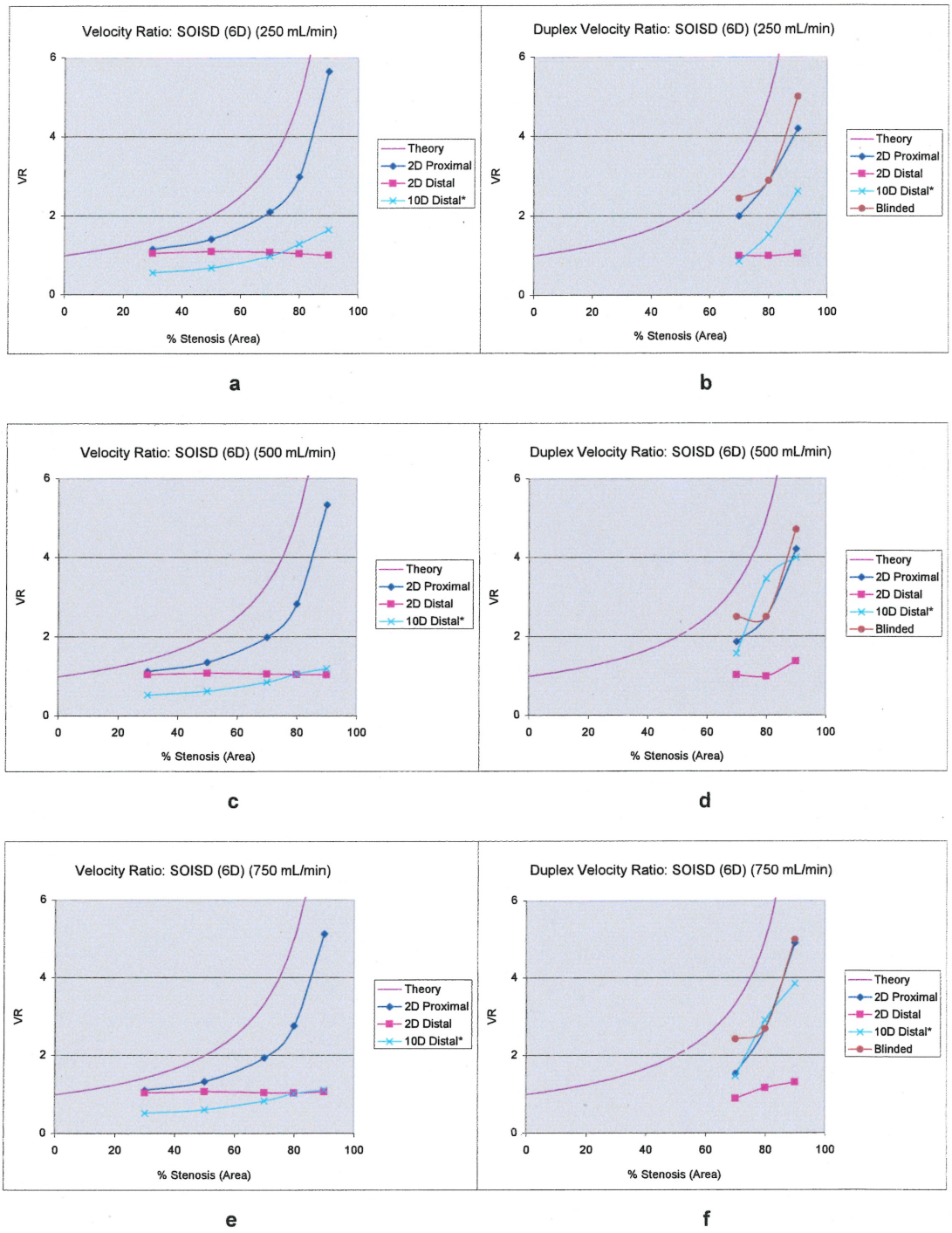

Figure AII-6. Velocity Ratios at SOI, for a stenosis at 6D distal to the SOI, from the simulations (left) and *in vitro* experiments (right). Flow rates increase from 250 mL/min (a and b), to 500 mL/min (c and d), and to 750 mL/min (e and f). The *in vitro* experiments for the 50% AR stenosis were not performed for lack of time.

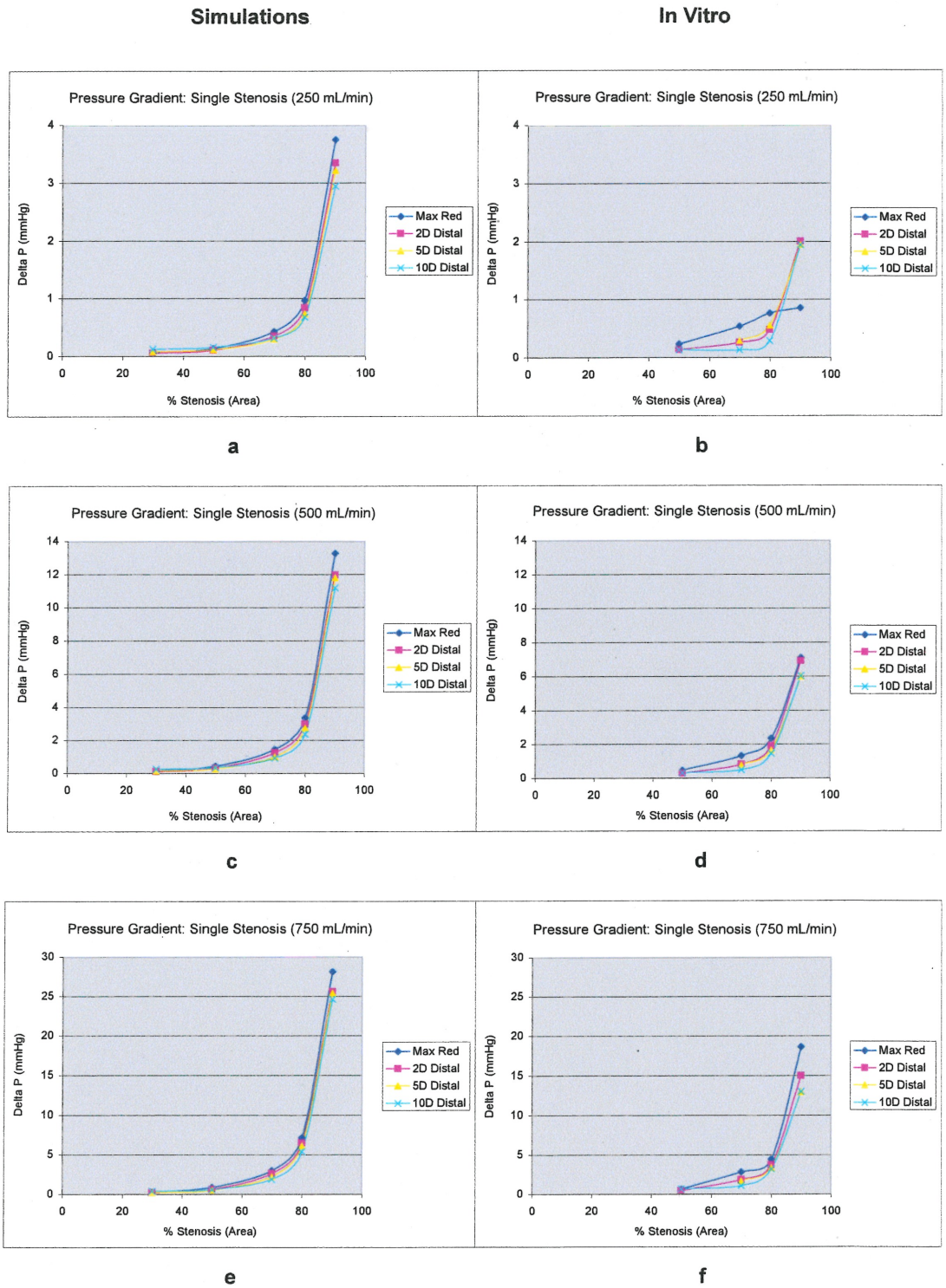

Figure AII-7. Pressure Gradients for a single stenosis from the simulations (left) and *in vitro* experiments (right). Flow rates increase from 250 mL/min (a and b), to 500 mL/min (c and d), and to 750 mL/min (e and f).

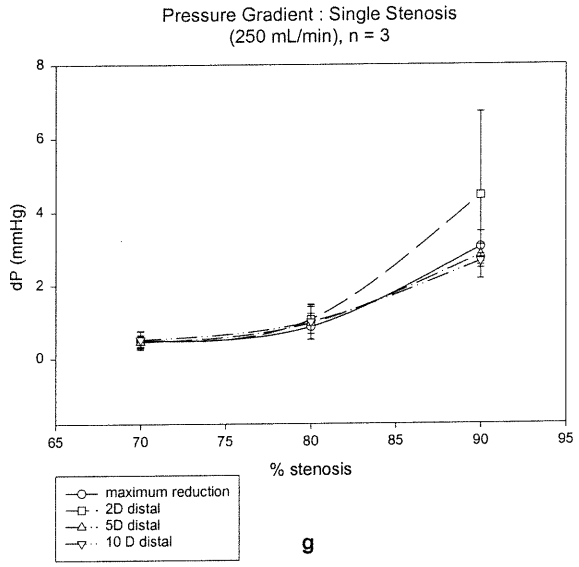

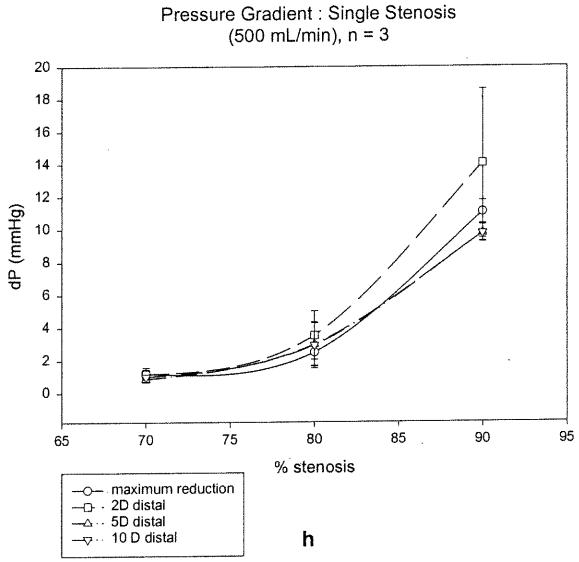

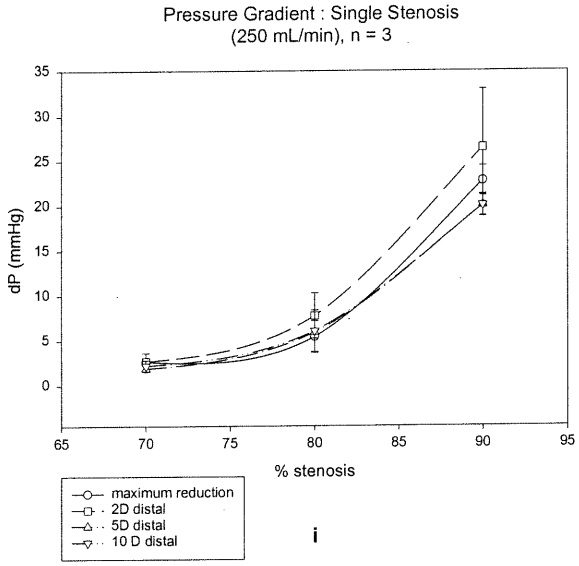

Figure AII-7 (continued). Pressure gradients for a single stenosis from the *in vitro* experiments of Qin. Flow rates increase from 250 mL/min (g), to 500 mL/min (h), and to 750 mL/min (i).

Simulations **In Vitro**

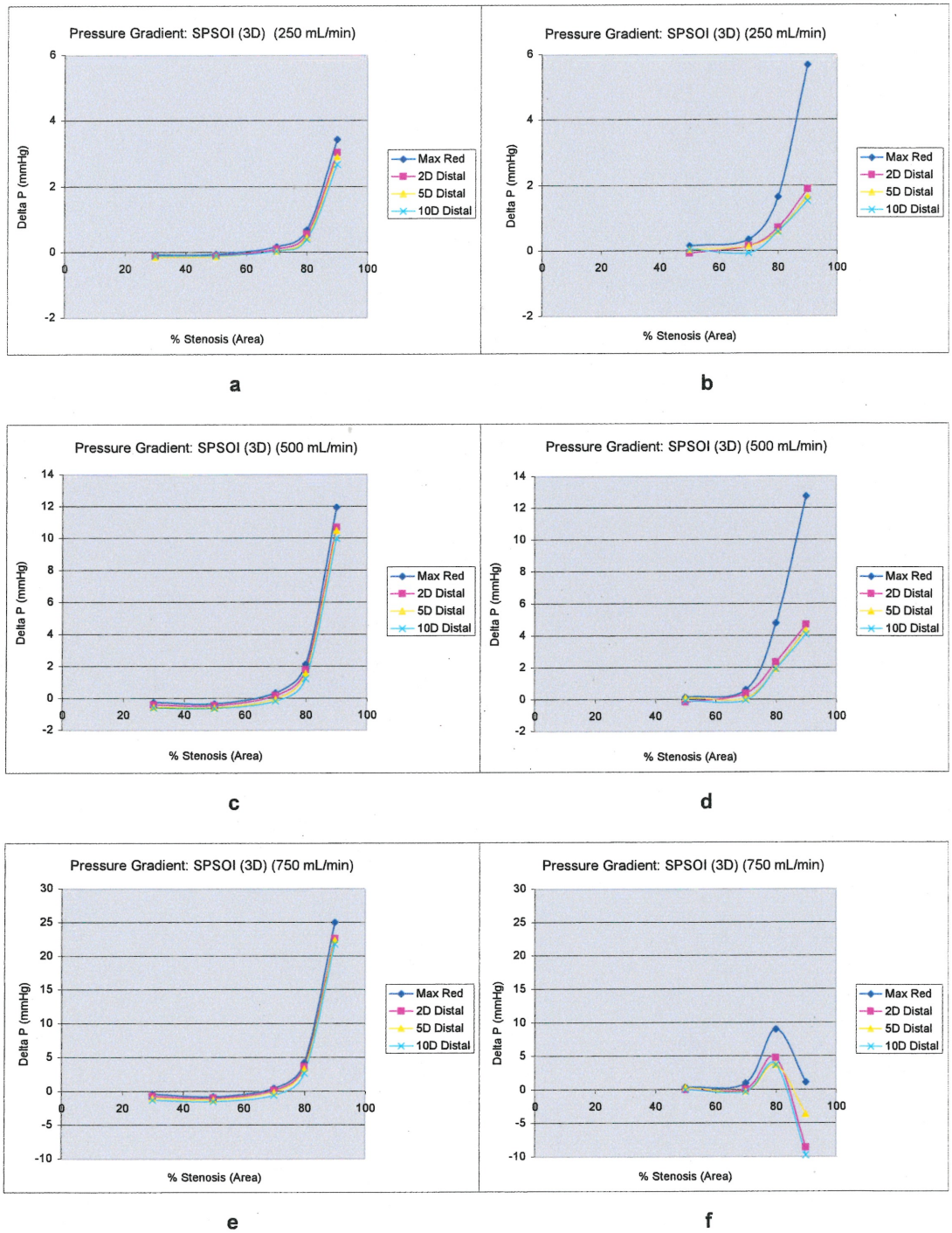

Figure AII-8. Pressure gradients at SOI, for a stenosis at 3D proximal to the SOI, from the simulations (left) and *in vitro* experiments (right). Flow rates increase from 250 mL/min (a and b), to 500 mL/min (c and d), and to 750 mL/min (e and f).

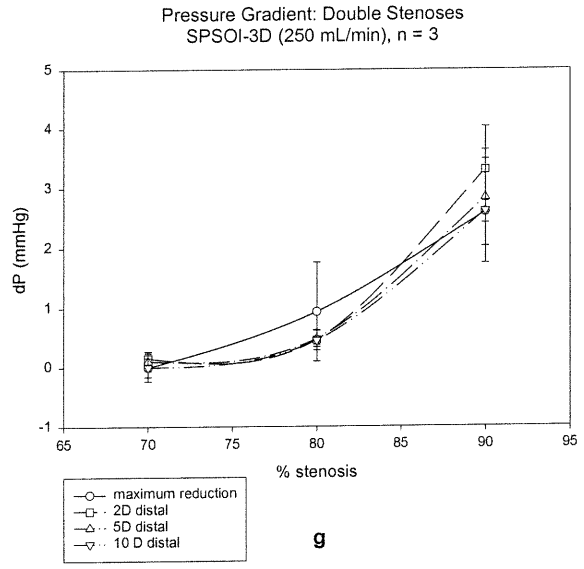

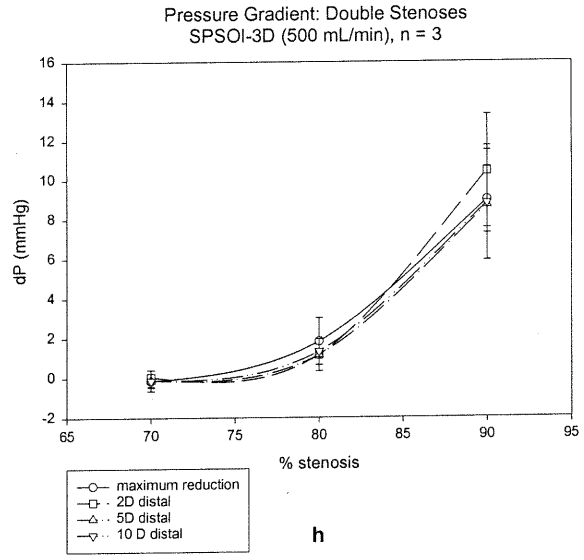

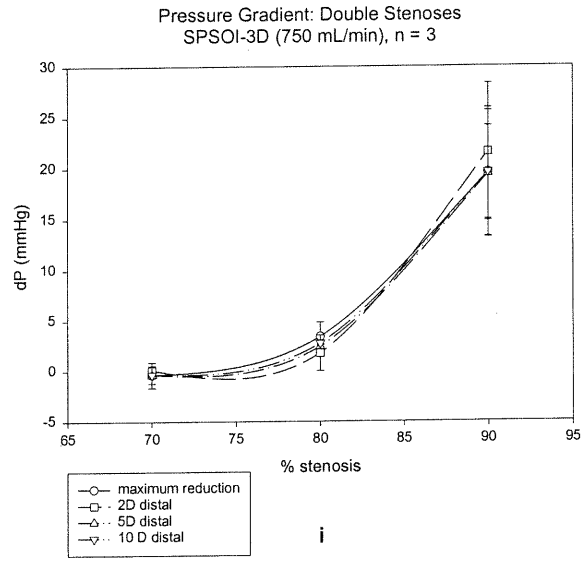

Figure AII-8 (continued). Pressure gradients at SOI, for a stenosis at 3D proximal to the SOI, from the *in vitro* experiments of Qin. Flow rates increase from 250 mL/min (g), to 500 mL/min (h), and to 750 mL/min (i).

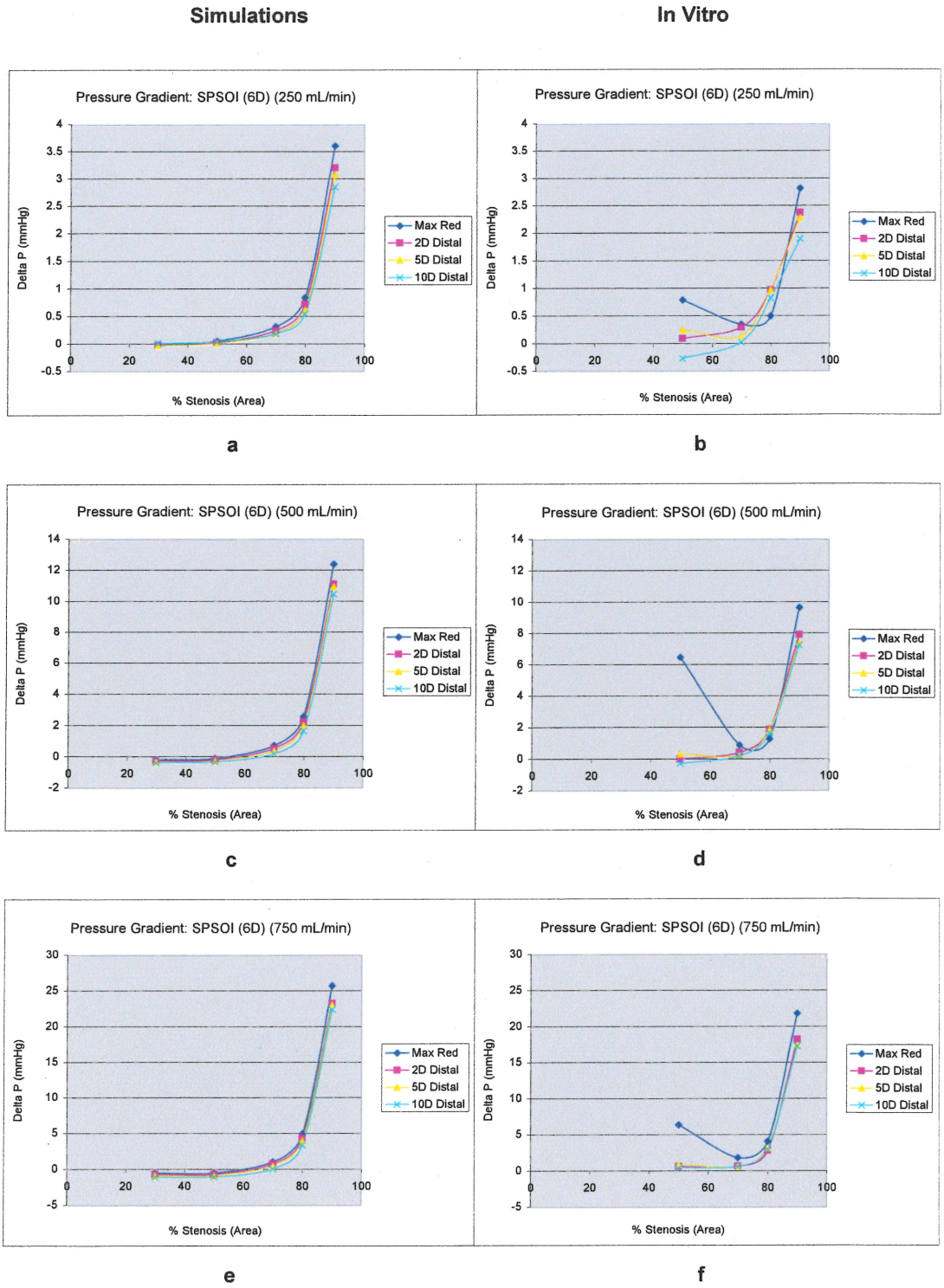

Figure AII-9. Pressure gradients at SOI, for a stenosis at 6D proximal to the SOI, from the simulations (left) and *in vitro* experiments (right). Flow rates increase from 250 mL/min (a and b), to 500 mL/min (c and d), and to 750 mL/min (e and f).

Simulations **In Vitro**

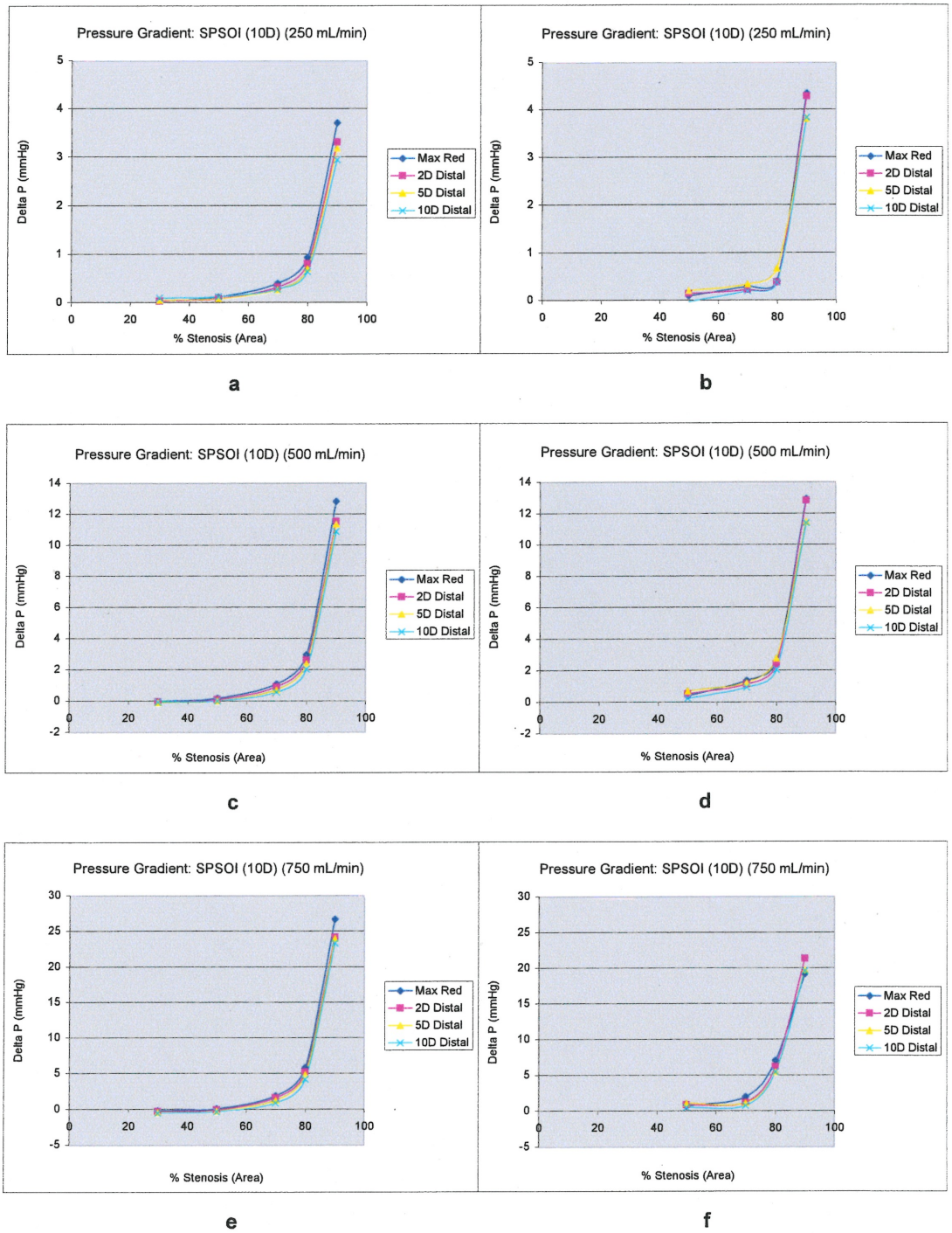

Figure AII-10. Pressure gradients at SOI, for a stenosis at 10D proximal to the SOI, from the simulations (left) and *in vitro* experiments (right). Flow rates increase from 250 mL/min (a and b), to 500 mL/min (c and d), and to 750 mL/min (e and f).

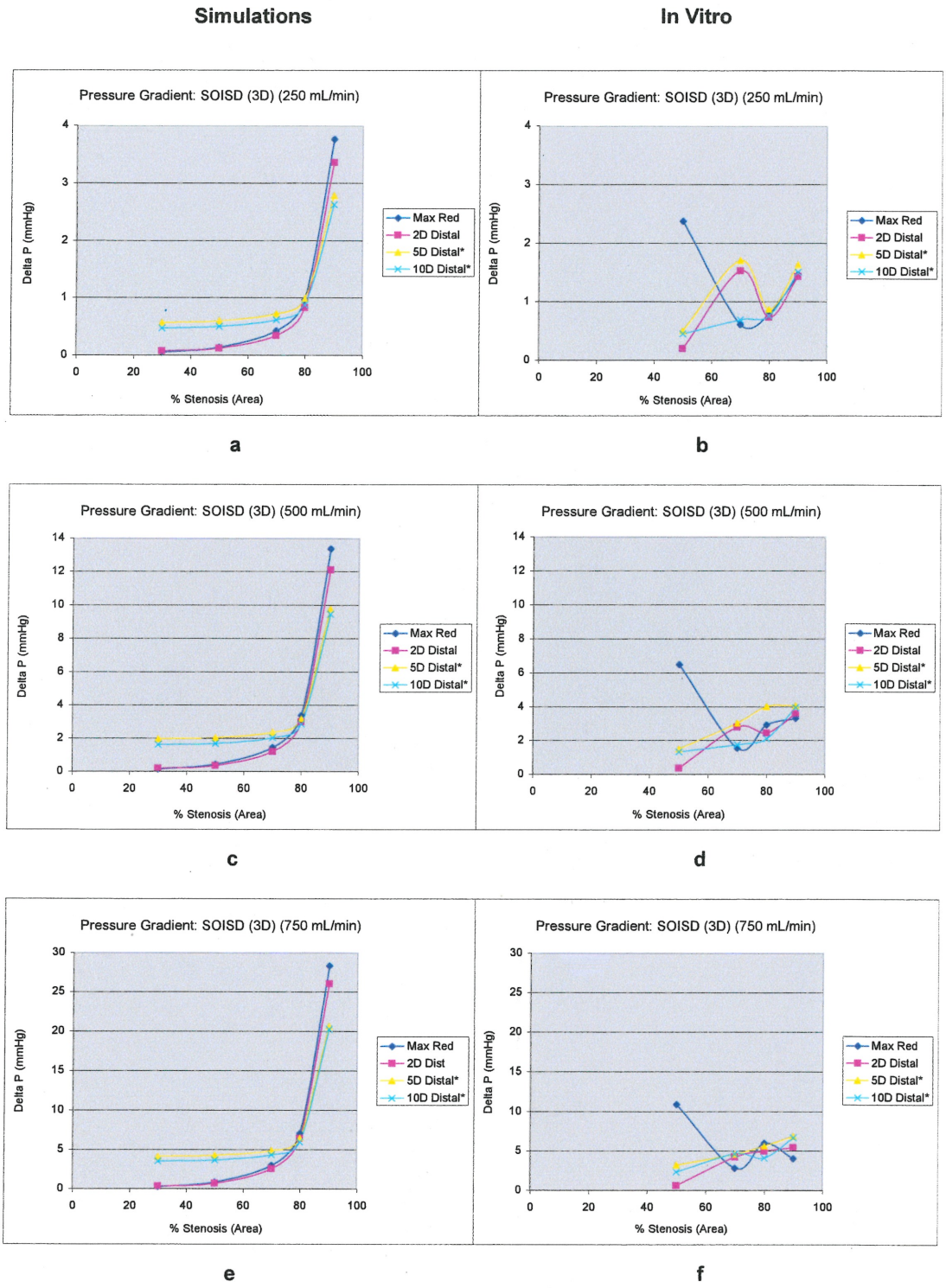

Figure AII-11. Pressure gradients at SOI, for a stenosis at 3D distal to the SOI, from the simulations (left) and *in vitro* experiments (right). Flow rates increase from 250 mL/min (a and b), to 500 mL/min (c and d), and to 750 mL/min (e and f).

Simulations **In Vitro**

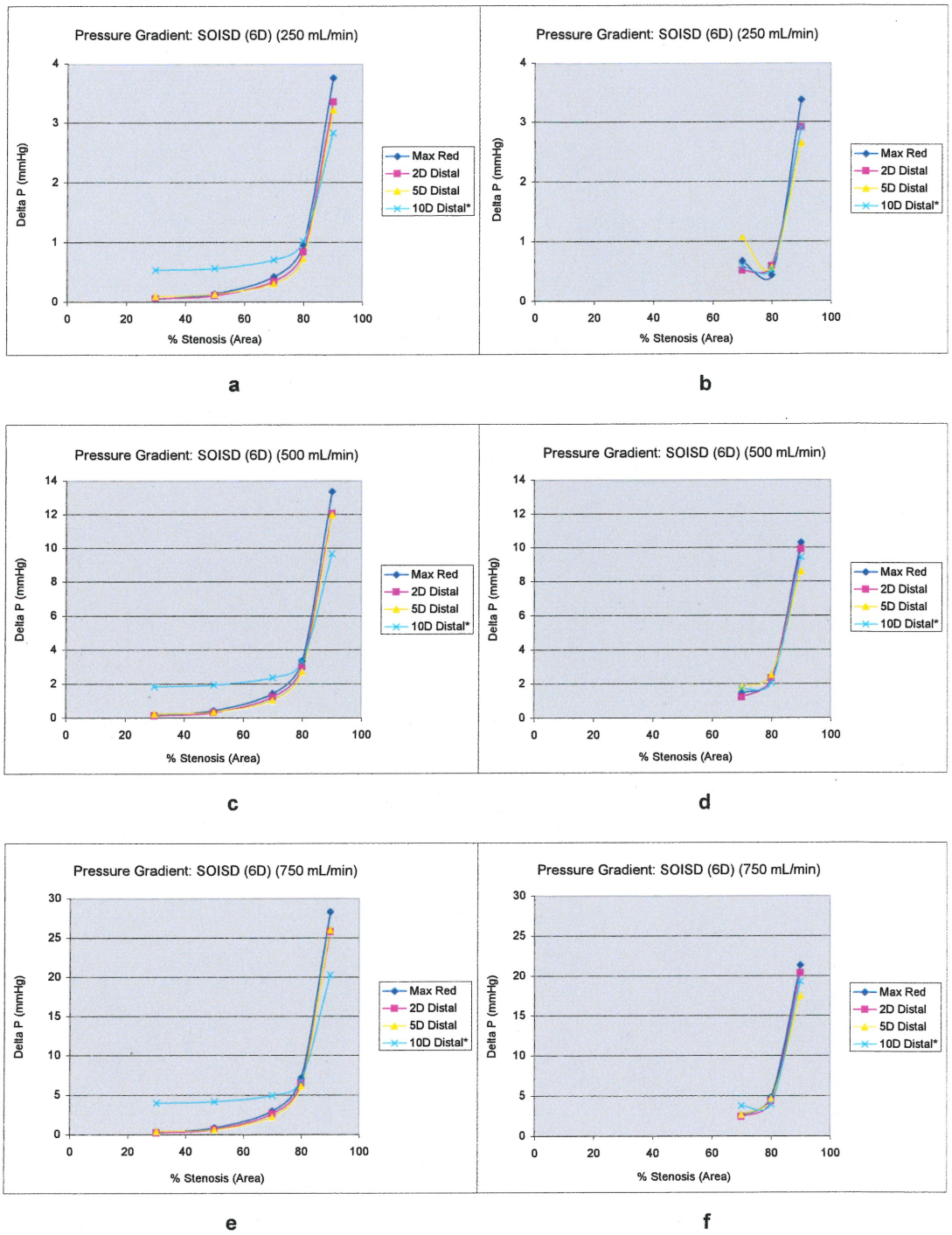

Figure AII-12. Pressure gradients at SOI, for a stenosis at 6D distal to the SOI, from the simulations (left) and *in vitro* experiments (right). Flow rates increase from 250 mL/min (a and b), to 500 mL/min (c and d), and to 750 mL/min (e and f). The *in vitro* experiments for the 50% AR stenosis were not performed for lack of time.